Delft University of Technology

Document Version
Final published version

Licence
CC BY-NC-ND

Citation (APA)
Roeplal, R., Pang, Y., Adema, A., van der Stel, J., & Schott, D. (2023). Modelling of phenomena affecting blast furnace burden permeability using the Discrete Element Method (DEM) – A review. *Powder Technology*, *415*, Article 118161. https://doi.org/10.1016/j.powtec.2022.118161

Important note
To cite this publication, please use the final published version (if applicable).
Please check the document version above.

Copyright
In case the licence states "Dutch Copyright Act (Article 25fa)", this publication was made available Green Open Access via the TU Delft Institutional Repository pursuant to Dutch Copyright Act (Article 25fa, the Taverne amendment). This provision does not affect copyright ownership.
Unless copyright is transferred by contract or statute, it remains with the copyright holder.

Sharing and reuse
Other than for strictly personal use, it is not permitted to download, forward or distribute the text or part of it, without the consent of the author(s) and/or copyright holder(s), unless the work is under an open content license such as Creative Commons.

Takedown policy
Please contact us and provide details if you believe this document breaches copyrights.
We will remove access to the work immediately and investigate your claim.

This work is downloaded from Delft University of Technology.

Powder Technology 415 (2023) 118161

Contents lists available at ScienceDirect

Powder Technology

journal homepage: www.journals.elsevier.com/powder-technology

Review

Modelling of phenomena affecting blast furnace burden permeability using the Discrete Element Method (DEM) – A review

Raïsa Roeplal [a,*], Yusong Pang [a], Allert Adema [b], Jan van der Stel [b], Dingena Schott [a]

[a] Department of Maritime and Transport Technology, Delft University of Technology, Mekelweg 2, Delft, the Netherlands
[b] Tata Steel Europe, Wenckebachstraat 1, Velsen-Noord, the Netherlands

GRAPHICAL ABSTRACT

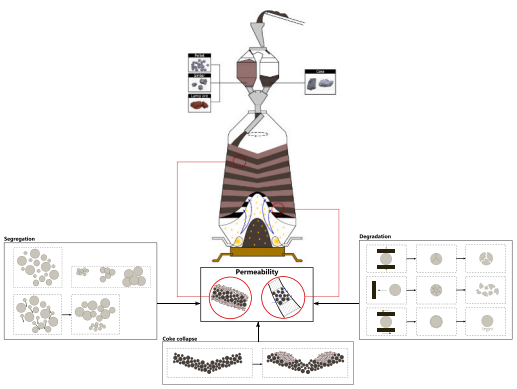

ARTICLE INFO

Keywords:
Blast furnace
Burden distribution
Permeability
DEM

ABSTRACT

Bed permeability is a crucial factor in blast furnace efficiency and stability. The Discrete Element Method (DEM) has been used extensively to model material flow in different parts of the furnace and holds great potential for optimizing the permeability. The inherent computational load is the main bottleneck in using this method to provide detailed descriptions of different blast furnace granular phenomena on an industrial scale. In recent years, computing capabilities have been rapidly increasing and more elaborate models are being developed for the furnace as a whole. This paper reviews the recent progress in modelling relevant phenomena related to the burden distribution, and how they affect the bed permeability, using DEM. We conclude that significant efforts have been made in modelling the burden distribution; however, these models generally do not investigate the permeability. Hence, understanding of how the permeability can be optimized still requires significant efforts towards model development.

* Corresponding author.
E-mail address: r.n.roeplal@tudelft.nl (R. Roeplal).

https://doi.org/10.1016/j.powtec.2022.118161
Received 12 September 2022; Received in revised form 10 November 2022; Accepted 8 December 2022
Available online 14 December 2022
0032-5910/© 2022 The Authors. Published by Elsevier B.V. This is an open access article under the CC BY-NC-ND license (http://creativecommons.org/licenses/by-nc-nd/4.0/).

1. Introduction

Steel is the most important engineering and construction material worldwide. The majority of energy consumed in an integrated steel plant is attributed to the smelting unit, a counter-current reactor commonly known as a blast furnace, where liquid iron is produced through a series of mostly endothermic chemical reactions occurring between ascending hot gas which is injected through tuyeres at the bottom of the furnace and a descending packed bed of raw materials (collectively referred to as the "burden") which are charged at the furnace top. Fig. 1 shows the general layout of the blast furnace including its charging system. Two types of charging systems are often encountered in blast furnace operation: bell-type (BT) and bell-less type (BLT). Bell-less systems are typically used in large and new blast furnaces with an improved design providing greater flexibility of charging method and more efficient burden distribution control when compared to bell-type systems [1]. The burden is charged in alternating layers of ferrous components (combinations of pellets, sinter and lump ore [2]) which may be mixed with additives, and coke. Since the gas temperature is highest at some distance above the tuyeres, the charged ores are progressively heated towards this point and will eventually melt. The consumption of solids and extraction of liquid products allows the packed bed to continuously travel downwards and a new batch of burden materials is added once the stock line level has decreased to a set-point height. Thus, the blast furnace can be regarded as a continuous reactor in which the solid-gas interactions control the process.

For many years, researchers have emphasized the importance of the burden distribution in furnace productivity [3–7]. How the bed layers are formed during furnace charging and how they subsequently deform during the burden descent are important as the burden distribution is closely linked to the permeability. Depending on the operation strategy, furnace operators aim for a certain burden distribution to control the

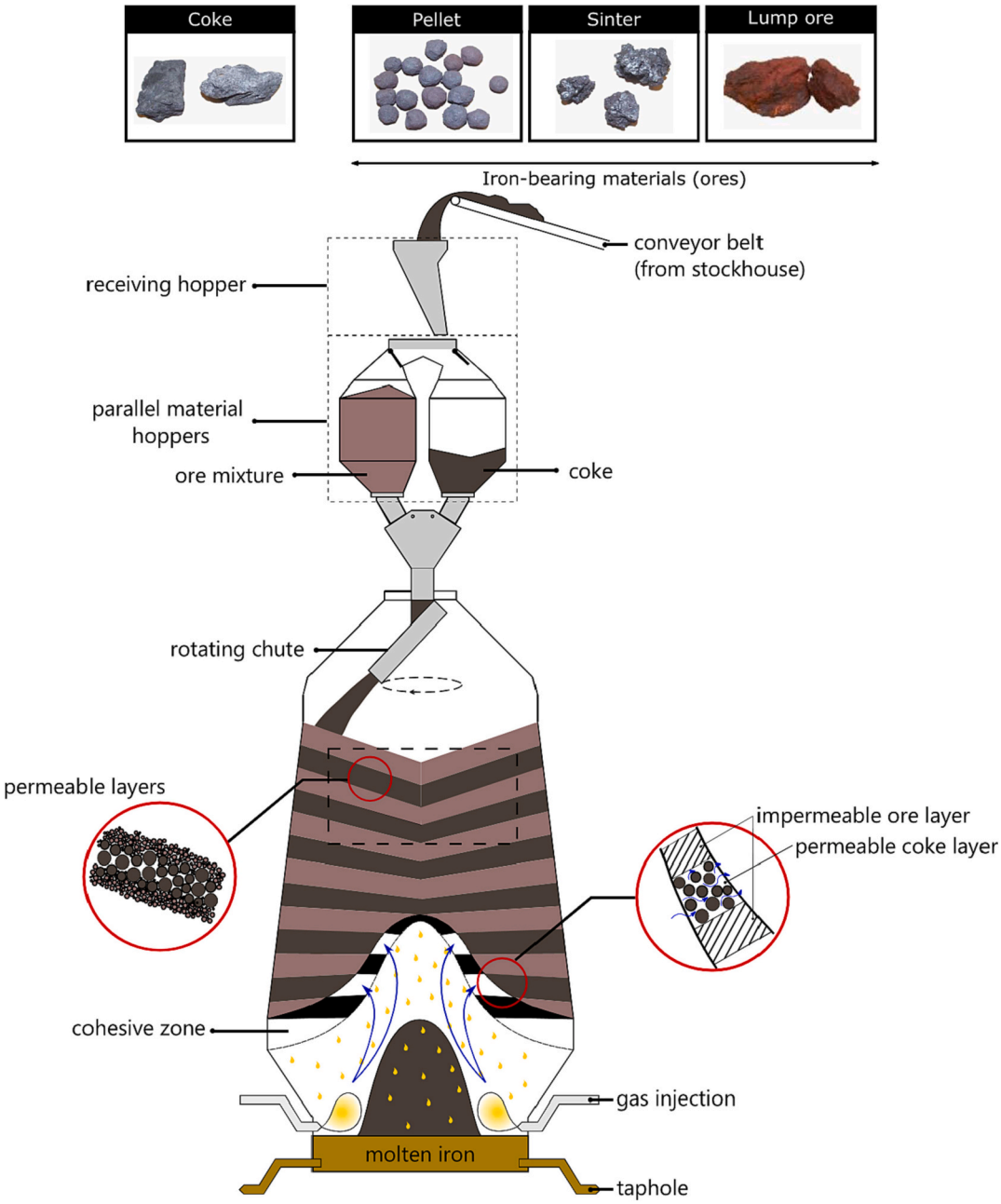

Fig. 1. Illustration of the packed bed structure, the (bell-less top) charging system and raw materials involved in blast furnace ironmaking.

bed permeability, and therefore the gas flow, along the shaft radius [8–10]. In practice, however, it is difficult to achieve the targeted distribution due to the complex interplay of granular phenomena which occur during charging and descent. Hence, there is a need to investigate how the material behaves during operation and whether the burden distribution can be improved. Since physical inspections and real-time measurements are very difficult and expensive to execute during furnace operation, a more feasible approach to predict the true burden distribution, and how it affects the permeability, is required.

Computational modelling is considered to be a powerful research tool which allows for saving time and costs when optimizing industrial processes. The Discrete Element Method (DEM) [11] quantifies the forces acting on each particle and can therefore predict the spatio-temporal evolution of a granular flow. The strength of DEM lies in the fact that both the bulk and particle-level characteristics of a flow can be analyzed, making this technique particularly suitable for scrutinizing the burden distribution and its effect on bed permeability. A DEM model requires input parameters which must be carefully selected such that the real-life flow behavior can be predicted at the lowest possible computational cost; the latter is especially true for large-scale applications. This balance of accuracy and efficiency requires the modeler to make certain modelling choices, which generally depend on the process or phenomenon being modelled. Hence, developing a model for optimizing the burden and subsequent gas flow distribution through charging requires a thorough understanding of the phenomena which are important to consider and how they can be modelled by DEM.

The objective of this work is twofold. First of all, we aim to provide a clear understanding of burden permeability, and how it is affected by different granular phenomena occurring during the charging and descending process according to literature. As DEM is particularly suited for modelling granular phenomena, our second aim is to review the state-of-the art in DEM models of the charging and descending phenomena for analyzing blast furnace permeability. Other reviews of blast furnace models have been published before [12–17], providing an overview of different modelling trends and discussing the use of both continuum and DEM models. The novelty of this paper is its focus on the permeability in particular, and the suitability of current blast furnace DEM models for this purpose. This paper could prove useful to modelers as it provides a summary on modelling and experimental methods and can serve as a guide for making certain choices based on literature.

This paper is divided into two main parts based on our objectives. In Section 2, we provide an understanding of blast furnace burden distribution and its effect on permeability based on the current blast furnace DEM literature. In Section 3, we recommend a DEM model development framework based on general DEM literature and review the modelling methods used in current blast furnace DEM literature using this framework. We conclude this work in Section 4 by stating the knowledge gap and providing an outlook on focus areas for future studies.

2. Granular phenomena affecting bed permeability

In Section 1 we touched upon the importance of burden distribution on bed permeability. In this section, we first describe in more detail how the two are related (Section 2.1). Next, we discuss important granular phenomena which are expected to affect blast furnace burden permeability during charging and descent according to literature (Section 2.2). At the end of this section, we synthesize the practical findings of these studies which can be applied in industry (Section 2.3).

2.1. Burden distribution and bed permeability

As mentioned previously, the resources involved in blast furnace ironmaking are ferrous materials (iron ores), coke and hot gas. The furnace is divided into four main zones based on the thermal and chemical state of the raw materials. In summary, ferrous solids contain iron oxides which need to be reduced to iron by the hot gas, while the coke burden has multiple functions [18,19]: (1) it fulfils the thermal and chemical requirements for the reduction process; (2) it acts as a carburizer; (3) it ensures adequate drainage of liquid products below the cohesive zone and passage for gas to and throughout the upper portion of the bed. The latter is possible due to the higher permeability of the coke bed compared to the ferrous bed, and the fact that only the coke layers remain permeable in the cohesive zone.

The permeability of a packed bed provides a measure for how well the voids between particles comprising the bed (i.e., the pores) are connected [20]. This generally depends on the bed configuration; i.e., on factors such as the packing fraction, and geometrical features (shapes and sizes) of the particles [21]. In the context of blast furnace productivity, the permeability determines to what extent the ascending gas is in contact with the ores, and therefore how well the reduction-melting process takes places. The literature suggests the following burden distribution guidelines regarding the permeability:

1. In the cohesive zone, there should be a minimum number and size of coke slits to allow adequate gas passage to the upper layers [22–24]. It is also important to have evenly sized coke slits, so that the gas flow is even in radial direction [10].
2. In the lumpy zone:
   (a) Each coke layer should have a sufficient and even thickness in radial direction in order to provide adequate gas flow to the subsequent ore layer along the radius [9,10,25]. In general, the permeability increases with the coke layer thickness [9]; however, as the steel industry faces increasing pressure to minimize its carbon footprint, the coke layer thickness is minimized as much as possible in modern operation. Pulverized coal is injected with the blast to account for the reduced metallurgical coke rate. To maintain permeability in the cohesive zone, coke is added to the ore burden in the form of small (nut) coke [19].
   (b) The ferrous layers should be as thin as possible to enhance gas-ore contact and have a uniform thickness along the radius [9]. Also, due to morphological differences, the different types of ore should be evenly distributed to provide a homogenous packing structure and therefore an even gas flow through the layer. Another (perhaps more important) reason for homogeneously distributed ores is the differences in chemical properties. Since the ores reach their melting point at different temperatures, an uneven radial and circumferential distribution at the top of the furnace could lead to problems in forming the cohesive zone, of which the shape plays an important role in gas flow distribution.
   (c) In general, an even particle size distribution throughout the layers is desired. The emphasis in this regard is on the even distribution of fines throughout the layers, as concentrated deposition of fines will result in localized clogging.

These guidelines aim to diminish spatially separated regions of strong and weak gas flow throughout the packed bed. In practice however, this is not exactly aimed for by blast furnace operators. As shown in Fig. 2, two basic operation modes are often described in literature [9,26–28]: central gas flow operation and wall-working operation. The main difference between the two lies in the gas flow distribution. In central gas flow operation, a strong gas flow is achieved in the center while the flow is directed towards the walls in wall-working operation. Other operation modes can also be found in literature such as “double-peak” and “flat” [10], but we will not further discuss them here. The preferential direction of gas flow in different operation modes is achieved by selective deposition of coke, as can be seen Fig. 2. Depending on the operation strategy which is aimed for, an “optimal” burden distribution can be defined. However, very little information on the burden distribution requirements corresponding to different operation strategies can be found in literature. According to Liu [10], wall-working operation is not desirable since wall erosion is highest and gas utilization is poor, while central gas flow operation has lowest wall erosion and

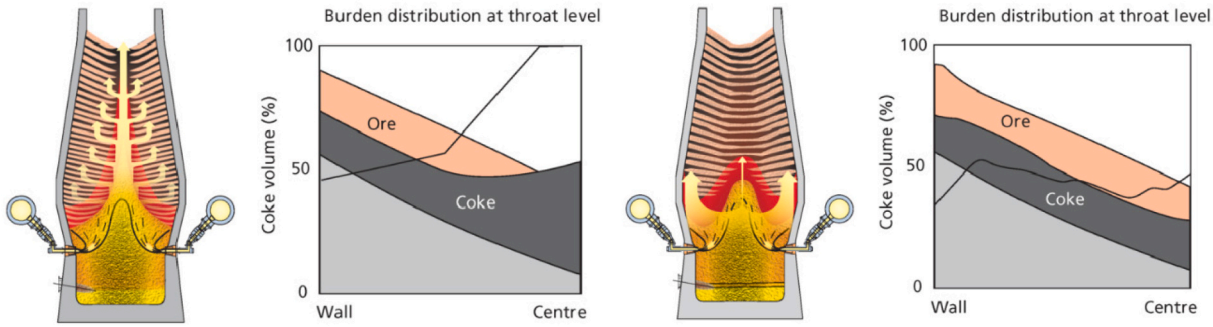

Fig. 2. Two basic gas flow distribution strategies used in industry (from left to right): (a) central gas flow operation, (b) wall-working operation; images adopted from [9].

better gas utilization. The flat operation mode has even better gas utilization, but does not offer the same degree of wall protection. Geerdes et al. [9] provide a clear set of requirements which, according to them, provides the ideal burden distribution for modern blast furnaces operating under high pulverized coal injection rates: "(1) an ore-free center, (2) nearly horizontal layers of coke and ore burden, (3) some nut coke in the ore burden in the wall area and (4) fines distributed over the radius".

Based on these findings, we conclude that not only should the material distribution within each layer be homogeneous in size (and composition, for the ore layers), but the amount of fines should be limited and an even radial and circumferential mass distribution should be strived for. In the following, we review to which degree these aspects of the burden distribution have been studied in the past using DEM.

2.2. Phenomena affecting burden distribution

2.2.1. Segregation

Segregation, also referred to as reverse mixing or de-mixing, is a widely-studied phenomenon occurring in granular flows which involves spatial arrangement of mixture components (pattern formation) due to differences in material properties such as size, density, shape and surface roughness [29]. Blast furnace operation involves different equipment which induce a variety of flow behaviors, and the burden differ in various material properties. Hence, segregation is expected to occur in different stages of the material handling process. In blast furnace operations, a burden layer is formed by charging concentric rings, usually starting at the throat periphery and ending at the center. Segregation during charging of these individual rings can pose an impediment to achieving a homogeneous size and component distribution within a layer as a whole [30], which might affect the initial permeability distribution [31] and the subsequent redistribution caused by the deformation of burden layers during their descent. Hence, it is important to understand how the multi-component burden segregates during charging and descent, and how this affects the permeability distribution.

- During flow through the charging apparatus

The coke and ore burden are charged into the parallel hoppers either from a conveyor belt or a skip [9]. In the case of a conveyor belt, some segregation of material can already occur during transportation on the belt due to its bouncing motion as it rolls over idlers. The small particles settle to the bottom of the belt while the coarse particles rest upon them. Going even further upstream, segregation also occurs as materials are discharged from storage onto the belt or into the skip. Only very little amount of research has been done on the occurrence of segregation as the material is handled upstream of the hoppers. Spence [32] undertook a thorough experimental investigation on size segregation within the charging system, which included the entire material transportation from the stock-house to the receiving hopper, material hopper, rotating chute and finally the furnace throat. They concluded that the segregation patterns emerging during material hopper discharge can be linked to segregation during filling of the receiving hopper. Another example is the work of Mio et al. [33], where a 1/3-scale furnace was used to investigate the distribution of coke and sinter in the throat after charging. In their system, the parallel hoppers received the burden materials from a surge hopper through a belt conveyor, and discharged into a funnel. By measuring the mass fraction different sized sinter particles as a function of time discharged from the funnel, they concluded that particle size segregation occurred during charging and discharging at the surge hopper and parallel hoppers since larger sinter particles were discharged later. While these experiments demonstrate that size segregation occurs upstream of the hoppers, and during filling of the hoppers, surprisingly little has been done to model the flowing behavior for this portion of the charging process, especially when it comes to loading and unloading of the skip cars or conveyor belt.

Most DEM blast furnace research has been done by modelling the system starting with the parallel hoppers. For example, Zhang et al. [34], Wu et al. [35] and Xu et al. [36] all studied size segregation during hopper charging using a fictitious filling method in their simulations. Since the material being fed to the hoppers was assumed to be non-segregated in these works, the results on size distribution in the hopper may not be representative of the actual operation. Nonetheless, these works have all shown that small particles tend to remain close to the stream impact point while large particles tend to roll away during heaping. The authors all concluded that the size distribution in the hopper changes as a function of the filling position and angle. Size segregation during hopper discharge is dictated by the order in which segregated material groups flow out of the hopper. This depends on

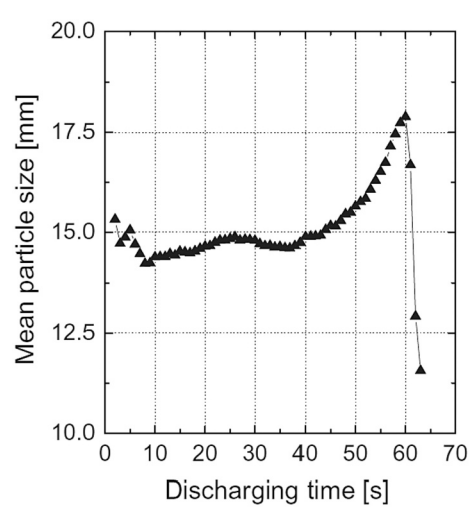

Fig. 3. Mean particle size in the flow at the outlet of a hopper; image adopted from [37].

primarily the hopper design, but it is generally seen that large particles are discharged later than small particles [35–38] (cf. Fig. 3). Since the burden is charged in rings to form a layer, size segregation during hopper filling and subsequent discharge can result in a non-homogenous size distribution in both circumferential and radial directions. It should be noted that actual blast furnace operation involves charging of an ore mixture, rather than one material component. As stated in Section 2.1, it is important for the ore layers to have an homogenous composition. The segregation behavior of ore mixtures during hopper filling and discharge has been studied by Xu et al. [39,40]. As the different types of ores are generally charged to the hopper in batches rather than a mixture, they investigated how the order of charging ores to the hopper affects the order of discharging and the final component distribution in the throat. They found that the trend of each component's mass fraction from the periphery to the center of the throat followed the mass fraction trend during discharging. Their work shows that component segregation within the ore layer is a direct consequence of the ore mixture's discharging behavior.

The next part of the charging apparatus which has received much attention is the rotating chute. The chute is the most flexible part of the system, as it can be controlled with respect to tilting angle (the angle between the chute baseline and the vertical centerline of the furnace) and rotating speed, which in turn affects the material flow within the chute itself, as well as the distribution on the stock surface in the throat. Researchers have mainly focused on understanding two main aspects: (1) how the material segregates as it flows through the chute, and (2) how the bulk flow behavior on the chute affects segregation of the material in the furnace throat. With respect to point (1), several researchers [38,41–43] have reported the occurrence of size segregation during chute flow. This is evident from the fact that the stream at the chute outlet has small particles at the inner part of the trajectory and large particles at the outer part. This pattern has been seen in both stationary and rotating chutes at different tilting angles [42]. As the particles flow through the rotating chute, they are subject to a variety of forces including inter-particle forces, particle-chute force, gravitational force, Coriolis force and centrifugal force [38]. The reader is referred to the work of Teng et al. [44] for a more in-depth description if these forces. The interplay of these forces determines the bulk behavior of the flow in the chute, specifically how compact/dilute the flow is at the chute outlet. When it comes to point (2), researchers have researchers have studied the effect of chute design [45] and operation [46,47] on the stream width and thickness, and how these factors affect segregation during layer build-up. These aspects are discussed later, in Section 2.3.

- During layer build-up

Segregation during layer build-up can occur due to different phenomena occurring simultaneously. First of all, when the particles exiting the chute are charged onto the stock surface, segregation due to heaping occurs. Each layer is formed by charging multiple rings, which are essentially heaps of material along the throat circumference. Hence, it is important to understand how the heaping process occurs as the rings are charged in order to understand the burden distribution. Xu et al. [48] performed a simple investigation in which a binary mixture of two particle sizes was charged to a 1/15th size blast furnace throat through a rotating chute. They only charged a single ring of material and found that the larger particles concentrated near the furnace wall while the small particles were near the center. Mio et al. [37] simulated the charging behavior of polydisperse sinter through multiple rings in a full-scale furnace. They found that ultimately the average particle size was largest at the furnace center, while the smallest average size was found at around half of the radius (cf. Fig. 4). They later confirmed this radial size distribution through experiments [33]. According to the authors, small particles are relatively immobile after impacting the stock surface and therefore stay in the vicinity of the burden stream's impact point, while large particles are able to roll towards the center during charging

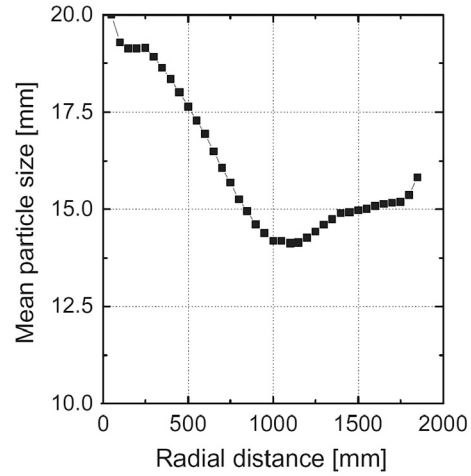

Fig. 4. Relation between mean sinter particle size and radial distance; image adopted from [37].

of the rings. Therefore, there are more large particles in the center of the furnace. Other researchers [38,49,50] provided a similar explanation after observing this accumulation trend in their DEM results. Yu & Saxén [51] also found this trend in their study of pellet charging, but they reported that the degree of segregation was much less compared to sinter due to the relatively narrow size distribution of pellet particles. The focus of these studies has been on size segregation when charging a single material to the furnace. Investigations of segregation during multi-component mixture charging are scarce. Xu et al. [48] extended their aforementioned size segregation study by varying the densities of the large and small particles individually and scrutinizing the effect on segregation. Their results showed that radial size segregation was reduced as the density of small particles increased, while the opposite was true when the density of large particles was increased. In reality, the ore mixture contains three materials (or four, if nut coke is present), each with their own size distributions. Hence, further investigation is required to understand the segregation behavior of blast furnace mixtures during heaping.

A second form of segregation occurs when ores are charged onto a layer of relatively light coke particles; this is referred to as the phenomenon of coke layer collapse (also referred to as coke-push or gouge formation). The ores "push" the coke particles aside, thereby deforming or shifting the coke layer which ultimately changes the coke-ore distribution, and therefore the permeability [52], in radial direction. An example of the coke collapse phenomenon is shown in Fig. 5. As the top surface of the burden is V-shaped, the coke particles roll down towards the center of the furnace. However, other surface shapes (e.g. "A" or "M" or "W") are also possible, and the direction in which the coke is shifted depends on the location of impact with respect to the peak [53]. Zulli et al. [54] performed experiments using a full-scale furnace model to investigate the coke collapse degree when sinter was charged onto preexisting coke layers. They found that the radial ore-to-coke distribution was significantly affected by this phenomenon. Ho et al. [4] used spheres made of different materials to study gouge formation experimentally in a lab-scale charging setup. They found that the gouge size increases as with the density of the charged material. Mitra & Saxén [55,56] used DEM to simulate the coke push effect when charging pellets onto a coke layer using a 1/10th scale blast furnace model, showing that DEM was able to predict this phenomenon. Mio et al. [42] simulated sinter charging onto a coke layer using a full-scale model, showing that the coke layer thickness changes significantly in radial direction after coke collapse. Kou et al. [46] also used a full-scale model to investigate coke collapse after sinter charging. They found that the severity of coke collapse depends on the chute angle, rotational speed and the amount of sinter being charged. Zhou et al. [57] developed a more realistic

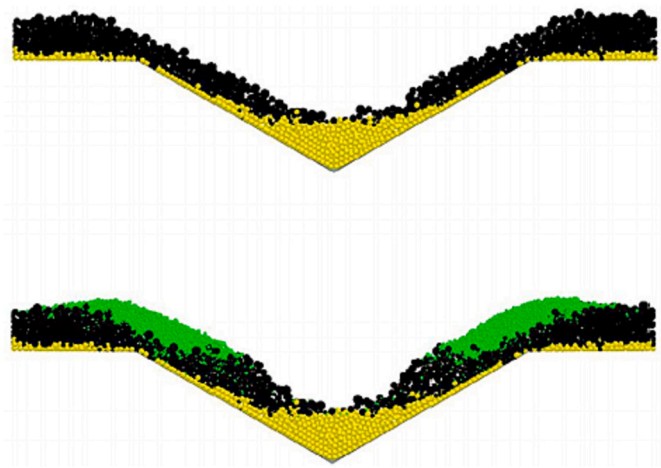

Fig. 5. Radial burden profiles before (top) and after (bottom) collapse, where yellow, black and green particles represent sinter base, coke and charged sinter, respectively; image adopted from [46]. (For interpretation of the references to colour in this figure legend, the reader is referred to the web version of this article.)

simulation where pellets, sinter and lump ore were mixed and charged on top of a coke layer in a full-scale furnace model. They investigated the effects of different charging practices such as reverse charging and central coke charging on coke collapse. These aspects are discussed later, in Section 2.3.

Until this point we discussed how radial segregation occurs during layer build-up. Segregation in the vertical direction also occurs due to the sieving phenomenon: small ore particles become embedded in the upper part of the coke layer during charging, and proceed to travel towards the bottom of the coke layer. This phenomenon results in the formation of a mixed coke-ore layer (cf. Fig. 6), which is densely packed and has a lower permeability than the individual coke and ore layers [49]. Kajiwara et al. [58] performed full-scale experiments of charging ore onto a coke layer and observed both the coke push phenomenon and the mixed layer formation. Several researchers [59–62] have shown experimentally that, depending on the size ratio between particles of the individual layers, this "interface resistance" can have a significant effect on the pressure drop over a stagnant bed. Wei et al. [49] used DEM to simulate sinter and coke layer formation using a small-scale setup. They

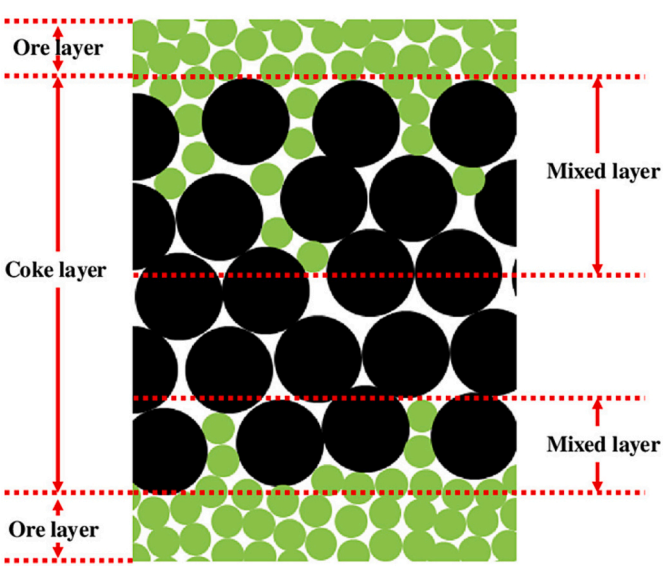

Fig. 6. Illustration of coke-ore mixed layers; image adopted from [182].

charged three alternating layers of sinter and coke, and studied the effect of segregation and mixed layer formation on the porosity distribution within the entire bed. They found that the porosity varied in both radial and axial directions: a higher porosity was found in the center of the furnace due to the higher average particle size in that region and a lower porosity was found in the bottom layers due to the presence of small particles and the compaction caused by the top layers. In general, the porosity of coke layers was highest while that of the mixed layers was the lowest. Li et al. [50] used a full-scale model to investigate both vertical and radial segregation when charging ore onto a layer of coke particles. For simplicity, they used a binary mixture of large and small particles for both materials and investigated the effect of the size ratio (defined as the ratio of small to large particle diameters) of the particles on segregation. Not surprisingly, the radial segregation worsened as the size ratio decreased. As this study was performed at full-scale, the flow conditions were representative of an actual blast furnace; however, the materials were not. Future studies should include more realistic size distributions to study the vertical segregation more accurately.

- During burden descent

As the packed bed descends, the coke and ore mixture layers tend spread out due to the gradual widening of the furnace [7]. Consequently, the voids between particles in each layer become larger and the ore particles are able to further infiltrate underlying coke layers. Hence, the mixed layers formed during charging become thicker, and individual coke and ore layers become thinner. This process has not been studied extensively in a setting representing actual blast furnace operation. Although inter-particle percolation has interested researchers for many years now, most of the work in this field involves analysis of the percolation behavior of only few particles in a simplified setup (e.g. a static, cylindrical packed bed) using idealized materials such as beads. These analyses have been done both experimentally [63,64] and numerically [65–69], primarily to gain fundamental understanding of the percolation phenomenon.

When it comes to blast furnace materials, only Yu & Saxén [70] attempted to study percolation during burden descent experimentally. The authors developed an experimental setup (described in Section 3.5.3) which allowed for visual inspection of pellet-coke mixed layer formation due to furnace widening. They also developed DEM counterpart to study the effect of different model parameters on the extent of percolation. The findings are discussed in Section 3.3.

2.2.2. Degradation

Degradation involves the generation of fines and broken particles during transportation and handling. Different types of degradation can occur, depending on the type and magnitude of forces causing degradation [71]. The furnace permeability is directly affected by the proportion of fines in the packed bed. This is true for all burden materials, but perhaps more important for the coke layer which is responsible for gas passage and liquid drainage in lower parts of the furnace. Hence, it is important to quantify degradation of burden materials at each handling stage.

Researchers have performed experiments to investigate degradation of coke [72–75], lump ore [72,76–78], pellet [79,80] and sinter [72,75] using drop tests, impact tests, slow compression tests and tumbling tests. The purpose of these tests is to relate the forces responsible for degradation to the particle size and shape distributions resulting after degradation has occurred. Tavares et al. developed a model to predict the breakage behavior of these materials under different conditions. This model is currently implemented in EDEM and RockyDEM [81]. Despite the possibility to model breakage phenomena using DEM, we have not encountered any studies focusing on blast furnace burden breakage modelling in literature. Instead, we find that researchers have used DEM to determine different aspects associated with breakage. For example, Nouchi et al. [82] assessed where stresses exceed the compressive stress

of coke and therefore could result in abrasion. Zhang et al. [83] determined optimal furnace wall angles based on the stress levels and therefore the expected degree of abrasion occurring for different furnace designs. In these studies, the particles in DEM were modelled as spheres and the breakage mechanism itself was not modelled. Natsui et al. [84] used DEM-CFD to determine the effect of coke degradation on the permeability of a coke packed bed. Rather than modelling the degradation process, they assessed how permeability changes after degradation in separate simulations. They initially performed simulations using virgin coke particles. The true shape of the particles was included in their work by attaching multiple spheres together such that coke shapes obtained through 3D scanning were approximated, as shown in Fig. 7. Through tumbler experiments, they could identify the volume of coke fines generated after 50 drum revolutions. Next, they performed simulations of the degraded particle bed by adding a representative amount of fines to a bed of coke particles which had decreased in size, compared to the initial simulation. They analyzed and compared the fines and gas velocity distribution for both cases, as shown in Fig. 7.

2.2.3. Flow deviation

Fig. 8 illustrates the basic material handling equipment involved in blast furnace charging using BLT. Compared to the serial-type BLT, the parallel-type requires an additional connection chute (also referred to as the "funnel" or "Y-tube") to direct the material discharged from the bunkers to the rotating chute. Fig. 9 shows that, unlike in a serial-type BLT, the flow discharged from the bunker is de-centered inside the funnel. This deviation of the material stream's centroid from the centerline results in a variation of its collision point on the chute as it rotates [85–88] and this imbalance ultimately causes an uneven circumferential burden distribution in terms of the charged mass flow and the material falling point just above the stock surface. Xu et al. [89] used DEM to investigate the difference in burden distribution when using a serial and parallel-type BLT. They found an even mass distribution in circumferential direction when using a serial-type BLT. For the parallel-type BLT, the mass distribution plot resembled a cosine-like curve, thereby demonstrating the circumferential imbalance. Narita et al. [90] performed experiments using a 1/5 scaled model of a charging apparatus and confirmed the existence of the circumferential imbalance. Using DEM, they looked at the forces acting on the particles upon entering the chute and claimed that the material is forced to travel along one side of the chute due to its curvature. When the centrifugal force acts in the same direction as the curvature force, then the material discharges at a higher position than when these forces oppose each other. Hence, the authors claimed that this difference in material stream discharge height causes an uneven falling point along the circumference. Using their DEM model, they investigated how the Y-tube design can be adjusted to mitigate the circumferential imbalance. Sun et al. [91] used DEM to analyze how the material flow on the chute changes with the collision point. They stated that when the collision point is located higher on the chute, then the flow of material on the chute is relatively sparse. When the striking point is lower, the particles falling down from the funnel tend to accumulate on top of material which already on the chute, making the flow denser. Hence, alternately sparse and dense granular flow exit the chute as it rotates, causing the uneven circumferential mass distribution in the throat. Chen et al. [92] used DEM to perform a thorough investigation of how the circumferential imbalance occurs. They claimed that the deflection of particle flow on the chute depends on the interplay between Coriolis force and curvature force, which in turn depends on the collision point on the chute (as summarized in Fig. 10). Next, they investigated how the mass flow rate and Y-tube design affect the circumferential imbalance. Xu et al. [39,93–95] investigated how design and operational factors can be adjusted to mitigate the circumferential imbalance. The results of all studies related to equipment and operation design are discussed in Section 2.3.

2.3. Effect of design and operational parameters on burden distribution

The design of equipment has a large influence on the burden flow behavior, and therefore the material distribution on the stock surface [35,95]. Hence, design modification should be considered when exploring the possibilities for enhancing gas-solid interactions in the furnace. However, it is generally more practical to consider how operational conditions can be adjusted, rather than modifying existing equipment design. Operational conditions refer to parameters which can be changed for a given system design. In this section, we discuss how design and operational aspects for different parts of the system can be

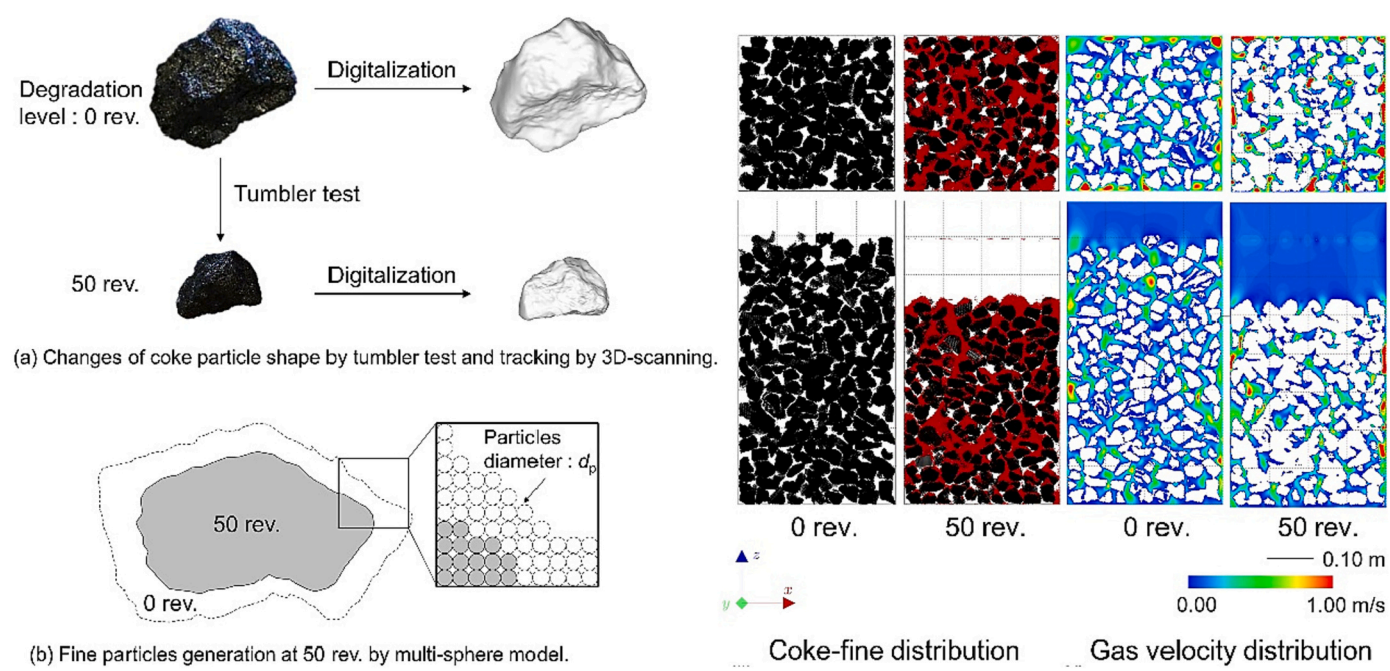

Fig. 7. Schematic of the coke deformation model (left) and simulation results for a packed bed of coke particles before and after degradation; images adopted from [84].

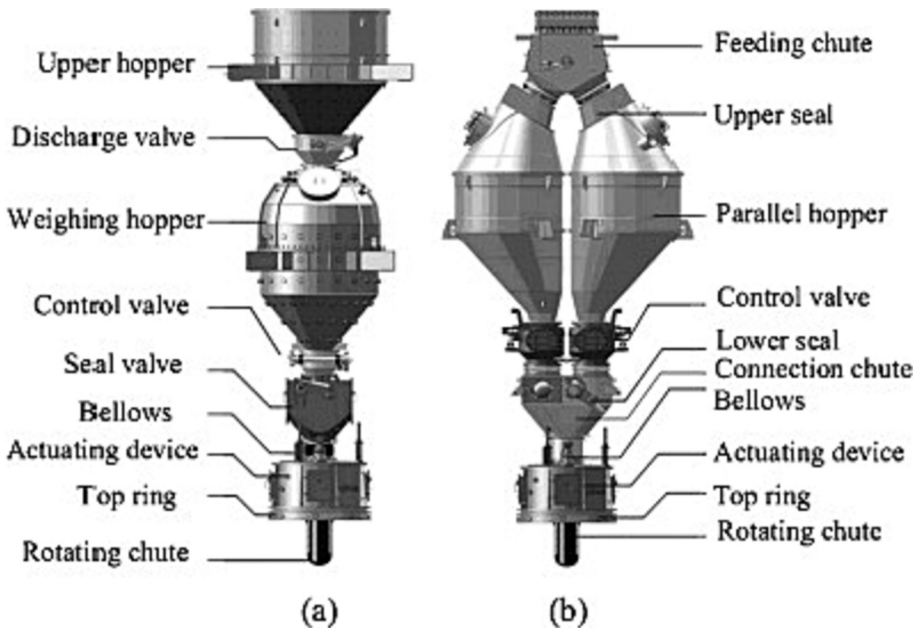

Fig. 8. Basic material handling equipment in (a) serial-type and (b) parallel-type BLT systems; image adopted from [38].

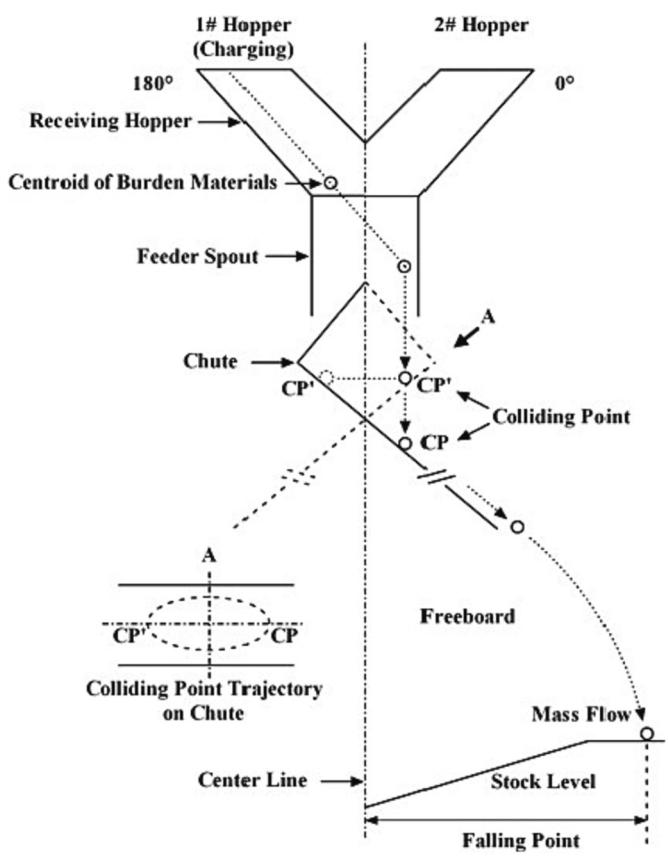

Fig. 9. Particle flow trajectory in a parallel-type BLT; image adopted from [87].

modified to improve the resulting material distribution according to blast furnace DEM studies.

2.3.1. Parallel hoppers

As mentioned previously, the hoppers can be loaded using a conveyor or skip hoists. The loading method is expected to affect how the burden segregates as it is charged to a Paul-Wurth hopper. Zhang et al. [34] investigated the effects of the angle and position of a feeding chute on size segregation during loading of a binary coke mixture to a hopper. The filling procedure in simulations was as follows: pre-mixed particles were generated randomly in a conical feeder bin above the hopper and subsequently discharged through the feeding chute, which replaced the belt charging used in practice. Since the conical feeder bin produced a mass flow upon discharging, the degree of segregation in the hopper after charging was solely the result of segregation during the confined heap formation in the hopper. Parameter studies were performed by adjusting the angle and endpoint of the inclined surface, as shown in Fig. 11. It was seen that the degree of segregation became less as the filling position was closer to the center of the hopper, and as the filling angle was more vertical. Wu et al. [35] performed a similar analysis for the filling position (either left, center or right, as shown in Fig. 12), but they considered a ternary mixture of sinter particles and they used a virtual factory rather than a mass flow hopper to generate particles. Their results showed that small particles are generally located near the burden apex, indicating that small particles always tend to accumulate around the striking point during hopper filling. They also concluded that segregation was different for each filling position; but, contrary to the results of Zhang et al. [34], it could not clearly be seen that the degree of segregation was less in the case of a centered apex. Xu et al. [93] also studied hopper filling, but they simulated the filling process using a feeding belt which resembles the actual hopper filling process. As shown in Fig. 13, the material discharged from the feeding belt entered a switch chute, which directed the flow to the parallel hoppers. They found that when the centerline of the feeding belt did not coincide with the symmetry plane of two parallel hoppers, there was a difference in the velocity of the flow to and subsequent burden distribution in the left and right hopper. The burden apex positions were different in the two hoppers, as well as the volume distribution in radial and circumferential directions. The effect on segregation was not investigated.

Segregation during hopper discharge is a result of the sequence of discharge of material. It has been claimed that the discharge sequence depends on hopper design, how the material is initially arranged in the hopper, and the discharging mass flow rate [40,96]. When it comes to design aspects, Wu et al. [35] scrutinized the effect of hopper outlet slope on size segregation. Keeping in mind that the parallel hoppers

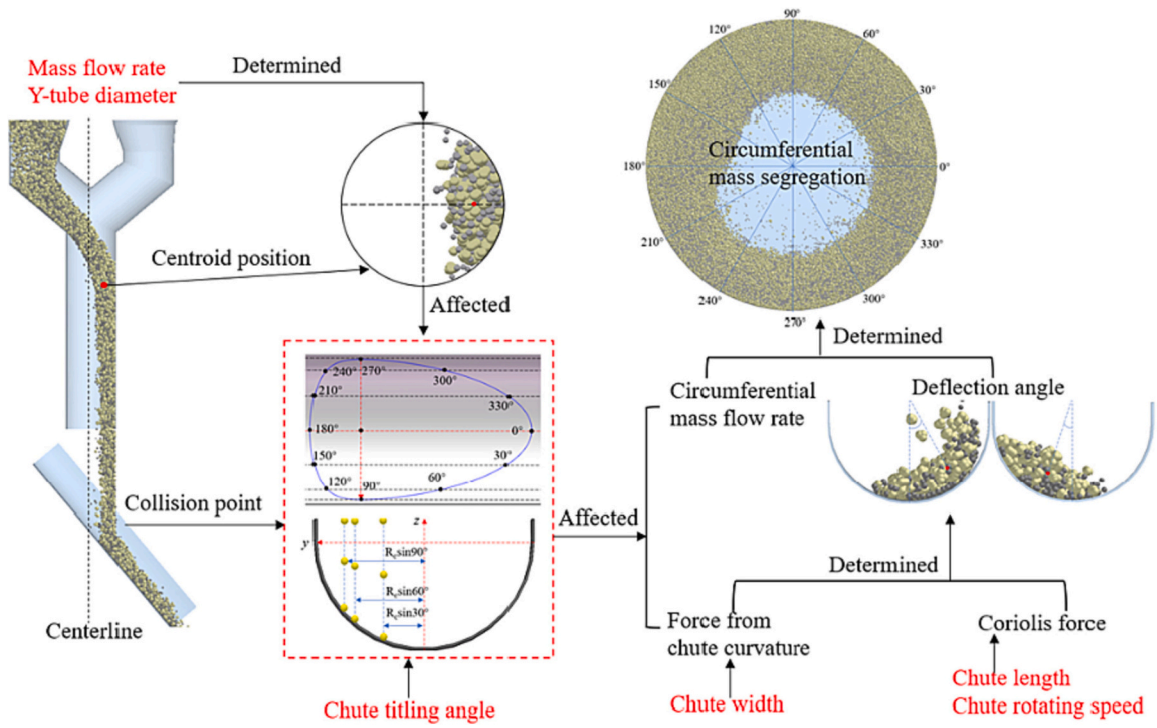

Fig. 10. Factors affecting circumferential imbalance; image adopted from [92].

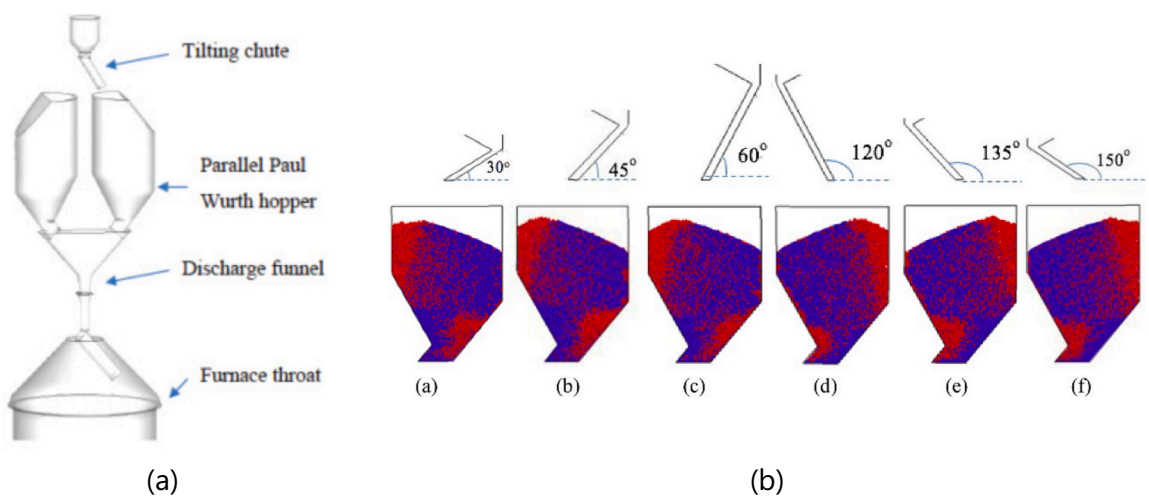

Fig. 11. Different tilting chute designs for charging the P-W hopper; images adopted from [34].

should be designed such that the outlet is close to the furnace center, they considered three hoppers with varying slope outlets but each discharging close to the furnace center (cf. Fig. 14). They found that the material discharging sequence was completely different for each design. In fact, for the left outlet hopper the material at the left side was discharged first, while the opposite was true for the right outlet hopper. Moreover, the right outlet hopper had a long outlet pipe which enhanced size segregation. Another design aspect is the hopper outlet size, which was studied by Zhang et al. [34]. They described the existence of the so-called "engulfing phenomenon", which involves the formation of a dip in the material during discharge. The dip engulfs large particles in its vicinity so that the discharge composition fluctuates. As the outlet size increases, the moving layers become larger and there is less time for the engulfing mechanism to take place; hence, there is less fluctuation and segregation decreases. When it comes to initial material arrangement, Xu et al. [39,40] scrutinized the discharging behavior of a pellet, sinter and lump ore mixture. In practice, these materials are charged to the hopper in batches rather than as a mixture. The authors investigated how the charging sequence of the materials to the hopper affects the discharging sequence. They found that particles charged first into the hopper were in fact not discharged first and that different initial arrangements of pellet, sinter and lump ore in the hopper resulted in different (radial and circumferential) burden distributions in the throat. Since each component has a different permeability, the authors pointed out the importance of studying how the initial distribution in the hopper affects the final distribution in the throat.

2.3.2. *Funnel (Y-tube)*

As discussed in Section 2.2.3, the deviation phenomenon occurring in the funnel of a parallel-type BLT charging system eventually leads to a

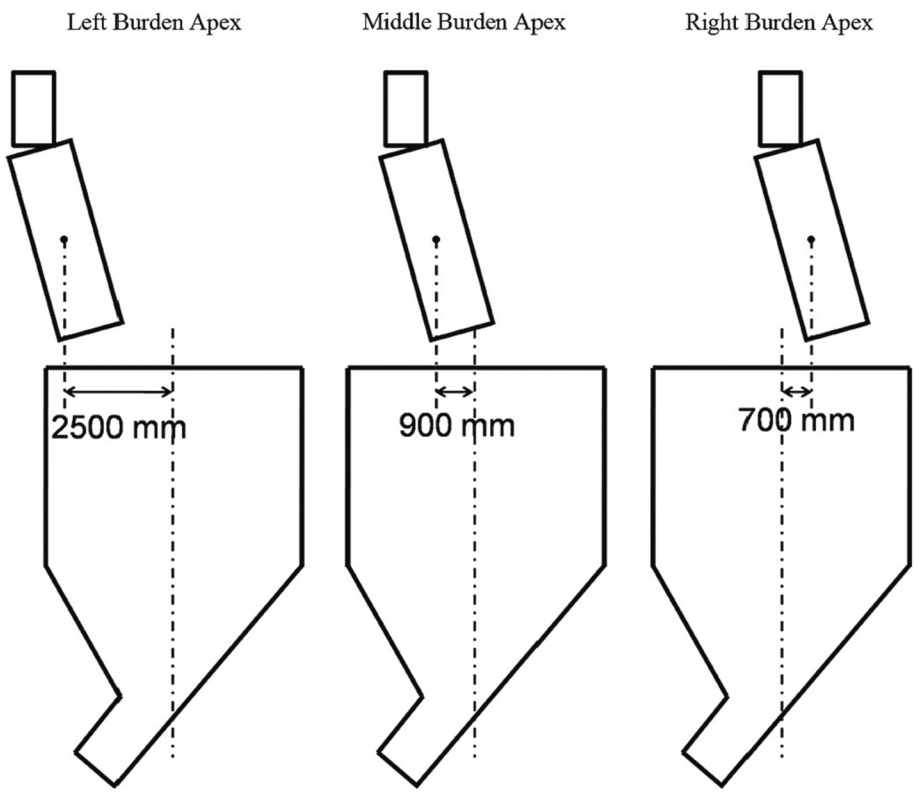

Fig. 12. Different locations of the charging chute for the P-W hopper; images adopted from [35].

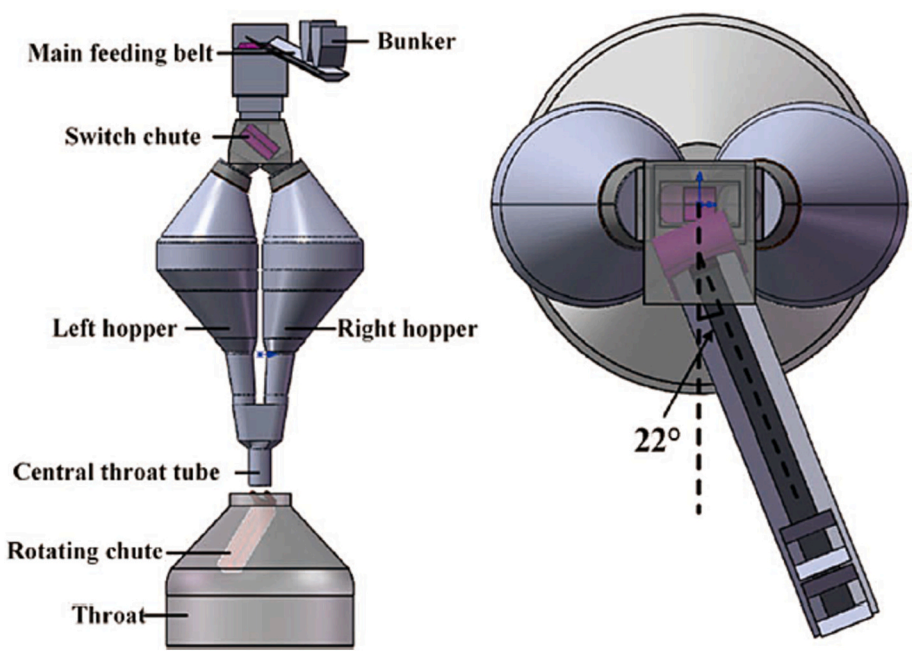

Fig. 13. Layout of a BLT-charging system with parallel hoppers (left) and the angle between the centerline of the main feeding belt and the symmetry plane of two parallel hoppers; image adopted from [93].

circumferential imbalance of the burden mass in the throat. The burden does not flow through the center of the funnel but rather concentrates either at the right or left side, depending on which hopper is being discharged. Narita et al. [90] studied whether the funnel outlet design can be adjusted to produce a more centered burden flow through the funnel outlet, with the aim of mitigating the circumferential imbalance. They considered two adjustments of the funnel outlet, as shown in Fig. 15a: a smaller outlet diameter compared to the original design, and a tapered outlet rather than a straight pipe. The authors found that particles easily de-center when the original funnel outlet design is used, and that the burden's falling point trajectory depends on the chute tilting angle. Using a smaller funnel outlet was not effective in reducing the imbalance; instead, the burden accumulated inside the funnel. On the other hand, the tapered chute outlet created a "push-back" effect on

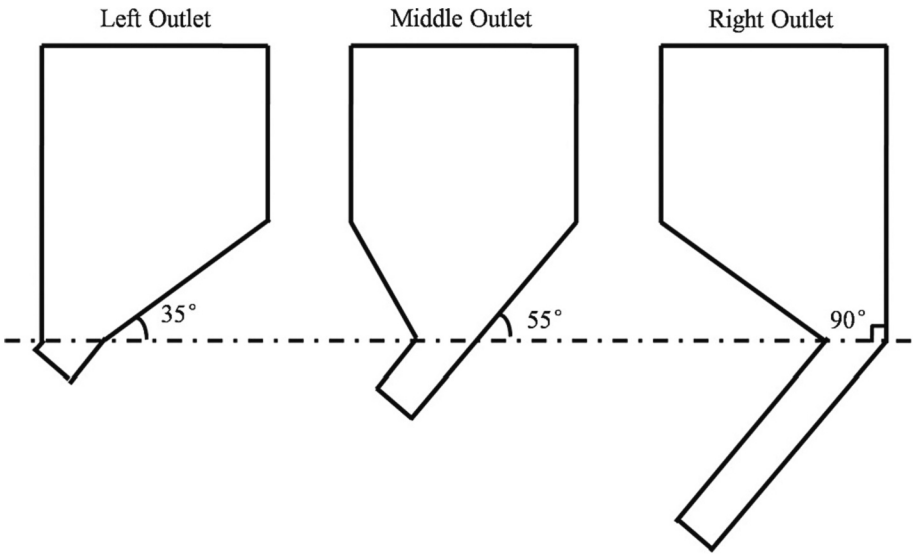

Fig. 14. Different hopper designs used for analyzing the effect of hopper outlet slope on size segregation during hopper discharge, from left to right: left outlet, center outlet and right outlet; images adopted from [35].

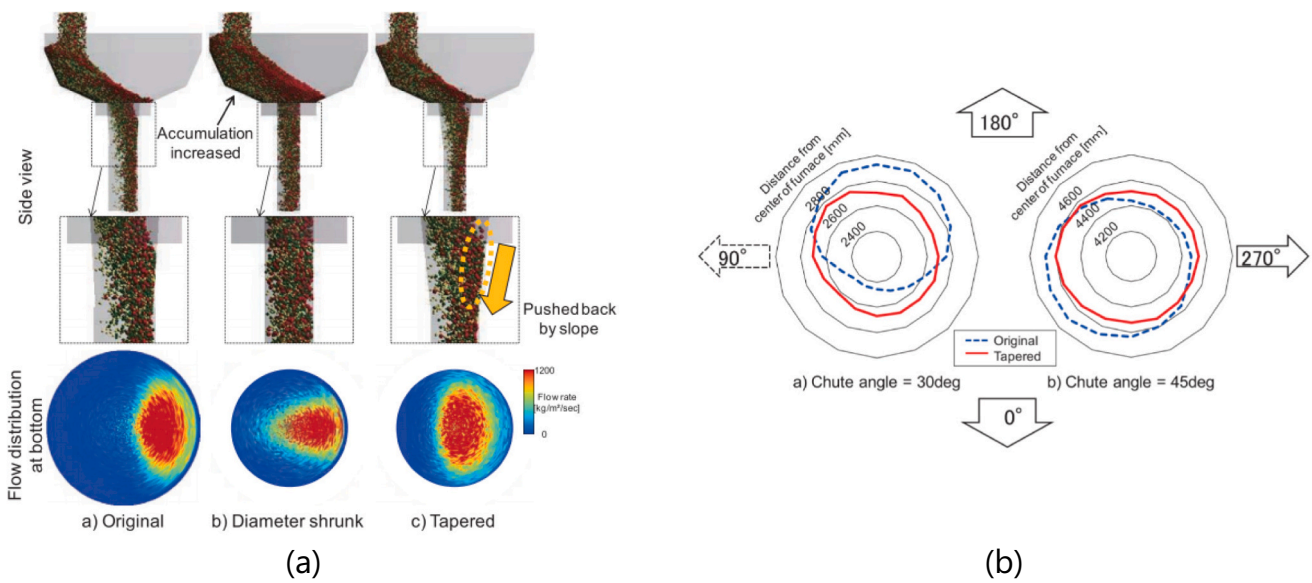

Fig. 15. Effect of funnel outlet shape on: (a) Burden de-centering in the funnel and (b) circumferential particle trajectory; images adopted from [90].

the de-centered burden stream and, as shown in Fig. 15b, resulted in a more even circumferential distribution at different chute titling angles. Chen et al. [92] also investigated the effect of funnel outlet diameter and found that increasing the outlet diameter had an adverse effect on the circumferential mass imbalance. Compared with the findings of Narita et al. [90], we conclude that there exists an optimal outlet diameter for which there is no accumulation of burden in the Y-tube while the circumferential mass imbalance is minimal. This can be a topic of investigation in future studies.

2.3.3. Rotating chute

- Tilting angle, length and rotational speed

The chute's tilting angle, rotational speed and length all affect the magnitude of centrifugal and Coriolis forces acting on the material as it flows through the chute. As the tilting angle and length increase, the particles' residence time on the chute becomes longer and therefore, the particles experience centrifugal and Coriolis forces for longer times. Consequently, the material stream will tend to move along one side of the chute and, according to Hong et al. [47], this tendency increases with the chute angle and length. Fig. 16 illustrates how three performance indicators (stream width, thickness and main striking point or MSP) for characterizing the burden distribution during charging are defined. Kou et al. [45] and Hong et al. [47] studied the effect of, among other factors, the chute angle, speed and length on these performance indicators. Despite using the same system, particles, particle sizes, interaction parameters, mass flow rate, amount of material and definitions of performance indicators, Hong et al. reported that the stream width increases with the chute angle, while Kou et al. reported the opposite. Their results on the effect of chute angle on stream thickness were also not in agreement, while they both stated that the MSP increases with the tilting angle. Zhang et al. [38] stated that the stream width increases with the chute angle, thereby forming a heap with a

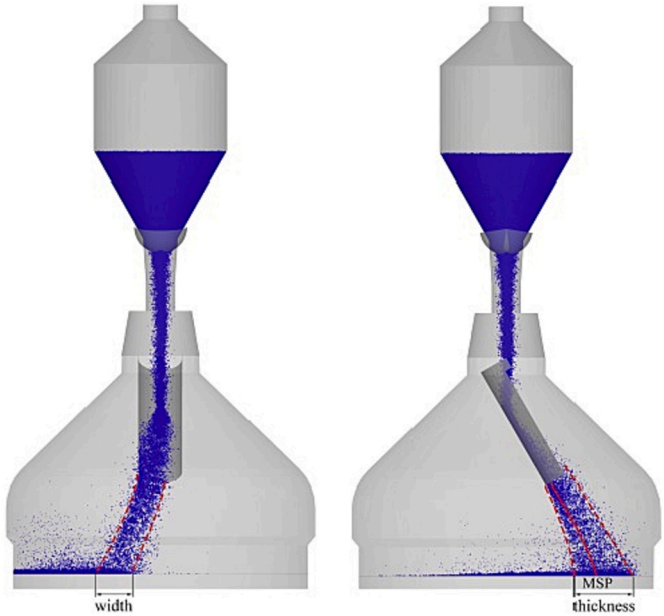

Fig. 16. Definition of stream width, thickness and main striking point above the burden surface; image adopted from [45].

lower peak compared to a heap formed at small tilting angles. They state that large particles can easily roll off this relatively flat heap towards the center of the furnace. As the centrifugal and Coriolis forces increase with the rotational speed, the material also tends to collect at one side of the chute as the rotational speed increases. Also, the particles at the chute outlet have a higher tangential velocity as the speed increases. Kou et al. [46] found that a high tangential velocity of ores is favorable with respect to coke collapse, since the particles tend to move in tangential direction rather than in radial direction, and therefore the amount of radial coke collapse is reduced for higher rotational speeds.

- Cross-section and surface profile

The chute's cross-section shape has a noticeable effect on the motion of particles in the chute and the burden distribution in the furnace throat. Kou et al. [45] considered semicircle, trapezoid, and rectangle shaped chutes and found that particles are more "spread out" at the outlet of a rectangular chute when compared to the other two shapes since there is more available space for particles to roll around on the flat rectangular surface. They also found that the MSP is larger for semi-circular chutes and successively smaller for trapezoidal and rectangular chutes, and the difference in MSP becomes larger for higher chute angles. Since their study involved a mixture of pellet, sinter and lump ore, they also investigated the effect of chute shape on size segregation in the furnace throat at different chute angles. The authors found that semi-circular chutes produce a more uniform radial size distribution at low and middle chute angles while the same is true for trapezoidal chutes at large angles. Xu et al. [94] performed a similar study for coke charging, focusing on both radial and circumferential distribution when using a semicircular and rectangular chute. They concluded that a rectangular chute outperforms a semi-circular chute in different respects when considering the circumferential distribution. First of all, a rectangular chute provides an almost perfectly circular falling point distribution, unlike the semicircular chute (cf. Fig. 17). Also, the charged volume distribution is more uniform. However, when it comes to segregation, the semicircular chute provided a slightly lower deviation of burden average diameter distribution.

Not only the cross-section shape, but also the design of the chute surface area plays an important role in burden distribution. Holmes et al. [97] considered three designs currently in use by Tata Steel (cf. Fig. 18): (i) straight, smooth design (not shown in the figure), (ii) rock-box design, with several open compartments along the chute length, and (iii) hybrid design, which is a combination of the first two. They scrutinized the performance of different chute designs in terms of mass distribution symmetry after charging coke and pellets. Fig. 19 shows an incomplete ring near the walls for all cases, which is the effect of an underdeveloped flow for a few seconds after starting the charging. Since material tends to accumulate in the rock-box compartments, the burden flows out at a later time for the rock-box chute; therefore, the tail of the outer ring is shorter for the rock-box chute when compared to the other chutes. Also, the rock-box chute appears to provide more scattering of the burden. These two aspects combined result in a better outer ring compared to the other chute designs. Looking at the distribution of the remaining rings, Fig. 19 also shows that the rock-box design produces a more uniform, symmetrical mass distribution for both coke and pellets when compared to the other designs. The authors stated that the instantaneous chute angle adjustment during ring charging generally results in a sudden unsteady burden delivery until the flow on the chute re-adjusts to the new angle. The authors found that the rock box design least suffers from this effect due to the its material accumulation capacity. These results indicate that the burden matrix needs to be carefully tuned based on the shape of the chute. Xu et al. [98] performed burden distribution measurements in a full-scale furnace to compare the performance of a smooth, semicircular chute to that of a plated,

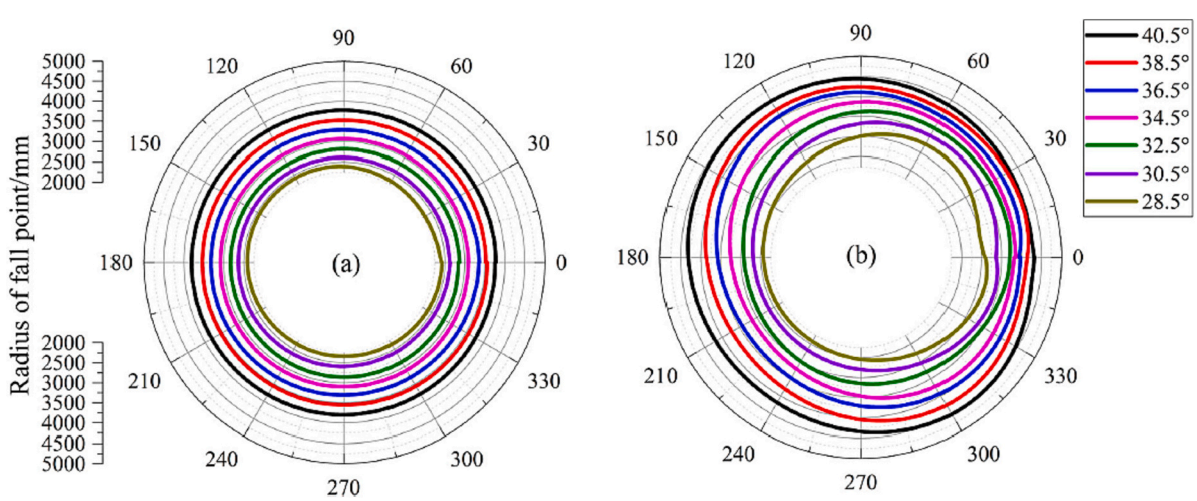

Fig. 17. Burden falling points distribution at different tilting angles when using rectangular chute (left) and a semicircular chute (right); image adopted from [94].

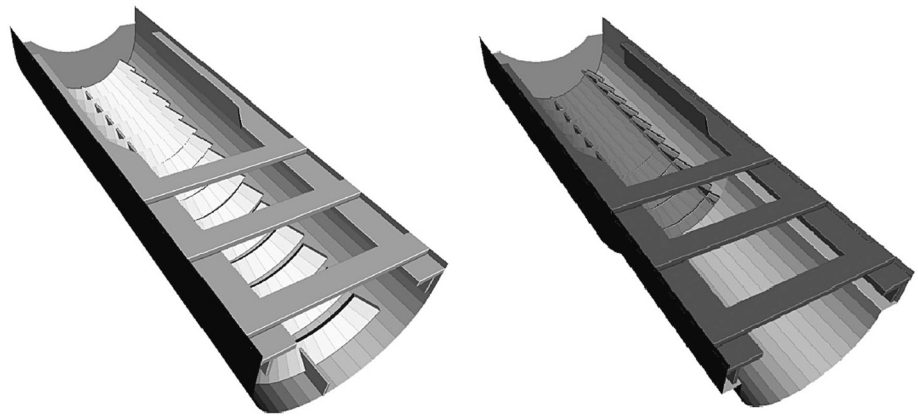

Fig. 18. Chutes with different surface designs: rock-box (left) and hybrid design (right); image adopted from [97].

rectangular chute at different chute angles (cf. Fig. 20). Their results showed that the rectangular chute produced a more uniform circumferential falling point distribution and smaller inner and outer falling point radii than the semicircular chute. These results are in line with DEM results from their earlier work [94].

- Outlet damper

Mio et al. [41] investigated the effect of using a damper on the segregation behavior of sinter particles as they are discharged from a stationary chute. Initially, it was observed that the burden at the chute was clearly segregated. Due to the percolation mechanism, small particles were concentrated at the bottom (along the chute surface) while large particles were at the top. By adding a damper at the chute outlet (cf. Fig. 21), the burden stream was agitated which resulted in local mixing of the smaller and larger particles. and segregation was reduced since the damper caused particle mixing at the outlet. In their study, Kou et al. [45] also briefly discussed the possibility of using a damper. They mentioned that the damper should be designed based on the shape of the chute: for semicircular chutes, the damper should produce a more uniform radial size distribution while it should produce a more aggregated stream for rectangular chutes. However, specific information on how these requirements should be translated to a damper design was not provided.

- Starting angle

The charging sequence generally starts at the outer ring so that burden is deposited near the walls (large tilting angle) first and at the center (small tilting angle) last. Zhou et al. [57] investigated the effect of reverse charging (i.e. starting at the center and ending at the walls) of ores on coke collapse. They found that the amount of coke collapse is nearly halved when ores are first charged in the center, since the displacement of coke particles is much less in the center and the material accumulation after charging the first rings prevents coke collapse towards the center when charging the outer rings. They also investigated the effect of central coke charging, i.e., increasing the amount of coke layer thickness in the center. Fig. 22 shows that the coke layer maintains its thickness almost perfectly when central coke charging is applied. According to the authors, the amount of coke collapse was almost 1/3 of the case without central coke charging since there is less available space for coke displacement towards the center.

2.4. Discussion

In this section we showed that there has been a significant amount of research focusing on blast furnace burden distribution and control using DEM models in recent years. Table 1 summarizes all DEM literature in which blast furnace materials have been modelled for studying different aspects of burden distribution. We have shown that the term “burden distribution” in the context of permeability refers to size, component and mass distribution, and that these are affected by segregation, degradation and the deviation phenomenon.

Our review has shown that segregation occurring in the charging apparatus and the top layers in the throat have mostly been studied, while segregation during descent has been considered to a much lesser extent. Also, size segregation has been the main focus to date, and segregation of multi-component burden mixtures which differ in size, shape and density has not yet been considered. While there is an overwhelming amount of literature emphasizing the need to study the occurrence of segregation and its effect on furnace performance, there is a lack of research focusing on the effect of segregation on permeability. Besides segregation, the deviation phenomenon has also received ample attention. Degradation on the other hand has only been considered in limited detail, with the main focus being the determination of stress distributions to predict whether particle degradation is expected to occur during charging and descent. Although it is currently possible to model breakage phenomena using some DEM software packages, this has not yet been done in the blast furnace context. Based on the current state-of the-art, we believe that modelling breakage phenomena is not yet considered a priority due to computational limitations.

The majority of work is focused on modelling the charging system, or parts thereof. This is understandable since there are little means for controlling the material distribution after the burden has been charged into the furnace. Although the charging system consists of numerous handling steps with raw materials being transported through a series of equipment from the stock-house up until the chute, the charging process is often simplified by considering the holding bins/hoppers as the starting point of material delivery, followed by a funnel and finally, the chute. Given the size of an industrial system, simulating the entire charging process starting at the stock-house would require huge amounts of computational power and this is expected to be investigated in the future.

A number of models have been used for investigating how the burden distribution is enhanced by adjusting design and operational conditions. How the bed permeability can be improved is not addressed in detail and should be the subject of future work. At the beginning of this section, we stated that it is often more practical to investigate how operational conditions can be adjusted for process optimization, rather than equipment design. Remarkably, only very few studies have focused on this aspect. Also, the case studies are mostly simplified since either a small part of the furnace is modelled, or not all burden components are included. Future case studies should aim to use models involving all burden components, thereby representing more realistic furnace operation.

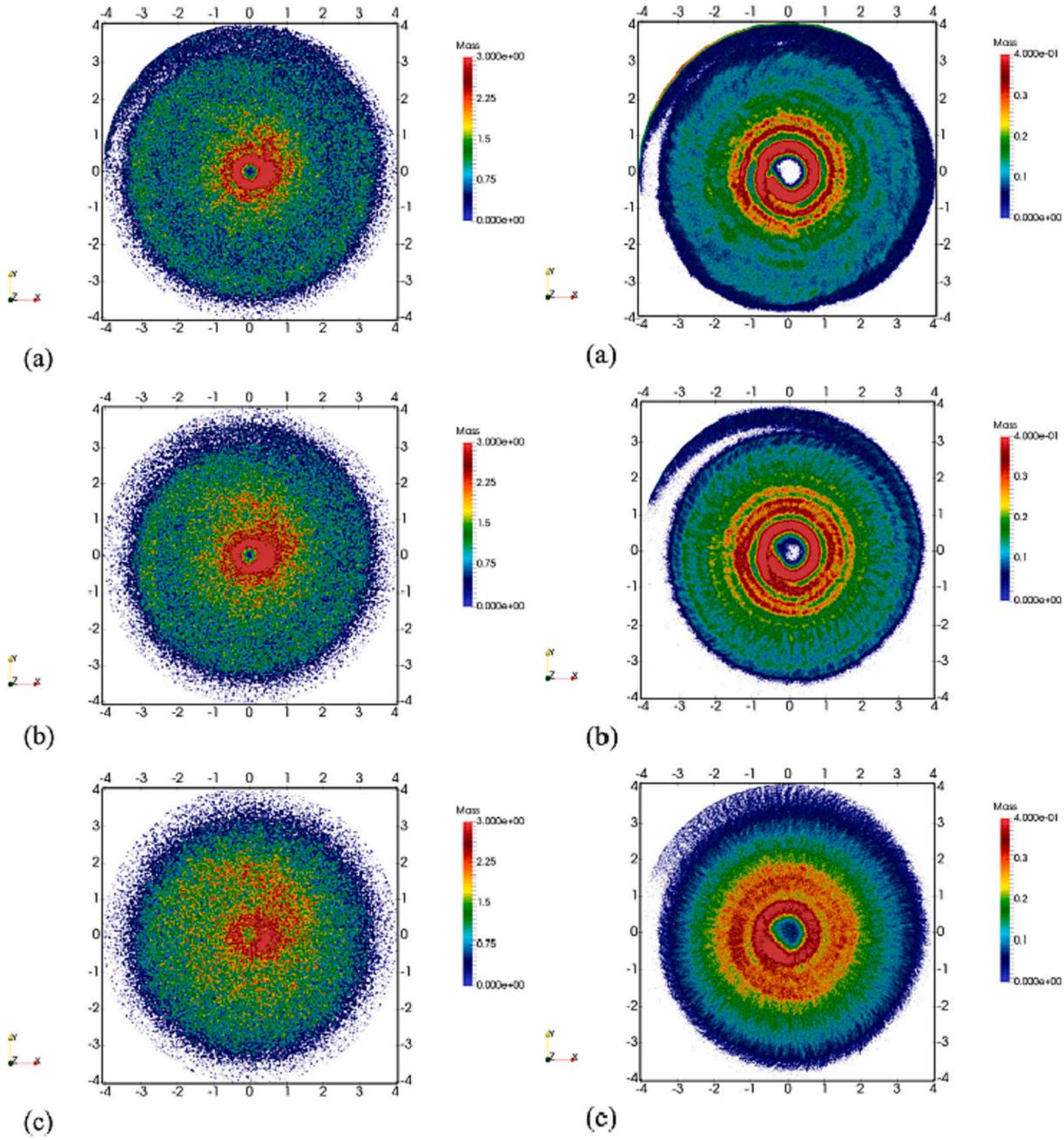

Fig. 19. Total mass delivery when using different chute designs for coke (left) and pellets (right): (a) straight chute, (b) hybrid chute and (c) rock box; images adopted from [97].

3. DEM modelling of blast furnace burden distribution and permeability

3.1. A brief note on model development

Developing a DEM model for large-scale granular flow applications is challenging from two perspectives:

- The model must be feasible: In DEM, numerical integration is performed to calculate the interactions of all particles with their surroundings at each time step. Hence, the computational efficiency increases as the number of particles decreases and as the time step increases. Since the time step in turn depends on the smallest particle size and certain material properties, there is often a need to use simplified particle sizes and fictitious properties to speed up simulations.
- The model must be reliable: As with any model, its input parameters must be selected such that the model's outputs reflect the actual flow behavior. The model inputs can be divided into three main categories: (i) morphological parameters, such as particle size and shape distributions; (ii) intrinsic material properties such as the density, Poisson's ratio and Young's modulus; (iii) interaction parameters such as restitution and friction coefficients, which generally depend on a combination of factors such as material type, particle shape and surface roughness. In theory, the parameters from the second and third category can be measured –albeit with great difficulty in some cases– and directly included as inputs for a DEM model. However, as the model becomes more idealized due to simplifications, the inputs are no longer reflective of actual measured properties and model

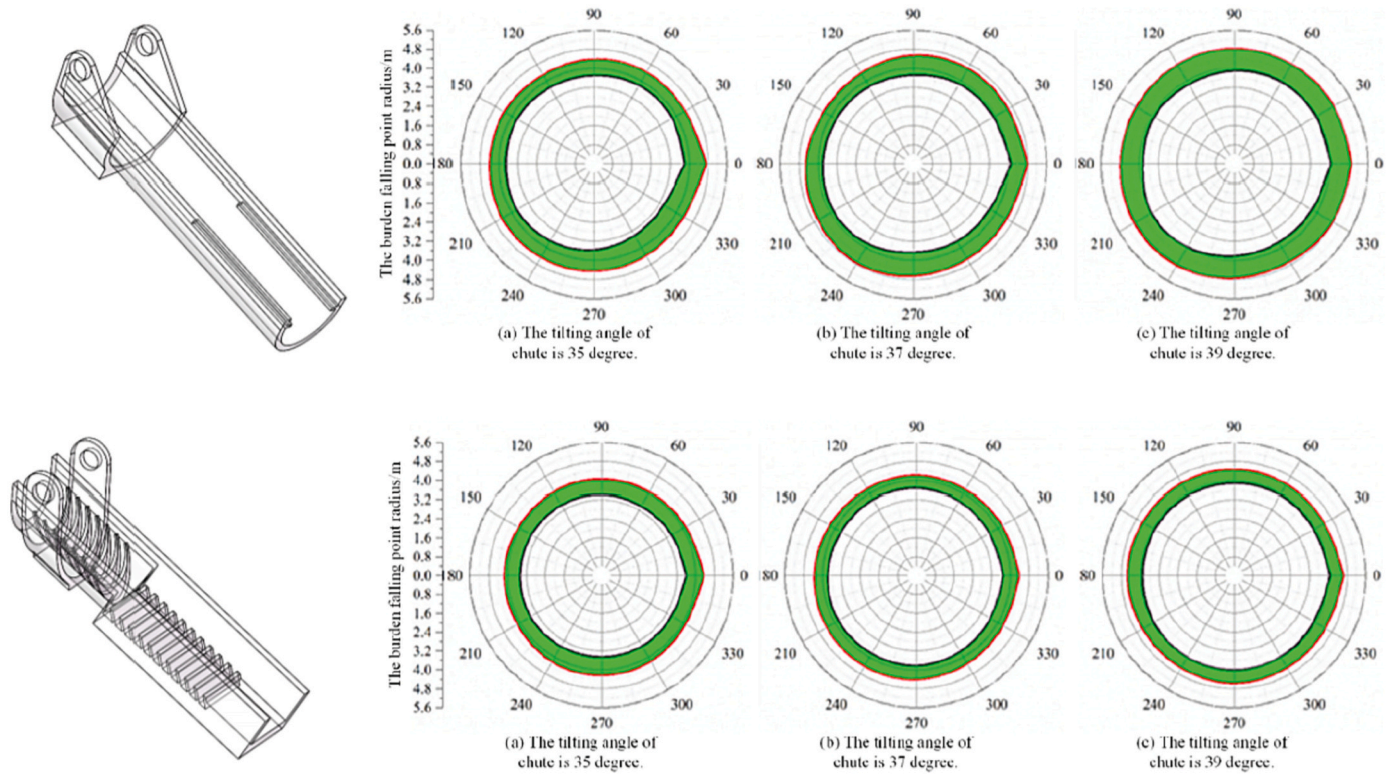

Fig. 20. Chutes with different cross-section profiles and surface design (left) and the corresponding burden falling point radius distributions; image adopted from [97].

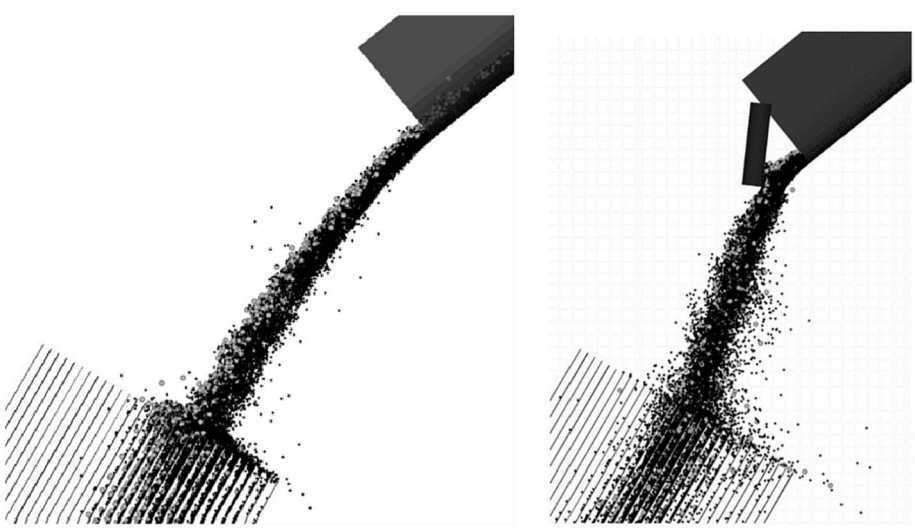

Fig. 21. Snapshots of particle discharging behavior at a chute inclination angle of 45° for (a) no damper and (b) using a damper at the chute outlet; images adopted from [41].

calibration is required. In this way, DEM model parameters are effectively parameters which must be carefully "tuned" such that the developed model reflects the true material behavior observed in experiments.

The conflict between model feasibility and reliability requires trade-offs between computational efficiency and accuracy to be made. This is an ongoing challenge in DEM model development and there are several publications focusing on different aspects of this topic [99–103]. We propose the following step-wise model development procedure based on our own insights and general recommendations from DEM modelers in literature:

1. Selection of a contact model: As many different force calculation models exist in DEM, the first step in model development is selecting a suitable model for the application and identifying the model inputs.
2. Sensitivity analyses for model inputs: The model's inputs can be determined through measurement and/or calibration. The calibration process involves changing input values iteratively in simulations until one (or more) targeted experimental response(s) is (are) met [100]. To avoid an unnecessary lengthy calibration process of many parameters, it is often more realistic to measure certain parameter

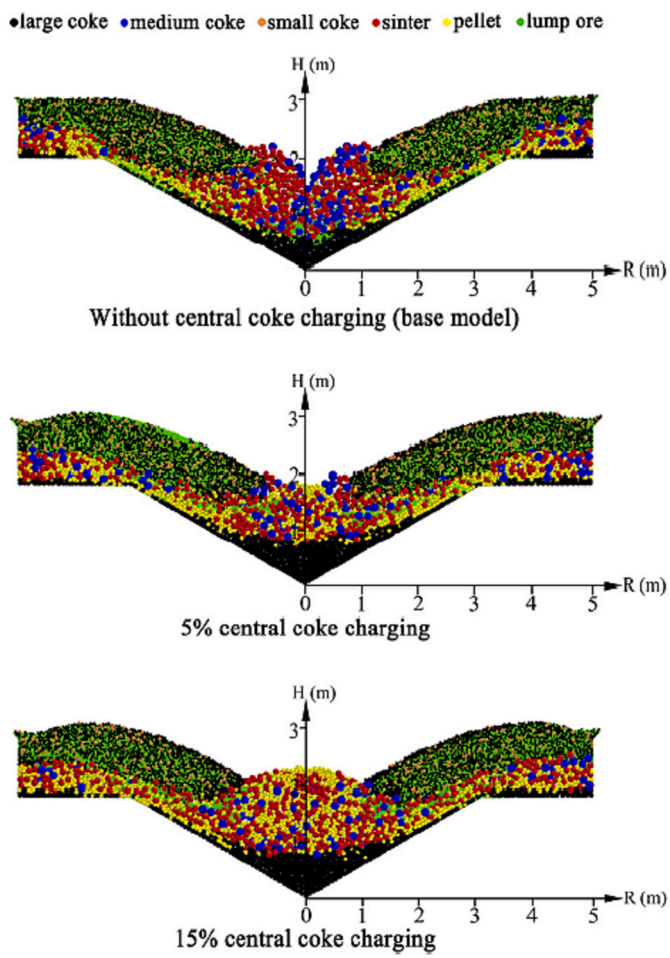

Fig. 22. Burden profiles after collapse for different amounts of central coke charging; image adopted from [57].

values, or obtain them from literature, and subsequently perform calibration for only the parameters which are most important for the process being modelled. Hence, before starting calibration, it is recommended to perform sensitivity analyses to identify which parameters must be carefully calibrated.

3. Determination of model inputs: During the calibration process, it is important to select experiments with calibration targets which are significantly affected by the parameters to be calibrated. Also, since it is known that multiple input parameters can affect a single calibration target, multiple targets are generally required to determine a unique solution for the parameters [101,102]. Finally, the flow conditions which are expected in the actual application should be reflected in the experiment. Finding the values of the inputs is traditionally performed in a trial-and-error fashion where input parameters are changed independently in simulations and the virtual calibration target values are compared to experiments. This method is usually inefficient, especially as the number of inputs increases [103], and rarely results in an optimal set of parameter values. More recent DEM studies incorporate optimization methods to address this shortcoming [104–110].
4. Verification and validation: After obtaining a solution to the parameter set, a verification step is required to ensure that the parameter values are remain valid for other experiments than the one(s) used for calibration. Once again, one must ensure that the selected test is sensitive to changes in the calibrated parameter values [100]. The final step involves using the calibrated model to simulate the actual (industrial) process, and comparing simulation data to operational data

Table 1
Summary of literature using DEM to model blast furnace material behavior.

Ref.	Materials	System	Focus
Segregation			
Mio et al., 2008 [41]	S	Hopper-chute	Size segregation during chute flow
Mio et al., 2009 [42]	S, C	BLT charging system[a] + furnace top	Size segregation during charging, coke collapse
Mio et al., 2010 [119]	S, C	BT charging system	Size segregation during furnace charging
Yu & Saxén, 2010 [111]	P	Hopper	Size segregation during hopper discharge
Yu et al., 2011 [120]	P, C	Furnace shaft (simplified)	Size segregation during burden descent
Mio et al., 2012 [37]	S, C	Delivery system + BLT charging system[b] + furnace top	Size segregation during furnace charging
Yu et al., 2012 [43]	P, C		
Yu et al., 2013 [51]	P, C	BLT charging system[a] + furnace top	Material behavior during charging, burden profiles
Wu et al., 2013 [35]	S	P-W hopper	Size segregation during hopper charging and discharging
Yu et al., 2014 [115]	C	P-W hopper	Size segregation during hopper charging and discharging
Zhang et al., 2014 [38]	O, C	BLT charging system[b] + furnace top	Segregation in BLT system
Liu et al., 2015 [116]	C	BLT charging system[a] + furnace top	Material behavior during furnace charging
Mitra & Saxén, 2015 [55]	P, C	BLT charging system[b] + furnace top	Coke-push effect
Mitra & Saxén, 2016 [56]	P, C	BLT charging system[b] + furnace top	Mixed-layer formation + coke-push effect
Schott et al., 2016 [122]	P, S, C	Conical hopper	Size segregation during heap formation
Xu et al., 2017 [36]	C	BLT charging system[b] + furnace top	Size segregation during furnace charging
Kou et al., 2018 [46]	S, C	BLT charging system + furnace top	Coke-push
Dianyu et al., 2019 [182]	S, O	Blast furnace shaft (without charging system)	Mixed layer formation and its effects on porosity distribution
Govender et al., 2019 [124]	S, C	BLT charging system[a] + furnace top	Burden topography and percolation
Mio et al., 2019 [114]	S	Hopper-chute	Particle charging trajectories after chute discharge
Xu et al., 2019 [94]	C	BLT charging system[b] + furnace top	Size segregation during charging
Chibwe et al., 2020 [125]	P, S	BLT charging system	Mixing and segregation within BLT charging system
Hong et al., 2020 [47]	P, S, L	BLT charging system + furnace top	Iron ore component segregation
Mio et al., 2020 [33]	S, C	BLT charging system + furnace top	Size segregation during and after furnace charging
Xu et al., 2020 [95]	C	Delivery system + BLT charging system[c] + furnace top	Size segregation during furnace charging
Wei et al., 2021 [49]	S, C	BLT charging system + furnace top	Porosity distributions in furnace top during and after charging

(*continued on next page*)

Table 1 (*continued*)

Ref.	Materials	System	Focus
Zhang et al., 2021 [34]	C	P-W hopper	Size segregation during hopper charging and discharging
Zhou et al., 2021 [57]	P, S, L, C	BLT charging system[a] + furnace top	Coke-push
Li et al., 2022 [50]	S, C	BLT charging system[a] + furnace top	Radial size segregation and mixed-layer formation
Degradation			
Ueda et al., 2010 [160]	O, C	Blast furnace shaft	Burden distribution and material stresses during burden descent
Burden distribution			
Park et al., 2011 [184]	O, C	BLT charging system[b] + furnace top	Burden distribution
Narita et al., 2017 [90]	O, C	BLT charging system	Circumferential imbalance
Holmes et al., 2018 [97,123]	P, S, C	BLT charging system[a] + furnace top	Circumferential imbalance
Kou et al., 2019 [45]	P, S, L	BLT charging system + furnace top	Burden distribution in the throat
Sun et al., 2019 [91]	O	BLT charging system[b] + furnace top	Particle velocities during chute flow, circumferential imbalance
Xu et al., 2019 [39]	P, S, L	BLT charging system + furnace top	Uniformity of burden distribution
Chakrabarty et al., 2021 [117]	C	Chute + furnace top	Burden distribution
Degrassi et al., 2021 [126]	P, S / C	Belt + hopper	Burden distribution in hopper
Zhou et al., 2021 [113]	P	BLT charging system[a] + furnace top	Burden distribution
Chen et al., 2022 [17]	P, S	BLT charging system[b] + furnace top	Mass flows and velocities in charging system, circumferential burden uniformity in throat
Di et al., 2022 [185]	O, C	BLT charging system[a] + furnace top	Burden surface shape and burden distribution in the throat
Holzinger & Schatzl, 2022 [118]	C	BLT charging system[b] + furnace top	Circumferential imbalance
Model calibration			
Liu et al., 2015 [116]	C		
Schott et al., 2016 [122]	P, S, C		
Wei et al., 2020 [167]	P, S, C		
Bester et al., 2021 [175]	C		
Degrassi et al., 2021 [126]	P, S, C		
Tripathi et al., 2021 [112]	P, S		
Chakrabarty et al., 2022 [145]	P, S		
Chen et al., 2022 [92]	P, S		

Legend: Materials: P = pellet; S = sinter; L = lump ore; O = ores, used when it is unclear which type of ore; C = coke; n.s. = not specified. System: BLT = bell-less type; BT = bell-type.

[a] Single/serial-type hopper system.

[b] Parallel-type hopper system.

This section reviews the methods which have been applied in blast furnace literature and the presented framework will serve as a guide for our review. Table 2 summarizes some important aspects of these studies which will be discussed throughout this section. Note that since we will focus on modelling details, the studies from Table 1 in which the materials were not clearly specified or distinguished from each other (for example where "ore" was used, rather than specifying the type of ore) are not included in Table 2 and are excluded from the discussion in this section.

3.2. Contact models

So far, the majority of blast furnace processes have been modelled using the non-linear Hertz-Mindlin no-slip model [127] and, to a lesser extent, the Kelvin-Voigt [128] model for normal and tangential interaction forces between particles. A DEM model based on these formulations requires the following inputs:

- Particle size distribution (PSD)
- Particle shape distribution, when non-spherical particles are used
- Particle density (ρ_p)
- Young's (or shear) modulus (E or G) for particle and equipment
- Poisson's ratio (ϑ) for particle(s) and equipment
- Sliding friction coefficient between particles ($\mu_{s_{pp}}$) and between particles and equipment ($\mu_{s_{pw}}$)
- Restitution coefficient between particles (ε_{pp}) and between particles and equipment (ε_{pw})
- Numerical time step Δt. For the Hertz-Mindlin model, the time step depends on the smallest particle's radius (R_{min}) and material properties according to

$$\Delta t = 0.1\ldots0.2\,\pi R_{min}\frac{\sqrt{\frac{\rho_p}{G}}}{(016319+0.8766)} \tag{1}$$

Non-spherical particles are often modelled as spheres in DEM to reduce computational effort, as will be discussed further in Section 3.3.1. In such cases, a rolling resistance model is generally applied to mimic the bulk friction of the non-spherical counterpart. The input parameters for a rolling resistance model are the rolling friction coefficient between particles ($\mu_{r_{pp}}$) and between particles and equipment ($\mu_{r_{pw}}$). Blast furnace modelers have used different rolling resistance models based on two main methods. The first and most common method involves a single (uniform) rolling friction coefficient between all particles of a material component. Ai et al. [129] summarized four classes of rolling friction models which are commonly used in DEM studies based on this approach: constant resistive torque (Model A), viscous resistive torque (Model B), elastic–plastic spring dashpot torque (Model C) and contact-independent resistive torque (Model D). Rolling models A and C are most often used in DEM simulations [130], although rolling model C performs better than model A in static situations, where model discontinuities may occur [129]. Another approach, originally suggested by Mio et al. [41] for modelling sinter behavior, involves a distributed rolling friction coefficient. It was argued that since sinter particles have many different shapes, a unique friction coefficient should be determined to account for each shape.

Table 2 shows that the distributed rolling friction (DRF) approach has only been utilized within the research group of Mio et al. and almost all remaining studies used rolling model A. The choice of rolling model used is obscure, which is interesting given the fact that Ai et al. [129] pointed out the difference in performance of the models. Moreover, the fact that model C is only encountered in the studies of Wei et al. [49] and Holzinger & Schatzl [118] while it is superior to model A is remarkable. A possible explanation for this overwhelming use of model A is its

Table 2
Details of modelling methods applied in previous studies. Legend: Model: specifies the contact model (CM) and rolling model (RM) used; Shape: indicates whether the material component was modelled using "spherical" or "non-spherical" particles, respectively, and the number of non-spherical shapes used to represent a material component is given in parentheses; Size: The first number in the size column denotes how many different sizes were used to model the material component, while the second (parenthesized) number indicates the factor with which particles were enlarged in simulations, when compared to experiments; Computational domain: specifies the scale of the simulated system relative to the true system and the type of computational domain, where Type I = full 3D model, Type II = slot model, Type III = sector model.

Ref.	Software	Model	Pellet		Sinter		Lump ore		Coke		Comp. domain	
		CM / RM	Shape (no.)	Sizes (UF)	Shape (no.)	Sizes (UF)	Shape (no.)	Sizes (UF)	Shape (no.)	Sizes (UF)	Scale	Type
Yu & Saxén [111]	EDEM	HMns / A	SP	3+	–	–	–	–	–	–	n.s.	I
Yu & Saxén [43]	n.s.	HMns / A	SP	3	–	–	–	–	–	–	1:10	I
Tripathi et al. [112]	EDEM	HMns / A	SP	PSD	–	–	–	–	–	–	N/A	N?A
Zhou et al. [113]	EDEM	HMns / A	SP	1	–	–	–	–	–	–	1;*	I
Mio et al. [41]	n.s.	Voigt / DRF	–	–	SP	3	–	–	–	–	1:3	I
Wu et al. [35]	n.s.	HMns / A	–	–	SP	3 (n.s.)	–	–	–	–	1:10	–
Mio et al. [114]	n.s.	Voigt / DRF	–	–	SP	8	–	–	–	–	1:3	I
Tripathi et al. [112]	EDEM	HMns / A	–	–	SP	PSD	–	–	–	–	N/A	N/A
Yu et al. [115]	EDEM	HMns / A	–	–	–	–	–	–	NSP (1)	3	n.s.	III
Xu et al. [36]	n.s.	n.s.	–	–	–	–	–	–	SP	PSD (1.5)	1:1	I
Xu et al. [94]	n.s.	n.s.	–	–	–	–	–	–	SP	PSD (1.5)	1:1	I
Liu et al. [116]	n.s.	HMns / A	–	–	–	–	–	–	SP	3	n.s.	I
Narita et al. [90]	n.s.	Voigt / n.s.	–	–	–	–	–	–	SP	3	n.s.	I
Xu et al. [95]	n.s.	n.s.	–	–	–	–	–	–	SP	PSD	1:1	I
Chakrabarty et al. [117]	EDEM	HMns / A	–	–	–	–	–	–	NSP (5)	PSD	1:1	I
Zhang et al. [34]	n.s.	HMns / A	–	–	–	–	–	–	SP	2	n.s.	II
Holzinger & Schatzl [118]	LIGGGHTS	HMns / C	–	–	–	–	–	–	SP	15	n.s.	I
Mio et al. [42]	n.s.	Voigt / DRF	–	–	SP	5	–	–	SP	4	n.s.	I
Mio et al. [119]	n.s.	Voigt / DRF	–	–	SP	5 (3.0)	–	–	–	–	1:1	I
Yu et al. [70,120]	EDEM	HMns / A	SP	1 (0.25)	–	–	–	–	SP	3 (0.25)	1:10	I
Mio et al. [37]	n.s.	Voigt / DRF	–	–	SP	5	–	–	SP	3	1:3	I
Yu & Saxén [70]	EDEM	HMns / A	SP	3	–	–	–	–	NSP (6)	3	n.s.	N/A
Yu & Saxén [51]	EDEM	HMns / A	SP	2	–	–	–	–	NSP (1)	6	1:10	III
Mitra & Saxén [55]	EDEM	HMns / A	SP	1	–	–	–	–	NSP (5)	3	1:10	III
Yang et al. [121]	n.s.	HMns / A	SP	1	–	–	–	–	SP	1	1:32	II/III
Mitra & Saxén [56]	EDEM	HMns / A	SP	1	–	–	–	–	NSP (5)	3	1:10	III
Schott et al. [122]	EDEM	HMns / n.s.	SP	m	NSP (1)	m	–	–	NSP (1)	m	n.s	I
Narita et al. [74]	EDEM	Voigt / n.s.	–	–	–	–	–	–	SP	3	n.s.	I
Holmes et al. [97,123]	n.s.	n.s.	SP	PSD	SP	PSD	–	–	SP	PSD	1:1	I
Kou et al. [46]	in-house code	HMns / A	–	–	SP	3 (2.0)	–	–	SP	3 (2.0)	1:1	I
Govender et al. [124]	LIGGGHTS	Voigt / n.s.	–	–	NSP	1 (0.05)	NSP	1 (0.05)	–	–	1:20	I
Kou et al. [45]	n.s.	HMns / A	SP	1 (2.0)	SP	1 (2.0)	SP	1 (2.0)	–	–	1:1	I
Xu et al. [39]	n.s.	HMns / A	SP	PSD	SP	PSD	SP	PSD	–	–	1:1	I
Chibwe et al. [125]	LIGGGHTS	HMns / A	SP	1 (2.5)	SP	2 (2.5)	–	–	–	–	1:5.8	I
Hong et al. [47]	n.s.	HMns / A	SP	1 (2.0)	SP	1 (2.0)	SP	1 (2.0)	–	–	1:1	I
Mio, 2020 [33]	n.s.	Voigt / DRF	–	–	SP	8	–	–	SP	5	1:3	I
Degrassi et al. [126]	RockyDEM	HMns / A	SP	PSD	SP	PSD	–	–	–	–	1:1	I
Wei et al. [49]	LIGGGHTS	HMns / C	–	–	SP	3	–	–	SP	3	1:10	I/II
Zhou et al. [57]	n.s.	HMns / A	SP	1 (2.0)	SP	1 (2.0)	SP	1 (2.0)	SP	3 (2.0)	1:1	I
Chen et al. [92]	EDEM	HMns / A	SP	3 (2.0)	NSP (3)	4 (2.0)	–	–	–	–	1:1	I
Li et al., [50]	n.s.	HMns / A	–	–	SP	1	–	–	SP	1	1:1	I

widespread implementation in different software packages at the time of execution. For example in EDEM, model C was made available only recently (version 2021.2) as a standard rolling model. However, we cannot investigate this further as the majority of the studies listed in Table 2 do not state which software package was used.

3.3. Sensitivity analyses for model input parameters

Sensitivity analyses provide an indication of which input parameters have the biggest impact on the simulation results. These analyses are useful for several reasons. As mentioned previously, one reason is for determining which set of input parameters must be carefully calibrated for a specific application. Also, as blast furnace studies are being

performed all around the world with raw materials which may differ in material properties, sensitivity analyses elucidate whether region-dependent custom modelling is required. Finally, it is useful to know whether adjusting certain inputs to speed up simulations still provides accurate results. In order to get insight into these aspects, we review the results of different studies focusing on such analyses in this section.

3.3.1. Effect of morphology

The morphological features of a granular material can be simplified in DEM simulations for computational efficiency. For example, modelling particles as spheres in combination with rolling resistance [99,130] results in faster simulations when compared to non-spherical particle approximations [131] such as ellipsoids, superquadrics, polyhedrons and clumps (also referred to as clusters, composite spheres or multi-spheres). The simulated flow behavior of irregularly shaped particles can be replicated to some degree by applying rolling resistance to the spherical particles. However, the packing behavior of a non-spherical assembly is different from a non-spherical assembly where interlocking of particles generally allows a higher maximum packing density to be achieved [131,132]. Hence, the particle shapes which are used to model burden distribution must be carefully considered. The true particle size distribution can also be simplified in simulations. Small particles are generally avoided since they prolong simulation in two ways: first, according to Eq. (1), the numerical time step becomes smaller as the particle size decreases and second, the number of particles required to model the flow increases as the particle size decreases. To increase computational efficiency, the general approach is to adjust particle-to-geometry size ratio such that particles are enlarged; this results in both a larger time step and a reduced number of particles. This can be done by either upscaling the particle size [133–135] or downscaling the geometry dimensions, or by applying a hybrid scaling approach in which both particle size and geometry dimensions are scaled using individual scaling factors [136,137]. When scaling the particle size, a distinction is made between coarse-graining and scalping [138]. The first method involves replacing a parcel of unscaled particles by a larger, coarse-grained particle, thereby reducing the number of particles required to simulate the process. In the second method, fines are neglected by "cutting off" the PSD at a certain particle size, which in essence comes down to coarse-graining only the fine particles below the cut-off size [138]. Another scaling technique often used is exact scaling, which involves using the same scaling factor for particles and geometry [139–141].

- Particle shape distribution

The literature review has shown that pellets are generally modelled as spherical particles due to their nearly spherical shape in reality. Sinter and coke have been modelled as both spherical and non-spherical particles (cf. Table 3) primarily using particle clumps, and using polyhedra in the study of Govender et al. [124]. Unlike pellets, coke and sinter particles do not closely resemble spheres and the spherical approximation method must be justified when used, since the particle shape affects important granular phenomena such as segregation and packing characteristics which determine the permeability. Some references state that the spherical approximation method provides suitable results when the goal is to model flowing behavior rather than packing behavior. Akashi

Table 3
Shape approximation methods used for modelling sinter and coke particles using DEM according to blast furnace literature. Images adopted from the corresponding citations.

Material	Non-spherical shape approximation method	Ref.	Illustration
Sinter	Clumped spheres	Schott et al. [133]	
		Chakrabarty et al. [145]	
		Chen et al. [17]	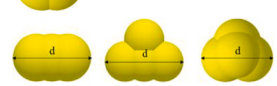
	Polyhedra	Govender et al. [124]	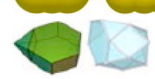
		Yu & Saxén [43]	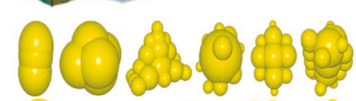
		Mitra & Saxén [55,56]	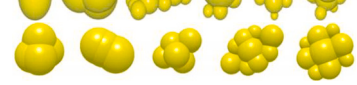
		Yu & Saxén [51]	
Coke	Clumped spheres	Schott et al. [122]	
		Chakrabarty et al. [117]	
		Bester et al. [175]	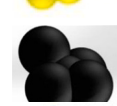
	Polyhedra	Govender et al. [124]	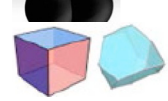

et al. [142] investigated the effect of particle shape on the flow and packing behavior of coal particles by using either spheres or clumped spheres in simulations and comparing the results to experiments. The spherical particles had a higher rolling friction coefficient than the clumped spheres; however, it is not clear how the values were determined. They observed that the effect of particle shape on flowing behavior (in terms of mean particle velocity and mean flowing angle) was insignificant, while the bulk density distributions in simulations using spherical particles did not correspond to experiments. Hence, they concluded that the particle shape plays an important role when modelling the packing structure. Mio et al. [114], in their study of sinter discharge from a chute, mentioned explicitly that they considered the spherical approximation method to be suitable because trajectories were being studied, rather than packing characteristics. When it comes to studies focusing on segregation, only Yu & Saxén [115] analyzed the effect of particle shape. They considered four different shapes (sphere, triangle, cylinder and hexahedron) for modelling size segregation during charging and discharging of a Paul-Wurth hopper in order to identify which shape showed the best agreement with experimental results. They found that the particle shape is insignificant during the charging process, while the spherical shape provided the best results during the discharging process. Therefore, they concluded that spherical particles are suitable for modelling size segregation of coke during hopper charging and discharging. Mitra & Saxén [55] studied the difference between using spherical and non-spherical coke particles when modelling the coke collapse phenomenon. It was shown that non-spherical particles performed better when considering the heap formation during coke charging. However, some aspects of the formed layers agreed equally well or even better to experimental results when using spherical particles.

It must be noted that the same rolling friction coefficient was applied to both spherical and non-spherical particles in the aforementioned studies. Hence, the models were not calibrated for each individual shape and the comparisons were therefore not objective. Wei et al. [143] studied the effect of particle shape (sphere, cone and cylinder) on the porosity distribution of a heap formed by hopper discharge after calibrating the model for each shape. Although these shapes did not resemble blast furnace material shapes, their study pointed out that particle shape plays an important role in the porosity distribution. They later studied packing behavior of pellet [144] and coke [49] in terms of porosity distribution, which is closely linked to permeability. They used spherical particles to model pellet and coke and in both cases and concluded that the porosity distribution obtained from simulations generally matched experimental results. It must be noted, however, that the match in the case of pellets was much better than in the case of coke. Interestingly, the authors attributed differences in results to "systematic errors" and "non-idealities in the experiment" and did not investigate whether non-spherical particles in the simulation would provide better results.

Clumps are formed by merging multiple overlapping spheres. The degree of overlap between mutual overlapping spheres and the size of each sphere can be chosen freely so that any arbitrary shape can be generated. While the computational cost increases as more and smaller spheres are used to form a clump, the shape approximation often becomes more accurate. Since actual coke and sinter particles are shape polydisperse [115], the main challenge is to select a representative shape and subsequently approximate the (clumped) shape using a minimum number of spheres which have the largest possible size. Although this an important task for both model accuracy and computational efficiency, the cited studies do not elaborate on the methods which were used to select the representative shapes, and how the clumps were optimized in terms of sphere count and size. It is generally stated that a number of common shapes within a material sample were selected and each shape was generated with equal probability in simulations. Another question which remains is: how many different clump shapes are assumed to be sufficient for representing the material? Yu & Saxén used six highly irregular shapes to model coke in [43], while they assumed only one of those shapes in [51], as shown in Table 3. Chakrabarty et al. [145] assumed a single shape to model sinter particles, which have high shape dispersity. While it is not clear how this specific shape was selected, they reported a good agreement between simulated and experimental repose angle and bulk density, and concluded that this simple shape was suitable for modelling the bulk behavior of sinter.

The use of other shape approximation methods for blast furnace materials has also been considered. Govender et al. [124] investigated the effect of coke and ore particle shape on chute discharge, charged burden topography and charged layer percolation using either polyhedra, which are angular in shape, or spheres in combination with rolling resistance. The size of spheres was equivalent volume of the polyhedra and rolling friction coefficients were determined by matching angle of repose of spherical and polyhedral burden discharged from a chute. The remaining input parameters were identical for both shapes. They concluded that there were significant differences in velocity and mass flow profiles between spheres and polyhedra, which is in contrast to the results of Akashi et al. [142]. Inter-layer percolation and packing density were also significantly affected by the particle shape. Hence, the authors concluded that modelling the burden as spherical particles in combination with rolling friction is not sufficient to account for particle shape effects when considering particle velocities, packing topography and permeability. Xia et al. [146] studied the effect of using spheres versus different super-ellipsoids to model the flowing and packing behavior of crushed material which, according to the authors, has shape characteristics similar to blast furnace materials. They used a pseudo-2D setup consisting of a hopper and a discharge bin to represent the furnace charging system in a simplified way. They scrutinized the performance of super-ellipsoid models by comparing the discharged material's macro-scale behavior in simulations to experiments and concluded that while spherical and super-ellipsoid particles were both able to predict the packing height, other aspects such as packing profiles, dynamic repose angle, and flow rate could not be predicted by spheres. Since the microscale performance of each model (for example in terms of the packing porosity) was not evaluated by comparison to experiments, it is not clear whether super-ellipsoids are also useful for predicting the packing behavior of materials with large size and shape dispersity.

- Particle size distribution

Similar to the particle shape, the use of a simplified PSD in simulations requires justification. Table 2 shows that only few researchers have modelled burden materials according to their true PSD. The majority of models has been developed using at most three particle sizes. We notice that the experimental counterparts of these studies are performed using more or less the same simplified PSD (this is achieved through sieving) and we conclude that these models are therefore not representative of actual burden behavior. The number of studies focusing on how the actual PSD can be simplified in simulations, through verification using the actual PSD in experiments, is scarce. Yu & Saxén [43] studied segregation of pellet and coke particles from a fixed chute, where both materials were modelled as a tridisperse mixture of fine, intermediate and coarse particles in simulations. The three particle sizes corresponded to the mean diameter of the size ranges used in the experiments. Unlike pellets, the coke particles were modelled as a combination of six different clumped spheres. To scrutinize the effect of particle size on the flow behavior in simulations, a test case was performed where the pellets were given the same parameters as the coke particles, except for the size. By comparing the results of this simulation to the original simulation of coke, it was concluded that pellets with the same parameters as coke behave in a similar way as coke with respect to the rotational and translational velocities in the chute. Schott et al. [122] investigated whether modelling the true PSD of individual components is required to model the tendency to segregate of a mixture of iron ore pellets, sinter and coke during hopper discharge and subsequent heap formation. It

was found that representing each of the materials by its mean particle size (d_{50}) reduces the number of particles and simulation time drastically without compromising the simulation results of the used material models.

Table 2 also shows that scaling has been applied frequently in blast furnace simulations. In general, either the particles or the geometry is scaled, or a hybrid scaling approach is applied. Regardless of the applied method, the choice of scaling factor(s) in these studies is not discussed and it is rarely verified whether the scaled model is indeed able to mimic the phenomena of an industrial furnace. This is an important point which must be considered since the principle of similarity states that "the behavior of two systems will be similar if the ratio of their linear dimensions, forces, velocities, reactions, etc., is the same" [147]. When it comes to studying aspects of the burden distribution on lab-scale, kinematic (motion) and dynamic (force) similarity with regard to the full-scale system should be considered. Otherwise, burden energy and momentum upon striking the stock surface in the furnace are lower in a downscaled system. In their 1/10-scale pilot setup, Mitra & Saxén [148] observed a the coke collapse phenomenon only slightly when charging pellets on top of coke layers. Large-scale simulations representing an actual blast furnace were also performed and the authors reported that the coke-push effect was much more pronounced, resulting in a significant redistribution of the burden. Using the same setup, they later investigated the formation of coke-ore mixed layers [56]. Since the materials and system were significantly downscaled in this study, the authors hypothesized that the mixed layer effect will be less pronounced in an actual, large-scale blast furnace. Narita et al. [149] experimentally investigated ore-coke mixed layer formation using a 1/10-scale charging setup and compared the findings to a full-scale setup. They observed that the mixed layer formation is less pronounced in the full-scale setup. Using the momentum balance, they showed that the coke to pellet (ore) mass ratio $\left(\frac{m_c}{m_p}\right)$ should be used as a scaling factor to obtain similar degrees of mixed layer formation. To verify this, they used smaller sized coke particles to reduce the value of $\left(\frac{m_c}{m_p}\right)$ and found that the volume of the mixed layer was comparable to the full-scale system. The studies listed in Table 2 generally aim to study the burden distribution during charging. Future DEM studies may focus on the descending behavior and analysis of the gas flow, which truly reflects the permeability. The scaling factor which should be considered for such studies is the Froude number, as reported in many blast furnace related publications [150–155].

3.3.2. Effect of material parameters

- Density

The density of an object is defined as the mass per unit volume of the material. Different types of density can be determined based on the volume which is considered in the calculation [156]. For a highly porous material, the true volume (i.e., the volume of the particle which excludes the volume of internal pores, either open or closed) occupied by a solid particle can be significantly lower than the total (encapsulated) volume of the particle. In DEM simulations, particles are modelled as non-porous; hence, the encapsulated density should generally be specified rather than the true (skeletal) density. For non-porous materials, these density values are equal. In Section 3.5 we show how both of these values can be measured, and that the skeletal density can be significantly higher than the encapsulated density for porous materials. It is therefore reasonable to question how significant a discrepancy in density value affects the simulation of different phenomena.

According to Katterfeld et al. [102], the particle density has a negligible effect on the bulk material's flowing behavior while it is strongly related to packing characteristics such as the bulk density and porosity. This was clearly demonstrated in the work of Tripathi et al. [112]. The authors used the method of interstitial fluid for measuring pellet and sinter particle density, resulting in a wide range of possible values (cf. Table 4) which could be used as inputs to their material model. In order to assess the effect of this range, they simulated dynamic angle of repose and bulk density tests using the extremes and compared the results to experimental results. They found that the repose angle was not significantly affected by changes between the extremes while the bulk density required an appropriate value within the range to be selected.

Ho et al. [4] experimentally studied the effect of particle density on

Table 4
Direct measurement methods for determining model input parameters from references related to blast furnace literature.

Parameter (unit)	Method (standard, if specified)	Pellet	Sinter	Coke
ρ_p (kg/m^3)	Gas pycnometer	3948 [166], 3990 [167]	–	–
	Envelope density analyzer	3552 [112]	3311 [112]	–
	Water displacement method	3126–3771 [112]	3041–3477 [112]	1021 [175]
	Drainage method	3674 [17]	3199 [17]	–
E (GPa)	Shimadzu autograph universal tester i.c.w. Eq. (2)	0.033 [169]	–	–
	Dynamic elastic modulus tester (ASTM E1876–01)	126 [167]	–	–
G (GPa)	Dynamic elastic modulus tester (ASTM E1876–01)	50.9 [167]	–	–
	Impact load cell	0.016 [166]	–	–
ϑ (–)	Dynamic elastic modulus tester (ASTM E1876–01)	0.24 [167]	–	–
ε_{pp} (–)	Drop test with glued particle surface	0.42 [167]	0.35 [167]	0.39 [167]
ε_{pw} (–)	Drop test with wall surface	0.62 (steel) [167]	0.4 (steel) [167]	0.42 (steel) [167]
$\mu_{s_{pp}}$ (–)	Pin-on-disk rotational tribometer	0.49 [166]	–	–
	Tilted table with two glued particle surfaces	0.65 [167]	0.76 [167]	0.87 [167]
	Poured repose angle test i.c.w. Eq. (7)	0.49 [112]	0.55 [112]	–
$\mu_{s_{pw}}$ (–)	Tilted table with one glued particle surface	0.36 (steel) [167]	0.52 (steel) [167]	–
	Pin-on-disk rotational tribometer	0.5 (steel) [166], 0.71 (rubber) [166]	–	–
	Inclined surface test	0.19 (glass) [112], 0.38 (acrylic) [112]	0.17 (glass) [112], 0.38 (acrylic) [112]	0.852 (rubber) [175], 0.24 (ceramic) [175]
$\mu_{r_{pp}}$ (–)	Particle velocity measurement i.c.w. energy balance equation	0.24 [167]	0.38 [167]	0.46 [167]
	2D Image analysis i.c.w. Eq. (8)	0.07 [112]	0.20 [112]	–

the coke push effect by using a simplified charging setup and balls of different densities, where low-density and high-density balls represented coke and ore, respectively. They concluded that the coke push effect becomes more pronounced as the density of the heavy material increases. More specifically, the gouge size increases as the density increases. The effect of particle density on spontaneous percolation of small particles into a packed bed of larger particles was investigated by Zhu et al. [153]. As they expected, there was no considerable effect of the percolating particles' density on their movement through the bed since a tightly packed bed was used in the analysis. The authors hypothesized that there might be a noticeable effect if the packing particles could move after impact with the percolating particles. Yu & Saxén [70] studied the layer expansion process during burden descent. A pellet layer was placed on top of a coke layer, and the percolation of pellets into the coke layer was analyzed for different densities of pellets ($\rho_p = \in \{1000,2284,3000\}$ kg/m^3) and coke ($\rho_c = \in \{500,1050,1500\}$ kg/m^3). The value of pellet density had no clear effect on the percolation behavior. On the other hand, the coke density of 1050 kg/m^3 provided the highest degree of percolation. The authors hypothesized that percolation in the case of lowest coke density was obstructed because the heavy pellet particles were able to move the coke particles such that the voids of the coke bed were sealed.

- Young's modulus

According to Eq. (1), the numerical time step for a simulation based on the Hertz-Mindlin contact model depends on the shear modulus, and therefore by definition, on the Young's modulus. By lowering the value of G (or E), the computational load can be reduced significantly. However, since a lower value of E corresponds to a softer material, it is important to asses to what extent a reduction in E can still provide accurate results [157]. Yu & Saxén [51] lowered the shear modulus of pellets from 10^9 to 10^7 Pa in their simulations of furnace charging and compared their results to a validated model (Okunu et al. [158]) for predicting mass fraction distribution of a pellet stream. They reported that both values of the shear modulus were in good agreement with the results of Okunu's model. Furthermore, the lowered value of G resulted in only a slight decrease of the total average force on small pellets, while the pellet (average, minimum, maximum and angular) velocities during charging as well as the charged radial burden distribution were practically unaffected. Based on this result, several other researchers [45,46,57,159] adopted the lowered value of 10^7 Pa in their work, applying this value to sinter and lump ore as well. When it comes to segregation, Zhu et al. [67] studied the effect of Young's modulus on the percolation of a single particle in a packed bed. They found no significant effect on the percolation behavior when lowering the Young's modulus of the percolating particle. Ueda et al. [160] studied how the descending behavior of coke and ore was affected by reducing the Young's moduli for both materials from $5 \bullet 10^9$ to $2 \bullet 10^8$ Pa. They concluded that the layer shapes did not change, while the stress distributions were clearly affected by the hardness reduction.

3.3.3. Effect of interaction parameters

Yu & Saxén [111] studied size segregation of pseudo-tridisperse pellets during discharge of a top bunker (conical) hopper, where pseudo-tridisperse indicates that there were three main size classes of particles with a narrow size distribution. The inter-particle and particle-wall sliding and rolling friction coefficients were varied as μ_s, $\mu_r = \in \{0.05,0.5,0.9\}$. It was concluded that the particle-wall friction coefficients affect the degree of segregation while the inter-particle friction coefficients do not.

In their sensitivity study for the percolation of pellets into a coke layer during layer expansion, Yu and Saxén [70] also scrutinized the effect of pellet-pellet (p-p) and pellet-coke (p-c) interaction parameters. It was clear that low values of the static friction coefficient ($\mu_{s_{p-p}} = 0.1$ and $\mu_{s_{p-c}} = 0.1$) promoted percolation which was expected since a low friction value means low contact resistance between particles. Less percolation occurred at higher static friction values, and there was no noticeable effect when $\mu_{s_{p-p}}$ and $\mu_{s_{p-c}}$ were increased from 0.5 to 0.9. When it comes to the rolling friction coefficient, high values of $\mu_{r_{c-c}}$ resulted in stronger percolation. This can be explained by the fact that coke particles' angular motion increases with rolling friction coefficient, therefore opening up the voids between the particles and allowing pellets to percolate. The values of $\mu_{r_{p-p}}$ and $\mu_{r_{p-c}}$ did not seem to have a noticeable effect on percolation, except that it was improved at very low values ($\mu_{r_{p-p}} = 0.05$ and $\mu_{r_{p-c}} = 0.04$). For the restitution coefficient is was found that ε_{c-c} had no effect on the pellet percolation, while lower values of ε_{p-c} and higher values of ε_{p-p} resulted in less percolation.

Liu et al. [116] modelled the trajectory of material after being discharged from a rotating chute, and its distribution in the furnace throat. It was concluded that inter-particle friction coefficients significantly affected the behavior of material which were in contact with the chute, while the effect on particles which were not in contact with the chute was negligible. When looking at the burden trajectories after being discharged from the chute, the effect of friction coefficients was negligible. However, they had a significant impact on the burden profile in the throat.

3.3.4. Effect of computational domain

The computational load of a full 3D (Type I) model is often reduced in simulations by using slot (Type II) or sector (Type III) models, as shown in Fig. 23. Since the walls (front/rear and side walls shown in Fig. 23b and c, respectively) may have a significant effect on the material behavior when using these simplified models, they are treated as either frictionless or periodic boundaries in simulations. The smallest slot thickness and the smallest sector angle for a given particle-to-vessel diameter ratio must be carefully determined to preserve the flow behavior of the actual system.

From Table 2 it can be seen that simplified computational domains have not been used extensively. Yang et al. [161] showed that sector models may be better suited to simulate material behavior in cylindrical systems such as conical hoppers. In a later study [121], they compared the use of slot and sector models for simulating the overall solid particle motion in a furnace shaft. The slot model produced different bed characteristics such as zone sizes and layer shapes, while the sector model produced results consistent with the full 3D model. The sector angle was also scrutinized and it was found that there were no significant differences in flow behavior between angles of 30°, 45°, 60° and 90°. The authors recommended the use of sector models in combination with circumferential boundary conditions for CFD-DEM studies of the gas-solid flow in a blast furnace. Zhang et al. [34] studied size segregation during discharge of a Paul-Wurth hopper using a slot model in combination with periodic boundaries at the front and rear walls. However, it is unclear how the slot thickness was determined. Wei et al. [49] developed a DEM model to study the evolution of axial and radial porosity distributions as the bed descends during and after charging. Using a rotating chute, alternating coke and sinter layers were formed in the furnace shaft. The simulation geometry represented the top of an experimental blast furnace, including charging hopper and chute which were fully three-dimensional, while a slot model with periodic boundaries was used for the furnace shaft. The particles which fell outside of the slot model during charging were simply removed from the simulation. The width of the slot model was 0.1 m, but the authors provided no explanation for the choice of this value.

3.4. Determination of model inputs

In this section, we review the measurement and/or calibration methods used to determine model inputs in blast furnace literature listed in Table 2.

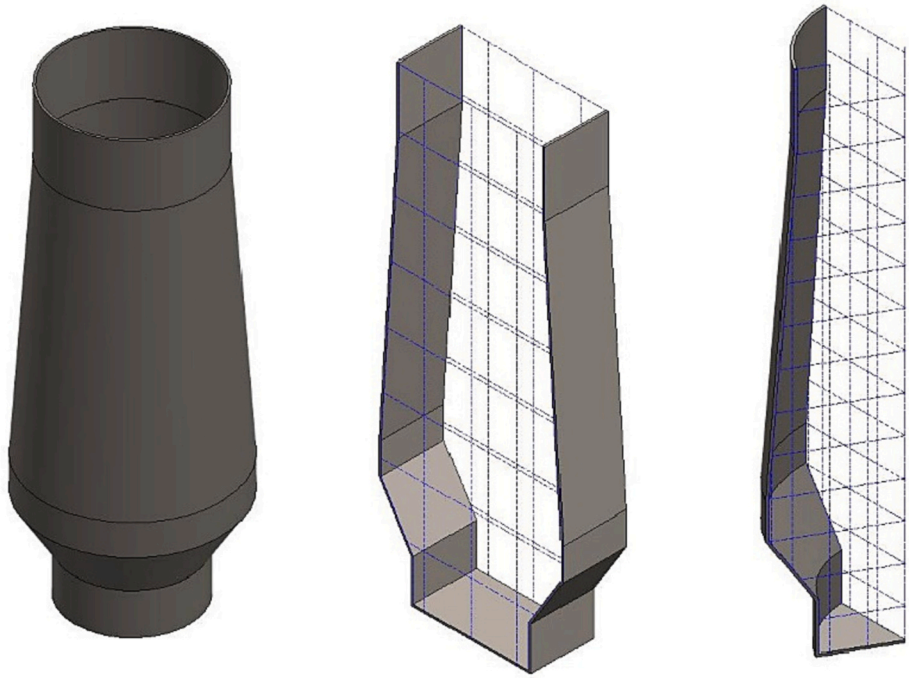

Fig. 23. Blast furnace computational domains used in simulations (from left to right): (a) full 3D (Type I) model, (b) slot (Type II) model, and (c) sector (Type III). The hatched surfaces indicate the periodic boundaries.

3.4.1. Direct measurement of inputs

The direct measurement approach has been applied for primarily iron ore pellet and to a far lesser extent for sinter and coke. Table 4 lists the test setups used for measuring different input parameters according to blast furnace literature.

- Morphology

The particle size and shape distributions are the first to be measured, as calibration is performed for material with a certain morphology. Size distributions are generally measured through sieving, either manually or using a vibration table. The former was reported to be more practical for iron ore pellets due to the relatively large particle size [162]. Although it is often reported that "pellets are approximately spherical" while "sinter and coke have highly irregular shapes", we have not encountered any blast furnace related publications in which the burden shape distributions are reported. Researchers generally select one or few irregular shapes to represent sinter and coke without stating how the number and type of shape was selected. For future work, a variety of shape descriptors based on 2D and 3D image analysis [163] can be used for particle shape characterization. Angelidakis et al. recently developed SHAPE [164] (cf. Fig. 24), a Matlab-based tool which performs morphological characterization of 3D particles obtained from imaging data. They also developed the CLUMP tool [165] for generating clumped particles from the data based on three different algorithms. The user specifies certain requirements of the clump, for example the number of spheres it may be comprised of. Generated clumps can subsequently be imported into different software packages.

- Density

In Section 3.3.2 we discussed how the magnitude of particle density depends on which volume was considered in its calculation. Fig. 25 illustrates the difference between skeletal volume and encapsulated volume which can be measured using a gas pycnometer and encapsulated density analyzer, respectively. A gas pycnometer uses an inert gas to fill a chamber of known volume containing a particle sample. Since the gas is able to penetrate open surface pores, the amount of gas supplied to the chamber, and therefore the true particle volume, can be approximated very closely. This method was used by Barrios et al. [166] and Wei et al.

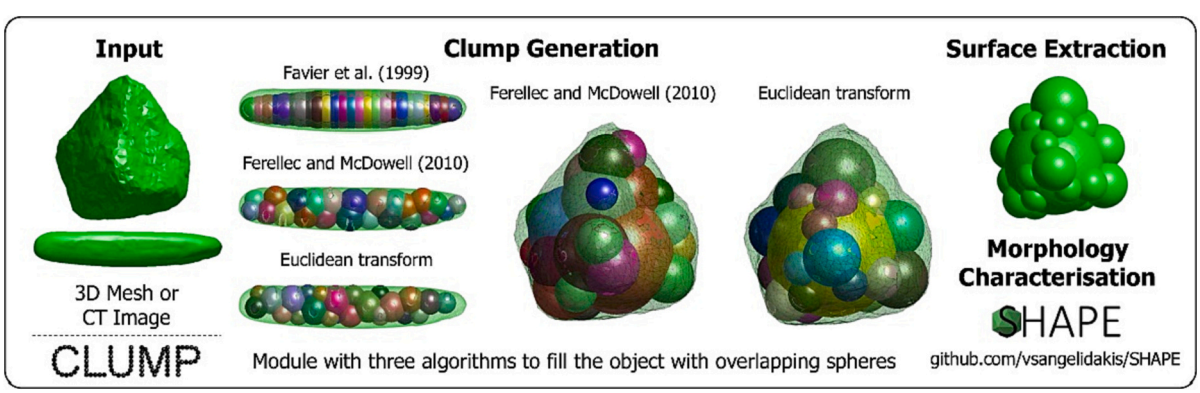

Fig. 24. The main modules of the CLUMP tool, illustrating how clumped sphere approximations of imaging data are created based on different algorithms. SHAPE can be used as a complementary tool to characterize particle morphology. Image adopted from [165].

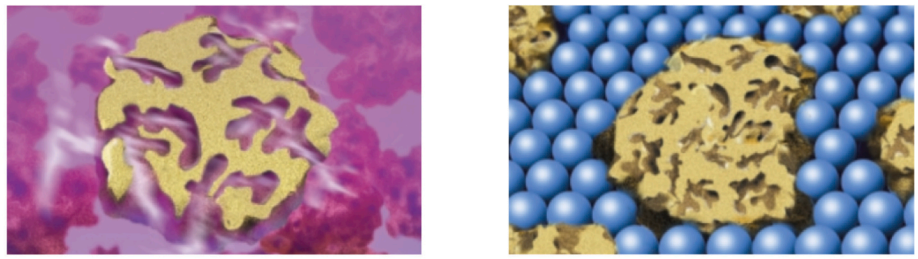

(a) (b)

Fig. 25. Particle volume estimation (from left to right, images adopted from [183]): (a) using a gas pycnometer, (b) using an envelope density analyzer.

[167]. An envelope density analyzer uses a granular material with high flowablity to achieve a close packing around a particle specimen by compaction using a piston. The packing particles are small enough to adhere closely to the specimen surface; however, they do not enter the open pores. The piston's displacement during compaction allows the encapsulated volume of the specimen to be approximated. Tripathi et al. [112] used the GeoPyc 1365TM [168] to determine the envelope density. While encapsulated density meters are relatively fast and easy to use, the main drawback is that such devices are generally limited in the particle size which can be used in the measurement due to the chamber size. Also, particles with very complex shapes (e.g. particles with deep concaves such as sinter) might not be suited for this device, as the packing particles may not be able to penetrate surface pores which are small compared to the packing particle size. An alternative is the fluid displacement method, as used by Tripathi et al. [112]. They filled a cylindrical container with particles and carefully added water to the brim. By assuming that no water entered the particles' pores, the volume occupied by the particles was determined as the container volume minus the volume of water which was required to fill the container. The envelope density was then determined as the ratio of material mass and volume in the container. To make the estimation more accurate, they excluded the volume of water which entered the pores from the calculation. This was done by measuring the mass of the wet particles and subtracting that value from the mass of the dry particles, which gave the mass (and volume) of water in the pores. This procedure resulted in a wide range of possible values for the envelope density. Chen et al. [92] used a similar method, but took measures to prevent water from entering the pores. They sealed the pores by immersing the particles in paraffin before bringing the particles in contact with water. This method is referred to as the "drainage method" and, according to Table 4, the measured density values of pellet and sinter were within the wide range of possible values produced by Tripathi et al. [112].

- Young's modulus, shear modulus and Poisson's ratio

Li et al. [169] used a Shimadzu Autograph universal tester to determine the Young's modulus of pellet. Their setup included a piston to apply a vertical (normal) force on a particle until breakage occurs. The force (F^n) and particle indentation (δ^n) were directly obtained from the user interface, and the authors subsequently estimated the Young's modulus from the Hertz contact law which reads

$$F^n = -\frac{4}{3}E^*\sqrt{R^*}(\delta^n)^{\frac{3}{2}} \tag{2}$$

This was done for pellets varying in size, and average value of all measurements was used. Wei et al. [167] used a dynamic elastic modulus tester to measure Young's modulus, Shear modulus and Poisson's ratio of pellet. Rather than accommodating particles directly, this setup requires a rectangular "plate" sample with a minimum size of 3 × 4 × 40 mm. The authors argued that the values of E, G and ϑ are independent of the material size and shape, and prepared rectangular samples to satisfy the setup requirements. The authors noticed a significant difference between their value of the Young's modulus (1.26×10^{11} Pa) and the value reported by Li et al. [169] (3.3×10^7 Pa) and other values from literature. They mentioned that differences could be attributed to the sample preparation process, which may have enhanced the material strength.

- Restitution coefficient

The restitution coefficient is generally determined through a drop test. In some cases, the dropping height (h_d) and rebound height (h_r) are measured using high-speed cameras, as described in [170], and subsequently used to calculated the restitution coefficient as

$$\varepsilon = \sqrt{\frac{h_r}{h_d}} \tag{3}$$

Since this calculation applies to central impact, it is less suitable for irregularly shaped particles. The following equation based on the ratio of rebounding and incoming velocities (v_r and v_i, respectively) has shown to be more appropriate [170].

$$\varepsilon = \frac{v_r}{v_i} \tag{4}$$

A detailed description on how the particle velocity is determined from image analysis is provided by [167]. Barrios et al. [166] used this approach for measuring the pellet-wall restitution coefficient using steel and rubber surfaces. For the pellet-pellet restitution coefficient, they followed the same method using a packed iron ore surface. Wei et al. [167] followed the same method, but instead glued particles to a plate for determining the particle-particle restitution coefficient. In order to reduce the effect of particle shape, they glued the particles such that a "flat" part faced upwards.

- Sliding friction coefficient

The most common setup used for determining the sliding friction coefficient involves a surface which is gradually titled until the particle starts to slide [117,167]. The surface angle (θ_s) on the onset of sliding is then measured, and the friction coefficient is determined as

$$\mu_s = tan(\theta_s) \tag{5}$$

The inclination angle must be increased gradually in order to identify the moment of sliding onset, and the operator should subsequently stop the surface inclination immediately. Another challenge is ensuring that particle rotation is excluded from the measurement. Wei et al. [167] did this by using a "particle plate" –which was constructed by gluing multiple particles together– instead of a single particle.

Barrios et al. [166] used a pin-on-disc tribometer to measure the particle-wall sliding friction coefficient. Their setup consisted of a rotating disc, covered with the different materials, which is brought in contact with a particle specimen. To determine the particle-particle friction coefficient, the disk surface was covered with ground particle pieces. The setup measures the tangential force (F^t) for different normal

forces (F^n), so that the sliding friction coefficient can be calculated as

$$\mu_{s_{pw}} = \frac{F^t}{F^n} \tag{6}$$

- Rolling friction coefficient

We highlight the work of Tripathi et al. [112], as they determined pellet and sinter model inputs using primarily the direct measurement approach. The authors first measured pellet and sinter particle density using the fluid displacement method. Next, they estimated the particle-particle sliding friction coefficient from the angle of repose (θ_r) of both materials using

$$\mu_{s_{pp}} = tan(\theta_r) \tag{7}$$

For the particle-particle rolling friction coefficient, they followed the 2D image analysis method of Wensrich et al. [130,171] which relates rolling friction to particle shape by

$$\mu_{r_{pp}} = \frac{< e >}{D} \tag{8}$$

where $<e>$ is the average eccentricity and D is the projected diameter for a given particle image. The remaining material properties (E or G, ϑ and ε) were obtained from literature. Assuming $\mu_{r_{pw}} = \mu_{r_{pp}}$ and using their estimated value of $\mu_{s_{pp}}$, they validated their approach by assigning these values to spherical particles in simulations of dynamic and poured repose angle tests, and comparing the results to experiments. Despite the fact that they used a 2D imaging technique, they reported a good match in both cases and concluded that their method allowed them to completely avoid a lengthy calibration process. Their work proved that the rolling friction coefficient is not purely a tuning parameter since it can be determined directly through measurable shape parameters, which is in contrast to previous belief [104].

3.4.2. Particle-level calibration

Some researchers employed an indirect measurement approach, in which they combined particle measurements with simulations to determine model inputs. The tests and measured values are summarized in Table 5. Barrios et al. [166] determined the particle-particle rolling friction coefficient using an inclined surface test. In their model, they used directly measured values of the other parameters while varying the value of$\mu_{r_{pp}}$. By comparing the simulated angle at which the particles start to roll with experiments, the value of $\mu_{r_{pp}}$ could be established. Next, they verified whether these single-particle measured values could be used as inputs to a DEM model for mimicking the bulk behavior through comparison of simulations with experiments. 37 Since pellets are not perfectly spherical, they attempted to represent the actual particle shape as much as possible in their simulations by using clumped spheres. For comparison, they also performed simulations using perfectly spherical particles. They concluded that, if pellets are modelled using clumps representing their actual shape, simulations of bulk flow provide realistic results. If pellets are modelled as spheres, the simulated results deviate from experimental results and a reasonable match is only found when the sliding friction coefficient is tuned. Their work demonstrates that even in the case of nearly-spherical particles, the bulk calibration approach should be applied rather than using parameters from direct measurement when the shape is idealized in simulations.

The research group of Mio et al. uses a distribution rolling friction model in combination with spherical particles to account for the actual shape of sinter in simulations, as mentioned earlier. In [41], they briefly described the approach for indirectly measuring the distributed rolling friction coefficient using an inclined surface.

Table 5
Particle-level calibration for determining model input parameters from references related to blast furnace literature.

Parameter (unit)	Method (standard, if specified)	Pellet	Sinter	Coke
ε_{pw} (−)	Drop test	0.39[a] / 0.42[b] (steel) [166], 0.29[a] / 0.32[b] (rubber) [166]	–	0.6[b] (rubber) [175]
$\mu_{r_{pp}}$ (−)	Inclined surface test	0.02[b] / 0.21[a] [166]	variable (cf. Fig. 9) [41]	–
$\mu_{r_{pw}}$ (−)	Inclined surface test	0.01[b] / 0.25[a] (steel) [166], 0.01[b] / 0.29[a] (rubber) [166]	variable (cf. Fig. 9) [41]	–

[a] Determined through simulation with spheres.
[b] Determined through simulation with overlapping spheres.

3.4.3. Bulk calibration

Bulk calibration involves experimentally measuring performance indices of the bulk material which are affected by model parameters, and subsequently determining the parameters' values such that the DEM model reproduces the experimental material behavior in terms of the performance indices. Table 6 summarizes the tests, calibration targets and values of calibrated parameters found when performing bulk calibration for individual materials and for mixtures in blast furnace literature.

- Interaction parameters for individual materials

From Table 6 it is clear that the calibration process is generally focused on determining inter-particle sliding and rolling friction coefficients. The repose angle is generally used as a calibration target since it is known to be affected by friction coefficients [143,172–174]. In some studies, the rolling friction coefficient is omitted when complex shapes are used to model irregular particles (e.g., the work of Schott et al. [122], Govender et al. [124] and Bester et al. [175]), so that the calibration procedure is directed towards only the sliding friction coefficient. Others included the rolling friction coefficient since they modelled particles as spheres (e.g., Liu et al. [116], Li et al. [169] and Chibwe et al. [176]), or even though non-spherical particles were used (e.g., Yu & Saxén [43], Chakrabarty et al. [145] and Chen et al. [92]).

We observe that several authors [116,169,176] have used the repose angle as the sole calibration target, despite calibrating for both rolling and sliding friction coefficients. Not surprisingly, they report multiple possible solution pairs for the friction coefficients. The general approach is to subsequently select a single solution pair somewhat arbitrarily. Li et al. [177] are the sole authors who acknowledged that an additional calibration target is required to obtain a unique solution to the calibration problem. They used the angle of repose of a pile formed through hopper discharging and the hopper discharge time as calibration targets. The set of friction coefficients which simultaneously satisfied both targets was then selected.

Table 6 summarizes the tests, calibration targets and values of calibrated parameters of the aforementioned studies. While the particle shapes used in the works of Chakrabarty and Schott were very similar, it can be seen that their calibration results for sliding friction are significantly different, especially for sinter (0.3 and 0.7 according to Schott and Chakrabarty, respectively). A similar observation holds for (spherical) pellets calibrated through ledge tests. Liu et al. and Chibwe et al. obtained sliding friction coefficient values of 0.7 and 0.4, respectively. The first possible explanation for these differences lies in the fact that materials used by different researchers are most likely not of the same origin, and the bulk behaviors can therefore differ, resulting in different calibration results. Even if materials are the same, differences in the material size distribution which is included in the model and/or experiments may also affect the calibration result. Another possibility is that researchers use different DEM software packages which may have slightly different implementations of the same contact model. These

Table 6
Bulk calibration methods for determining model particle-particle (pp) and particle-wall (pw) parameters found in blast furnace literature.

Ref.	ρ_p (kg/m^3)	$\mu_{s_{pp}}$ (−)	$\mu_{r_{pp}}$ (−)	ε_{pp} (−)	$\mu_{s_{pw}}$ (−)	$\mu_{r_{pw}}$ (−)	ε_{pw} (−)	Target / Test
Pellet								
Soda et al. [187]	–	0.70	–	–	–	–	–	AoR / Rotating drum test
Liu et al. [116]	–	0.70	0.05	–	–	–	–	AoR / Ledge test
Schott et al. [133]	–	0.45	–	–	–	–	–	AoR / Piling test
Li et al. [169]	–	0.50	0.30	–	–	–	–	AoR / Draw down test
Chibwe et al. [125]	–	0.40	0.20	–	–	–	–	AoR / Ledge test
Wei et al. [188]	–	0.55	0.20	–	–	–	–	AoR / Lifting funnel test
Chen et al. [17]	–	0.40	0.10	–	–	–	–	AoR / Piling test
Sinter								
Liu et al. [149][a]	–	0.70	0.10	–	–	–	–	AoR / Ledge test
Schott et al. [133][b]	–	0.30	–	–	–	–	–	AoR / Piling test
Wei et al. [186][a]	–	0.50	0.30	–	–	–	–	AoR / Lifting funnel test
Chen et al. [17][b]	–	0.60	0.20	–	–	–	–	AoR / Piling test
Coke								
Liu et al. [149][a]	–	0.70	0.10	–	–	–	–	AoR / Ledge test
Schott et al. [133][b]	–	0.20	–	–	–	–	–	AoR / Piling test
Chibwe et al. [179][a]	–	0.80	0.50	–	–	–	–	AoR / Ledge test
Chakrabarty et al. [161][b]	985	0.55	0.10	0.60	0.90 (steel)	0.20 (steel)	0.40 (steel)	(1) Bulk density / Container test (2) AoR / Ledge test (3) Sliding angle / Inclination test
Bester et al. [166][b]	–	0.20	–	–	–	–	–	
Wei et al. [186][a]	–	0.45	0.30	–	–	–	–	AoR / Lifting funnel test
Pellet-sinter								
Schott et al. [133]	N/A	0.10	N/A	n.s.	N/A	N/A	N/A	AoR / Piling test
Degrassi et al. [169]	N/A	0.40	0.40	0.30	N/A	N/A	N/A	–
Chakrabarty et al. [131]	N/A	0.60	0.07	0.55	N/A	N/A	N/A	–
Pellet-coke								
Schott et al. [133]	N/A	0.10	N/A	n.s.	N/A	N/A	N/A	AoR / Piling test
Sinter-coke								
Schott et al. [133]	N/A	0.10	N/A	n.s.	N/A	N/A	N/A	AoR / Piling test

Note: This distinction is not made for pellets as they are always modelled as spheres in current literature.
[a] Determined through simulation with spheres.
[b] Determined through simulation with overlapping spheres.

points demonstrate that adopting model parameters from literature should be exercised with caution.

- Interaction parameters for mixtures

According to Table 2, there are several studies in which interactions between different burden materials have been modelled. However, most of these works either mention that the interaction parameters between different material components were obtained from literature, or they completely omit the methods used for determining these parameters [92,177]. Only few researchers have explicitly reported their methods. Degrassi et al. [126], after calibrating the material models of pellet and sinter separately, assumed the average values of the individual sliding friction, rolling friction and restitution coefficients as the pellet-sinter interaction parameters. Their simple approach was only validated qualitatively by performing large-scale hopper filling simulations and visually comparing the material distributions inside the hopper to actual distributions using photographs. Chakrabarty et al. [145] took a similar approach to determine pellet-sinter interaction parameters. Using average values, they performed angle of repose experiments using pellet-sinter mixtures of different compositions. The authors reported a good match between simulations and experiments for all compositions and concluded that their method for mixture characterization was simple, yet effective. Schott et al. [122] took a different approach to mixture calibration. Instead of assuming the average friction coefficient value for the interaction between mixture components, the authors used a fixed mixture composition (20:10:1 for pellets, sinter and coke on mass basis) and determined the friction coefficient for which the repose angle matched between simulations and experiments. In this way, they determined a sliding friction coefficient of 0.1 between all mixture components. It is not clear how the restitution coefficient between different components was determined and, as mentioned previously, rolling friction was not considered since the particle shape was assumed to be approximated correctly. The obtained pellet-sinter sliding friction coefficient is clearly very different from the value obtained by Chakrabarty et al. This might be explained by the fact that Schott et al. [122] calibrated a mixture consisting of not only pellet and sinter, but also coke.

An important aspect of material model calibration is to include the flow conditions which are expected in the actual application in the calibration test. Considering the sheer size of industrial blast furnaces, the magnitude of flow velocity upon burden surface impact is expected to be in the order of 10 m/s [47]. Hence, models developed for predicating phenomena affecting the burden distribution should be calibrated against high-velocity experimental data. Surprisingly, this aspect has not been taken into account, nor is it even mentioned, in the current blast furnace literature. Another aspect which seems to be ignored completely is taking the stochastic nature of granular material behavior in both virtual and physical experiments into account during calibration, as investigated by Fransen et al. [178].

3.5. Validation

In the previous subsections we demonstrated that blast furnace modelers have employed different methods to simplify the model development process, first by reducing computational costs and

subsequently by minimizing calibration efforts. While these methods allow the development of large-scale DEM models to become more feasible, the modeler must avoid oversimplification by carefully assessing whether the model is able to capture phenomena of interest. Hence, validation is the final step in the model development process which investigates whether the modelling methods are acceptable for a specific model objective. This requires careful selection of key performance indicators (KPI's) for comparing numerical and experimental results. Table 7 provides a summary of the methods which have been applied to validate the models discussed in this review. While some models have not been validated against experimental results, the majority of the studies report that the developed models are acceptable according to the authors. Such findings are generally expected, as the opposite result would not have been reported scientifically. However, we notice that the KPI for judging model validity is typically related to burden flowing behavior rather than burden distribution characteristics, even when the objective is to analyze the burden distribution. The experimental methods used for validation are discussed in more detail in this section.

The burden distribution is studied in simulations using a variety of KPI's, including burden trajectories after being discharged from the chute, degree of segregation, radial coke-to-ore ratio and height of charged layers. While obtaining the data for determining these indicators is relatively easy in simulations, it is often quite difficult to physically reproduce tests and extract particle data in a non-destructive manner. In this section, we discuss the reported experimental counterparts for these tests.

3.5.1. Particle trajectories

Mio et al. [114] used a relatively large experimental apparatus (1:3 scale model of an actual blast furnace charging system, as shown in Fig. 26a) to observe the behavior and measure the trajectory of sinter which was being discharged from a chute rotating at 13.4 rpm. The particles' trajectories at the chute outlet were captured using high-speed video recording while the flow inside the chute was recorded using pressure-sensitive sheets.

Zhang et al. [38] used a laser grid method to measure the stream of burden materials as they were charged into an actual furnace with an inner volume of 3200 m^3. A laser grid was projected as a frame of reference and a video camera was installed in a direction perpendicular to the plane of the laser grid (cf. Fig. 26b). As the material ejected from the rotating chute cut into the laser grid, an image of the burden trajectory was captured by the video camera and transmitted to a computer. An image processing system was used to extract the burden trajectory data at different chute angles.

3.5.2. Burden profiles

Mitra & Saxén [148] designed a test setup to gain insight into the arising layers of a charging program (cf. Fig. 27). The setup was a 1:10 scale model of an industrial bell-less charging system. To mimic the shape of the burden surface in an actual furnace, a conical surface was placed into the throat and a layer of coke particles was glued on the cone. This represented a coke layer with an inclination similar to the angle of repose of coke. After charging a layer of material, the throat was lowered in order to maintain a constant burden level. A mechanical device was used to determine the layer thickness. By computing the difference between measurements before and after charging, the layer thickness could be approximated. This setup was used to study the charging behavior of pellets on top of a coke layer [55] through both simulations and experiments. When charging pellets on top of the coke layers, the coke collapse effect was observed slightly using the pilot-scale setup. The disadvantage of their measuring technique was that only the layer profile could be mapped, but it could not distinguish where the particles of each layer ended up. Therefore, effects such as coke collapse, which were clearly seen in simulations, were not seen in the experimental layer plots.

Table 7
Details of validation methods applied in blast furnace literature.

Ref.	KPI	Method	Conclusion by authors
Yu, 2010 [148]	Mass fraction of fine, intermediate and coarse particles during discharging	Comparison with experiments using "stop-start" sampling method [171]	The model was able to qualitatively reproduce discharge trends. The extent of segregation was slightly under-predicted, which may be due to non-optimal parameter settings, idealization of the shape and differences in initial filling between simulations and experiments
Yu, 2012 [41]	(1) Mass fraction of fine, intermediate and coarse particles in sampling box after being discharged from chute; (2) Mean particle velocities	Comparison with experiments using (1) sampling box rig; (2) high-speed video recording	The model predicted the overall behavior well
Mio, 2008 [39]	(1) Mass fraction of fine, intermediate and coarse particles in sampling box after being discharged from chute; (2) Distribution of discharging velocity	Comparison with exp. Measurements using (1) sampling box rig; (2) high-speed video recording	The simulated distributions of collected particle agree with those of experimental very well
Mio, 2012 [37]	N/A	N/A	N/A
Wu, 2013 [35]	Radial particle size distribution in hopper	Comparison to experimental results of Aminaga et al. [188]	The simulation results agreed well with the results of Aminaga et al. [188]
Mio, 2019 [127]	(1) Particles' velocities; (2) Particles' trajectories	Comparison with experiments using (1) high speed video camera; (2) pressure sensitive sheet and a high speed video camera	The simulated and experimental velocities and trajectories matched very well
Yu, 2014 [128]	Mass fraction of fine, intermediate and coarse particles during discharging	Comparison to experimental results of Standish et al. [172] using continuous or "stop-start" method	N/A
Liu, 2015 [149]	(1) Particle trajectories; (2) Layer height along radius	Comparison with experiments using: (1) horizontal bars layered with carbon paper; (2) unclear	(1) Generally speaking, the simulated results match the experiments, with minor differences which can be ignored because of the different treatments in determining the stream line; (2) Simulated burden profile agrees well with the experimental results
Xu, 2017 [36]	N/A	N/A	N/A
Xu, 2019 [91] Xu, 2020 [93]	N/A	N/A	N/A

(continued on next page)

Table 7 (*continued*)

Ref.	KPI	Method	Conclusion by authors
	Falling point distribution	Comparison with experiments using circumferential poles	Outer collision region in simulations agrees well with experiments
Chakrabarty, 2021 [161]	Angle and height of belt-discharged coke	Comparison with experiments	Simulation and experimental results match well
Zhang, 2021 [34]	N/A	N/A	N/A
Mio, 2009 [40]	N/A	N/A	N/A
Mio, 2010 [176]	N/A	N/A	N/A
Yu, 2011 [67,177]	Bed height along the width for different expansions	Comparison with experiments	The simulated and experimental burden heights are in good agreement and slight differences can be ascribed to idealization of shape and PSD of coke
Yu, 2012 [41]	Bed height along the width for different expansions	Comparison with experiments	The simulated and experimental burden heights are in good agreement and slight differences can be ascribed to idealization of shape and PSD of coke
Yu, 2013 [48]	(1) Mass fraction distribution in particle trajectories, (2) Layer height along radius	(1) Comparison with validated mathematical model of Okuno et al.; (2) Comparison with experiments	The model was able to reproduce the overall burden behavior; discrepancies may be due to non-optimal parameter settings and idealization of PSD
Schott, 2016 [133]	N/A	N/A	N/A
Narita, 2017 [87]	Particle mass distribution	Comparison with experiments using sampling boxes	Circumferential imbalance was confirmed by experiments
Holmes, 2018 [95]	N/A	N/A	N/A
Kou, 2018 [43]	N/A	N/A	N/A
Govender, 2019 [125]	N/A	N/A	N/A
Kou, 2019 [42]	N/A	N/A	N/A
Xu, 2019 [92]	N/A	N/A	N/A
Chibwe, 2020 [179]	N/A	N/A	N/A
Hong, 2020 [44]	N/A	N/A	N/A
Mio, 2020 [33]	(1) Mass fraction of each size range during funnel discharge (2) Burden profile (shape); (3) O/C-ratio	Comparison with experiments using (1) n.s.; (2) n.s.; (3) digging up burden at different radial distances and determining the size distribution	A good agreement between simulated and experimental results was obtained
Wei, 2021 [46]	Porosity distribution	Comparison with experiments using the beaker method	The DEM results show general agreement with experimental findings, but there are some differences which may arise from systematic errors and non-idealities in the experiments
Zhou, 2021 [54]	N/A	N/A	N/A
Zhou, 2021 [182]	N/A	N/A	N/A

3.5.3. Segregation

Segregation has been quantified experimentally using different methods, depending on the type of equipment. For hoppers, the "start-stop" sampling method, originally described by Standish & Kilic [179], has been applied to analyze size segregation during hopper discharge on lab-scale [111,115] and industrial scale [58]. The hopper is equipped with a sliding plate at the outlet, which is kept closed during the charging process. The sliding plate is removed at various time intervals during discharging, allowing material to be collected intermittently until the hopper is fully discharged. The samples obtained at different discharged mass ratios are measured by a balance below the exit of the hopper. The contents of each sample are then screened and weighed to determine the mass fraction of each particle size as a function of the total discharged mass. Size segregation during hopper filling has also been investigated experimentally. This is more challenging, as the spatial distribution of particles within the hopper must be determined. Standish [180] proceeded to fill the charged hopper with water and subsequently freeze the contents. Then, volume elements from different positions were melted off and dried to analyze the size distribution within the sample.

Size segregation during chute flow occurs due to the kinetic sieving mechanism. The sampling box method, as shown in Fig. 21, is very popular for observing this effect [41,43]. As the name suggests, a sampling box with different compartments is placed at the chute outlet, allowing particles to be collected based on their horizontal position. The mass fraction of different sized particles in the compartments is determined, providing an indication of the degree of size segregation.

Segregation during burden descent has been mimicked by Yu and Saxén [70] using a specially designed expansion device (cf. Fig. 28). A layer of pellet particles was added on top of a coke layer and the device was slowly expanded, allowing the percolation of pellet into coke layers to be visualized. Although this method did not allow the degree of percolation to be quantified, the bed height at different expansion rates could be measured and compared to simulations, thereby providing an indication of the model accuracy.

3.5.4. Porosity distributions

The porosity, by definition, is the volume fraction of void space per unit volume of granular material. As this is a property of the internal structure, it is very difficult to quantify experimentally. Wei et al. [143,144] studied porosity distributions of a heap formed during hopper discharge on lab-scale. Measuring beakers were placed under the hopper prior to discharging and the filled beakers were carefully removed after a stable heap was formed, as shown in Fig. 29. The heap bottom porosity distribution was then determined by adding water from a measuring cup to each particle-filled beaker until the beaker was full. The amount of water required to fill the beaker was read from the measuring cup and this amount was assumed to represent the void volume in the beaker. The same method was used in a more advanced experiment in which a single coke layer was charged to a lab-scale furnace using a rotating chute [49]. The setup contained twelve identical small boxes (with a size of 50 mm × 100 mm × 40 mm) nested in a large box which was fixed to the bottom of the throat. The small boxes were dimensioned such that their size was more than 6 times the size of the largest particle and more

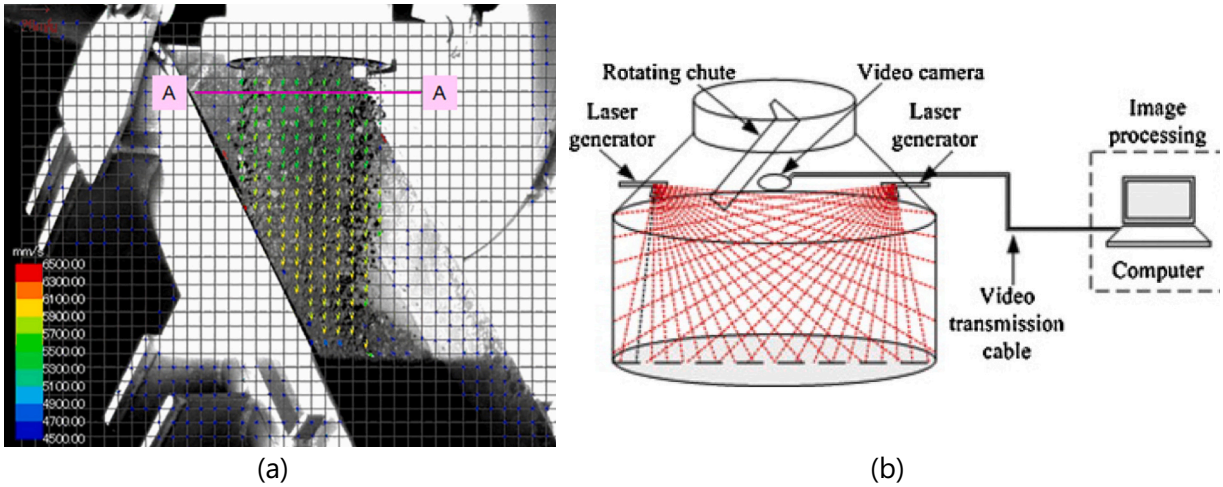

Fig. 26. (a) Example of velocity analysis by PIV \cite{Mio2019} (b) laser grid method to capture particle trajectories [38].

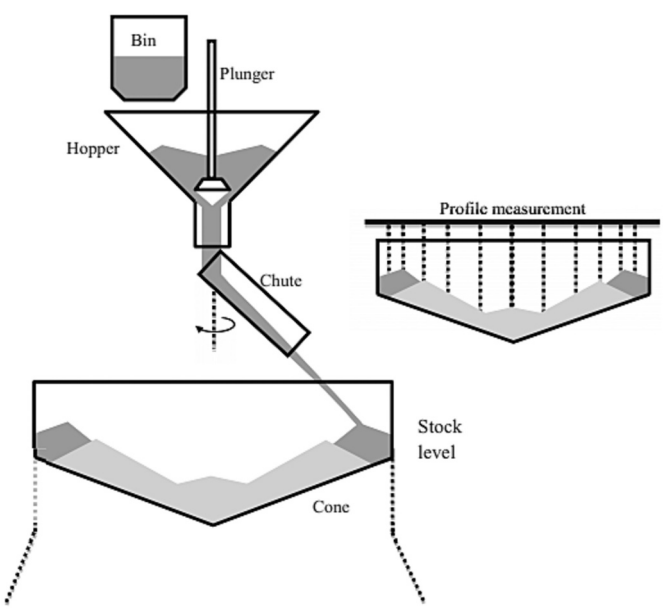

Fig. 27. Burden profile measurement setup of [148].

than 16 times the size of the smallest particle. This allowed the number of particles in each box to be over a hundred; hence it was assumed that the walls did not have an effect on porosity. In general, the authors found general qualitative agreement between simulated and experimental porosity distributions. The simulated porosity profiles were more symmetrical and fairly uniform when compared to the experimental profiles and the authors hypothesized that these differences were caused by systematic errors and non-idealities in the experiments.

3.6. Discussion

At the beginning of this section, we stated that developing a DEM model often requires simplifications of the actual system and materials to be made, and that the degree of simplification is driven by the model objective. The literature review has shown that the choice of particle morphology for blast furnace modelling is not straightforward. The studies using clumped spheres and polyhedra draw conflicting conclusions on whether spheres can be used in simulations to model how the burden components flow during charging, and where they subsequently end up in the furnace throat. There is clearly a need to systematically investigate whether different shape approximation methods provide comparable results for modelling the flowing behavior and which method is most suitable by comparison to experiments. This also holds for the permeability of the packed bed, as there is currently a lack of

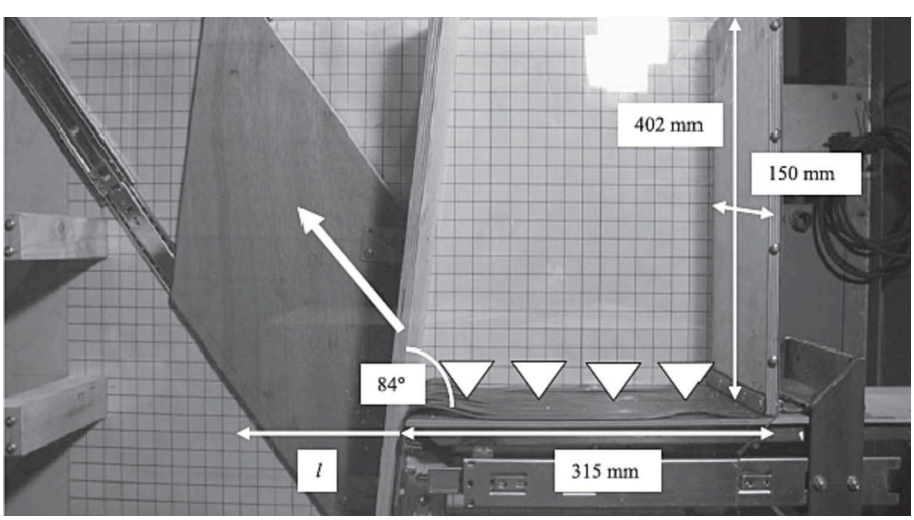

Fig. 28. Experimental device used to emulate percolation segregation during burden descent; image adopted from [70].

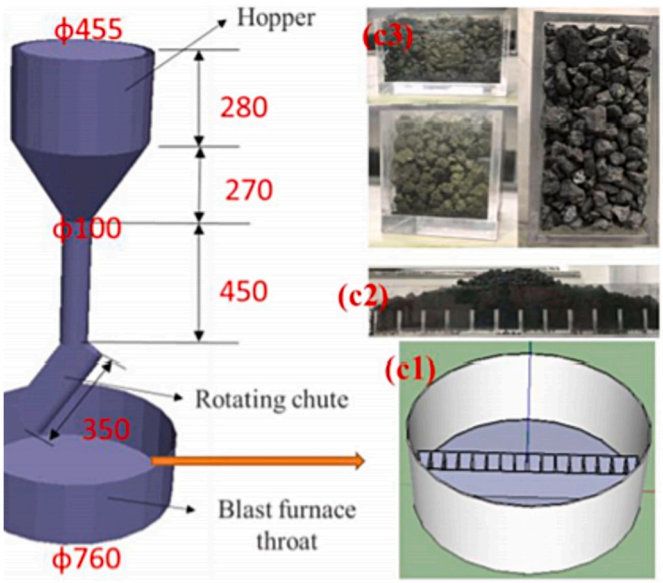

Fig. 29. Experimental device used to measure the porosity distribution in the throat (dimensions in *mm*; image adopted from [49].

studies focusing on structural aspects of the bed and how they are affected by modelling choices. Wei et al. [49] made progress in this regard by analyzing the permeability distribution in the throat using simulations and experiments. However, their results do not elucidate the effect of particle shape. By extension, the choice of particle size distribution used in simulation also requires further investigation.

Referring to our recommended model development procedure, we conclude that the current blast furnace literature lacks systematic model development procedures. Our review has shown that researchers often adopt values from previous research, often without consideration of the application and morphology which was used in the original work. Researchers are advised to adopt this strategy with caution, as the outcome of a calibration process may depend on modelling choices such as the morphology used to represent the material and even the software package used to develop the model [181]. Of the few studies involving calibration, we observe that friction coefficients are often determined through comparison with repose angle experiments and the combination of sliding and rolling friction coefficients is selected arbitrarily. Until now, Degrassi et al. [126] are the sole blast furnace modelers who adopted a structured calibration approach using an optimization algorithm. It must be noted that this method requires significantly more simulation runs, since sufficient data must be supplied to the optimization tool. Hence, the question which comes up is whether such an approach is required, or whether it is sufficient to select model inputs with a relatively high degree of freedom. Despite this seemingly unstructured approach, the authors of these studies generally report a good match between simulations and experiments (cf. Table 5). This can probably be attributed to the fact that small variations in the input parameters do not significantly affect burden trajectories, which are often used as the KPI to judge whether there is a good agreement between simulations and experiments. The sensitivity review showed that burden profiles are affected by friction coefficients, even though the trajectories are not. Hence, we conclude that KPI's should be carefully selected.

4. Conclusions and future perspectives

The objectives of this work were to review the state-of-the art in DEM modelling of blast furnace burden distribution during charging and descent and subsequently assess how the bed permeability can be enhanced according to these models. Our main findings are:

- Segregation, degradation during the deviation phenomenon the charging process are all expected to affect the burden distribution and resulting bed permeability. We found that the majority of blast furnace related literature focusses on these phenomena, and how they affect the burden distribution. However, the models are generally not reflective of actual blast furnace operations since materials and their mixtures are highly simplified. Also, many models are created using downscaled geometries which cannot reproduce the actual flowing behavior in a real blast furnace due to the lower mass flow rates and velocities. Full-scale geometries have become the standard in most recent studies, which indicates that computational power is increasing and DEM software packages are being made compatible with high-end solvers.
- While segregation and the deviation phenomenon have been studied frequently, investigations on how these phenomena are linked to permeability are currently missing. Future studies should focus more on this aspect, for example by developing DEM-CFD coupled models which can provide a detailed analysis of the gas flow for a certain burden distribution.
- The choice of particle morphology for blast furnace modelling is not straightforward. The studies using clumped spheres and polyhedra draw conflicting conclusions on whether spheres can be used in simulations to model how the burden components flow during charging, and where they subsequently end up in the furnace throat. There is clearly a need to systematically investigate whether different shape approximation methods provide comparable results for modelling the flowing behavior and which method is most suitable by comparison to experiments. This also holds for the permeability of the packed bed, as there is currently a lack of studies focusing on structural aspects of the bed and how they are affected by modelling choices. By extension, the choice of particle size distribution used in simulation also requires further investigation.
- The majority of models encountered uses parameters based on literature, rather than systematic calibration. While both direct measurement and bulk calibration of properties related to individual burden components have been reported to a limited extent, no literature on the systematic determination of interaction parameters between different burden components was found, neither through direct measurement nor through bulk calibration. Furthermore, the angle of repose is currently used as bulk calibration target to characterize the material flowing behavior. It is currently not clear whether the segregation and packing behavior are modelled correctly after calibration using this target. Hence, further investigation on the selection of calibration targets for capturing localized material behavior is required.
- Researchers generally report a good match between simulations and experiments based on KPI's relating to burden trajectories and burden distribution. In the future, appropriate KPI's for quantifying permeability in simulations, and how they can be measured experimentally, need to be determined.
- Encountered models have been used to investigate how system design and operational conditions can be adjusted to control the burden distribution more effectively. However, the case studies are mostly simplified since either a small part of the furnace is modelled, or not all burden components are included. Future case studies should be aimed at optimizing the permeability using models involving all burden components, thereby representing more realistic furnace operation.

This review has shown that significant efforts have been made to model the burden distribution; however, these models generally do not investigate the permeability. Hence, understanding of how the permeability can be optimized still requires a significant amount of effort towards model development.

Declaration of Competing Interest

The authors have no conflicts of interest to declare that are relevant to the content of this article.

Data availability

No data was used for the research described in the article.

Acknowledgements

This work was carried out as part of the "Industrial Dense Granular Flows" project, which received funding from the Dutch Research Council (NWO) in the framework of the ENW PPP Fund for the top-sectors and from the Ministry of Economic Affairs in the framework of the "PPS-Toeslagregeling".

References

[1] Yu. Yaowei, Experimental and Discrete Element Simulation Studies of Bell-Less Charging of Blast Furnace, PhD thesis,, Åbo Akademi University, Finland, 2013.
[2] Hans Bodo Lüngen, Peter Schmöle, Comparison of blast furnace operation modes in the world, Steel Res. Int. 91 (2020) 2000182.
[3] B.D. Pandey, U.S. Yadav, Blast furnace performance as influenced by burden distribution, Ironmak. Steelmak. 26 (1999) 187–192.
[4] C.K. Ho, S.M. Wu, H.P. Zhu, A.B. Yu, S.T. Tsai, Experimental and numerical investigations of gouge formation related to blast furnace burden distribution, Miner. Eng. 22 (2009) 986–994.
[5] Chin Loo, Leanne Matthews, Damien O'Dea, Lump ore and sinter behavior during softening and melting, ISIJ Int. 51 (2011) 930–938.
[6] Yongliang Yang, Yixin Yin, Donald Wunsch, Sen Zhang, Xianzhong Chen, Xiaoli Li, Shusen Cheng, Wu Min, Kang Zhi Liu, Development of blast furnace burden distribution process modeling and control, ISIJ Int. 57 (2017) 1350–1363.
[7] Haifeng Li, Henrik Saxén, Weiqiang Liu, Zongshu Zou, Lei Shao, Model-based analysis of factors affecting the burden layer structure in the blast furnace shaft, Metals 9 (2019).
[8] Zheng-Jian Liu, Jian-Liang Zhang, Tian-Jun Yang, Low carbon operation of super-large blast furnaces in China, ISIJ Int. 55 (2015) 1146–1156.
[9] Maarten Geerdes, Renard Chaigneau, Oscar Lingiardi, Modern Blast Furnace Ironmaking: An Introduction, Fourth edition, IOS Press BV, 2020. ISBN: 978–1–64368-123-8.
[10] Yuncai Liu, The Operation of Contemporary Blast Furnaces, Springer, Singapore, 2021. ISBN: 978-981-15-7074-2.
[11] P.A. Cundall, O.D.L. Strack, A discrete numerical model for granular assemblies, Géotechnique 29 (1979) 47–65.
[12] Xuefeng Dong, Yu Aibing, Jun ichiro Yagi, and Paul Zulli., Modelling of multiphase flow in a blast furnace: recent developments and future work, ISIJ Int. 47 (11) (2007) 1553–1570.
[13] Shigeru Ueda, Shungo Natsui, Hiroshi Nogami, Jun ichiro Yagi, and Tatsuro Ariyama., Recent progress and future perspective on mathematical modeling of blast furnace, ISIJ Int. 50 (2010) 914–923.
[14] Tatsuro Ariyama, Shungo Natsui, Tatsuya Kon, Shigeru Ueda, Shin Kikuchi, Hiroshi Nogami, Recent progress on advanced blast furnace mathematical models based on discrete method, ISIJ Int. 54 (2014) 1457–1471.
[15] Yu-zhu Pan, Hai-bin Zuo, Jing-song Wang, Qing-guo Xue, Guang Wang, Xue-feng She, Review on improving gas permeability of blast furnace, J. Iron Steel Res. Int. 27 (2) (2020) 121–131.
[16] Prakash B. Abhale, Nurni N. Viswanathan, Henrik Saxén, Numerical modelling of blast furnace – evolution and recent trends, Miner. Process. Ext. Metall. 129 (2020) 166–183.
[17] Jiansheng Chen, Haibin Zuo, Qingguo Xue, Jingsong Wang, A review of burden distribution models of blast furnace, Powder Technol. 398 (2022), 117055.
[18] Alexander Babich, Dieter Senk, Coke in the iron and steel industry, in: Isabel Suárez-Ruiz, Maria Antonia Diez, Fernando Rubiera (Eds.), New Trends in Coal Conversion, Chapter 13, Woodhead Publishing, 2019, pp. 367–404 (ISBN: 978-0-08-102201-6).
[19] D.J. Gavel, A review on nut coke utilisation in the ironmaking blast furnaces, Mater. Sci. Technol. 33 (4) (2017) 381–387.
[20] Krzysztof M. Graczyk, Maciej Matyka, Predicting porosity, permeability, and tortuosity of porous media from images by deep learning, Sci. Rep. 10 (1) (2020) 21488.
[21] Xu Wenxiang, Kaixing Zhang, Yufeng Zhang, Jinyang Jiang, Packing fraction, tortuosity, and permeability of granular-porous media with densely packed spheroidal particles: monodisperse and polydisperse systems, Water Resour. Res. 58 (2) (2022).
[22] Tatsuya Kon, Shungo Natsui, Shohei Matsuhashi, Shigeru Ueda, Ryo Inoue, Tatsuro Ariyama, Influence of cohesive zone thickness on gas flow in blast furnace analyzed by DEM-CFD model considering low coke operation, Steel Res. Int. 84 (11) (2013) 1146–1156.
[23] Shigeru Ueda, Tatsuya Kon, Hiroyuki Kurosawa, Shungo Natsui, Tatsuro Ariyama, Hiroshi Nogami, Influence of shape of cohesive zone on gas flow and permeability in the blast furnace analyzed by DEM-CFD model, ISIJ Int. 55 (2015) 1232–1236.
[24] Masahiro Yakeya, Akito Kasai, Rikizo Tadai, Kentaro Nozawa, Gas permeability improvement mechanism at the blast furnace cohesive zone by mixed coke charging in ore layer and effect of coke mixing for different cohesive zone condition on gas permeability, ISIJ Int. 60 (2020) 1438–1444.
[25] Kazuhira Ichikawa, Yusuke Kashihara, Nobuyuki Oyama, Toshiyuki Hirosawa, Jun Ishii, Michitaka Sato, Hidetoshi Matsuno, Evaluating effect of coke layer thickness on permeability by pressure drop estimation model, ISIJ Int. 57 (2) (2017) 254–261.
[26] A. Biswas, Principles of Blast Furnce Ironmaking: Theory and Practice, Cootha Publishing House, 2022. ISBN:978-0949917089.
[27] Yoshiyuki Matsui, K. Shibata, Y. Yoshida, R. Ono, The principle of blast furnace operational technology and centralized gas flow by center coke charging, in: KOBELCO Technology Review 12, 2005, pp. 12–20.
[28] Yu Xiaobing, Yansong Shen, Model study of blast furnace operation with central coke charging, Metall. Mater. Trans. B Process Metall. Mater. Process. Sci. 50 (5) (2019) 2238–2250.
[29] C.A. Kruelle, Physics of granular matter: pattern formation and applications, Rev. Adv. Mater. Sci. 20 (2009) 113–124.
[30] Tathagata Bhattacharya, Review Report on Granular Segregation in the Blast Furnace 1, Unpublished Work, 2008 available at: www.angelfire.com/my/tathabhatt/documents/segregation.pdf.
[31] S.H. Gharat. Flow and Segregation of Granular Materials during Heap Formation", in Progress in Fine Particle Plasmas, IntechOpen, London, United Kingdom, 2019 [Online]. Available: https://www.intechopen.com/chapters/69744.
[32] Andrew Spence, Improving Blast Furnace Burden Distribution by Stockfeed Segregation Control, Master's thesis, 1996.
[33] Hiroshi Mio, Yoichi Narita, Kaoru Nakano, Seiji Nomura, Validation of the burden distribution of the 1/3-scale of a blast furnace simulated by the discrete element method, Processes 8 (2020).
[34] T.F. Zhang, J.Q. Gan, A.B. Yu, D. Pinson, Z.Y. Zhou, Size segregation of granular materials during Paul-Wurth hopper charging and discharging process, Powder Technol. 378 (2021) 497–509.
[35] Wu Shengli, Mingyin Kou, Xu Jian, Xinying Guo, Du Kaiping, Wei Shen, Jing Sun, DEM simulation of particle size segregation behavior during charging into and discharging from a Paul-Wurth type hopper, Chem. Eng. Sci. 99 (2013) 314–323.
[36] Xu Jian, Hu Zhaowen, Xu Yang, Dongdong Wang, Liangying Wen, Chenguang Bai, Transient local segregation grids of binary size particles discharged from a wedge-shaped hopper, Powder Technol. 308 (2017) 273–289.
[37] Hiroshi Mio, Masatomo Kadowaki, Shinroku Matsuzaki, Kazuya Kunitomo, Development of particle flow simulator in charging process of blast furnace by discrete element method, Miner. Eng. 33 (2012) 27–33.
[38] Jianliang Zhang, Jiayong Qiu, Hongwei Guo, Shan Ren, Hui Sun, Guangwei Wang, Zhengkai Gao, Simulation of particle flow in a bell-less type charging system of a blast furnace using the discrete element method, Particuology 16 (2014) 167–177.
[39] Wenxuan Xu, Shusen Cheng, Qun Niu, Wei Hu, Jiawen Bang, Investigation on the uneven distribution of different types of ores in the hopper and stock surface during the charging process of blast furnace based on discrete element method, Metal. Res. Technol. 116 (314) (2019).
[40] Xu Wenxuan, Shusen Cheng, Changrong Li, Effect of the charging sequence of iron-bearing burden on burden distribution during the charging process of blast furnace based on discrete element method, Ironmak. Steelmak. 0 (2021) 1–9.
[41] Hiroshi Mio, Satoshi Komatsuki, Masatoshi Akashi, Atsuko Shimosaka, Yoshiyuki Shirakawa, Jusuke Hidaka, Masatomo Kadowaki, Shinroku Matsuzaki, Kazuya Kunitomo, Validation of particle size segregation of sintered ore during flowing through laboratory-scale chute by discrete element method, ISIJ Int. 48 (2008) 1696–1703.
[42] Hiroshi Mio, Satoshi Komatsuki, Masatoshi Akashi, Atsuko Shimosaka, Yoshiyuki Shirakawa, Jusuke Hidaka, Masatomo Kadowaki, Shinroku Matsuzaki, Kazuya Kunitomo, Effect of chute angle on charging behavior of sintered ore particles at bell-less type charging system of blast furnace by discrete element method, ISIJ Int. 49 (2009) 479–486.
[43] Yu Yaowei, Henrik Saxén, Flow of pellet and coke particles in and from a fixed chute, Ind. Eng. Chem. Res. 51 (2012) 7383–7397.
[44] Zhao-jie Teng, Shu-sen Cheng, Guo-lei Zhao, Du. Peng-yu, Effect of chute rotation on particles movement for bell-less top blast furnace, J. Iron Steel Res. Int. 20 (12) (2013) 33–39.
[45] Mingyin Kou, Xu Jian, Wu Shengli, Heng Zhou, Gu Kai, Shun Yao, Bingjie Wen, Effect of cross-section shape of rotating chute on particle movement and distribution at the throat of a bell-less top blast furnace, Particuology 44 (2019) 194–206.
[46] Mingyin Kou, Wu Shengli, Heng Zhou, Yu Yimin, Xu. Jian, Numerical investigation of coke collapse and size segregation in the bell-less top blast furnace, ISIJ Int. 58 (2018) 2018–2024.
[47] Zhibin Hong, Heng Zhou, Wu Jianlong, Longling Zhan, Yibo Fan, Zongwang Zhang, Wu Shengli, Xu Haifa, Li Wang, Mingyin Kou, Effects of operational parameters on particle movement and distribution at the top of a bell-less blast furnace based on discrete element method, Steel Res. Int. 92 (2020) 8.
[48] Xu Yang, Kaihui Ma, Chengfeng Sun, Zhehan Liao, Xu Jian, Liangying Wen, Chenguang Bai, Effect of Density Difference on Particle Segregation Behaviors at Bell-less Top Blast Furnace with Parallel-Type Hopper, Springer International Publishing, 2018, pp. 391–399.

[49] Han Wei, Weitian Ding, Ying Li, Hao Nie, Henrik Saxén, Hongming Long, Yu. Yaowei, Porosity distribution of moving burden layers in the blast furnace throat, Granul. Matter 23 (2021) 2.
[50] C.X. Li, K.J. Dong, S.D. Liu, G.R. Chandratilleke, Z.Y. Zhou, Y.S. Shen, DEM study of particle segregation in the throat region of a blast furnace, Powder Technol. 407 (2022), 117660.
[51] Yu Yaowei, Henrik Saxén, Particle flow and behavior at bell-less charging of the blast furnace, Steel Res. Int. 84 (2013) 1018–1033.
[52] S. Nag, S. Basu, A.B. Yu, A static approach towards coke collapse modelling in blast furnace, Ironmak. Steelmak. 36 (7) (2009) 509–514.
[53] Samik Nag, Somnath Basu, Tathagata Bhattacharya, Modelling of coke collapse in blast furnace – a static approach, in: Tata Search (ISSN: 0971–5975) 1, 2007, pp. 105–110.
[54] P. Zulli, W.B.U. Tanzil, J. Monaghan, M.J. McCarthy, K.L. Hockings, New technologies in blast furnace burden distribution - physical modelling, in: Chemeca 88: Australia's Bicentennial International Conference for the Process Industries; Preprints of Papers, 1988, 1988, pp. 450–454.
[55] Tamoghna Mitra, Henrik Saxén, Simulation of burden distribution and charging in an ironmaking blast furnace, IFAC-PapersOnLine 48 (2015) 183–188.
[56] Tamoghna Mitra, Henrik Saxén, Discrete element simulation of charging and mixed layer formation in the ironmaking blast furnace, Comp. Part. Mech. 3 (2016) 541–555.
[57] Heng Zhou, Wu Jianlong, Zhibin Hong, Li Pang Wang, Wu Shengli, Mingyin Kou, Guangwei Wang, Yiwa Luo, Numerical Simulation of Coke Collapse and its Optimization during Burden Charging at the Top of Bell-Less Blast Furnace vol. 389, Powder Technology, 2021, pp. 155–162.
[58] Yoshimasa Kajiwara, Takao Jimbo, Tadatsugu Joko, Yo Ichi Aminaga, Takanobu Inada, Investigation of bell-less charging based on full scale model experiments, Trans. Iron Steel Inst. Japan 24 (1984) 799–807.
[59] Mark Propster, Julian Szekely, The porosity of systems consisting of layers of different particles, Powder Technol. 17 (1) (1977) 123–138.
[60] Vladimír Staněk, Vit Eckert, Course of porosity in layered beds of spherical particles, Archiv für das Eisenhüttenwesen 50 (1) (1979) 19–24.
[61] Mriganshu Guha, Samik Nag, Pailola Kumar Swamy, Ramachandran Venkat Ramna, Effect of Interface resistance on gas flow in blast furnace, ISIJ Int. 51 (11) (2011) 1795–1799.
[62] Jinzhou Liu, Qingguo Xue, Xuefeng She, Jingsong Wang, Investigation on interface resistance between alternating layers in the upper of blast furnace, Powder Technol. 246 (2013) 73–81.
[63] J. Bridgwater, N.W. Sharpe, D.C. Stocker, Particle mixing by percolation, Trans. Inst. Chem. Eng. Chem. Eng. 47 (5) (1969).
[64] J. Bridgwater, N.D. Ingram, Rate of spontaneous inter-particle percolation, Trans. Inst. Chem. Eng. Chem. Eng. 49 (3) (1971).
[65] Franck Lominé, Luc Oger, Transport of small particles through a 3d packing of spheres: experimental and numerical approaches, J. Stat. Mech. Theory Exp. 2006 (07) (2006) P07019.
[66] Mahbubur Rahman, Haiping Zhu, Aibing Yu, John Bridgwater, Dem simulation of particle percolation in a packed bed, Particuology 6 (6) (2008) 475–482. Simulation and Modeling of Particulate Systems.
[67] H.P. Zhu, M. Rahman, A.B. Yu, J. Bridgwater, P. Zulli, Effect of particle properties on particle percolation behaviour in a packed bed, Miner. Eng. 22 (11) (2009) 961–969 (Special issue: Computational Modelling).
[68] Heng Zhou, Wu Shengli, Mingyin Kou, Zhi-Guo Luo, Zong-Shu Zou, Yansong Shen, Analysis of cohesive particle percolation in a packed bed using discrete element method, ISIJ Int. 58 (1) (2018) 43–51.
[69] S.M. Arifuzzaman, Kejun Dong, Haiping Zhu, Qinghua Zeng, DEM study and machine learning model of particle percolation under vibration, Adv. Powder Technol. 33 (5) (2022), 103551.
[70] Yu Yaowei, Henrik Saxén, Effect of DEM parameters on the simulated inter-particle percolation of pellets into coke during burden descent in the blast furnace, ISIJ Int. 52 (2012) 788–796.
[71] Willem J. Beekman, Gabrie M.H. Meesters, Brian Scarlett, Todd Becker, Measurement of granule attrition and fatigue in a vibrating box, Part. Part. Syst. Charact. 19 (1) (2002) 5–11.
[72] C. Teo, A.G. Waters, Stuart K. Nicol, Quantification of the breakage of lump materials during handling operations, Int. J. Miner. Process. 30 (1990) 159–184.
[73] R.K. Sahoo, D. Roach, Effect of different types of impact surface on coal degradation, Chem. Eng. Process. Process Intensif. 44 (2) (2005) 253–261. Pneumatic Conveying and Handling of Particulate Solids.
[74] Yoichi Narita, Hiroshi Mio, Takashi Orimoto, Seiji Nomura, Modelling of coke layer collapse during ore charging in ironmaking blast furnace by DEM, EPJ Web Conf. 140 (2018), 1 2017.
[75] Rodrigo Carvalho, Pedro Porto, Luis Tavares, Modeling Breakage and Mechanical Degradation of Steelmaking Materials during Handling, 2018.
[76] R. Sahoo, D. Roach, Quantification of the lump coal breakage during handling operation at the Gladstone port, Chem. Eng. Process. Process Intensif. 44 (7) (2005) 797–804.
[77] Luís Marcelo Tavares, Rodrigo M. de Carvalho, Modeling ore degradation during handling using continuum damage mechanics, Int. J. Miner. Process. 101 (1) (2011) 21–27.
[78] Luís Marcelo Tavares, Rodrigo M. de Carvalho, Modeling ore degradation during handling using continuum damage mechanics, Int. J. Miner. Process. 112-113 (2012) 1–6 (Special Issue Communition 2009).
[79] Pedro P.S. Cavalcanti, Horacio A. Petit, Anderson D. Thomazini, Rodrigo M. de Carvalho, Luís Marcelo Tavares, Modeling of degradation by impact of individual iron ore pellets, Powder Technol. 378 (2021) 795–807.
[80] Horacio A. Petit, Avneer Philippe, Anderson D. Thomazini, Luís Marcelo Tavares, Modeling breakage by impact of fragments of fired iron ore pellets, Powder Technol. 398 (2022), 117059.
[81] Luís Marcelo Tavares, Review and further validation of a practical single-particle breakage model, KONA Powd. Part. J. 39 (2022) 62–83.
[82] Taihei Nouchi, Takeshi Sato, Michitaka Sato, Kanji Takeda, Tatsuro Ariyama, Stress field and solid flow analysis of coke packed bed in blast furnace based on DEM, ISIJ Int. 45 (2005) 1426–1431.
[83] Jian Liang Zhang, Yong Xing Chen, Zheng Yun Fan, Hu Zheng Wen, Tian Jun Yang, Tatsuro Ariyama, Influence of profile of blast furnace on motion and stress of burden by 3D-DEM, J. Iron Steel Res. Int. 18 (11) (2011) 1–6.
[84] Shungo Natsui, Azuma Hirai, Koki Terui, Yusuke Kashihara, Akinori Murao, Yuji Miki, Hiroshi Nogami, Impact of high-temperature non-uniform degradation on fines clogging and gas flow in a coke bed, Chem. Eng. J. 427 (2022), 131484.
[85] Ting-zhi Ren, Xin Jin, Hong-yan Ben, Yu. Cheng-zhong, Burden distribution for bell-less top with two parallel hoppers, J. Iron Steel Res. Int. 13 (2) (2006) 14–17.
[86] Huatao Zhao, Minghua Zhu, Du Ping, Seiji Taguchi, Hongchao Wei, Uneven distribution of burden materials at blast furnace top in bell-less top with parallel bunkers, ISIJ Int. 52 (12) (2012) 2177–2185.
[87] Xu Jian, Wu Shengli, Mingyin Kou, Lihua Zhang, Yu. Xiaobo, Circumferential burden distribution behaviors at bell-less top blast furnace with parallel type hoppers, Appl. Math. Model. 35 (3) (2011) 1439–1455.
[88] Lin Shi, Guangsheng Zhao, Mingxin Li, Xiang Ma, A model for burden distribution and gas flow distribution of bell-less top blast furnace with parallel hoppers, Appl. Math. Model. 40 (23) (2016) 10254–10273.
[89] Xu Yang, Xu Jian, Chengfeng Sun, Kaihui Ma, Cheng Shan, Liangying Wen, Shengfu Zhang, Chenguang Bai, Quantitative comparison of binary particle mass and size segregation between serial and parallel type hoppers of blast furnace bell-less top charging system, Powder Technol. 328 (2018) 245–255.
[90] Yoichi Narita, Hiroshi Mio, Takashi Orimoto, Seiji Nomura, DEM analysis of particle trajectory in circumferential direction at bell-less top, ISIJ Int. 57 (2017) 429–434.
[91] Chengfeng Sun, Xu Jian, Zhehan Liao, Xu Yang, Mingyin Kou, Liangying Wen, Causes of particle trajectory fluctuation on the rotating chute in circumferential direction at bell-less top with parallel type hoppers, ISIJ Int. 59 (9) (2019) 1527–1533.
[92] Jiansheng Chen, Haibin Zuo, Hongbo Zhao, Qingguo Xue, Jingsong Wang, Burden circumferential mass segregation at the blast furnace with parallel hoppers, Powder Technol. 409 (2022), 117845.
[93] Xu Wenxuan, Shusen Cheng, Qun Niu, Guolei Zhao, Effect of the main feeding belt position on burden distribution during the charging process of bell-less top blast furnace with two parallel hoppers, ISIJ Int. 57 (2017) 1173–1180.
[94] Xu Wenxuan, Shusen Cheng, Qun Niu, Guolei Zhao, Effect of the cross-section shape of rotating chute on particle flow and burden distribution during the charging process of bell-less top blast furnace with two parallel hoppers, Ironmak. Steelmak. 46 (2019) 105–112.
[95] Xu Wenxuan, Shusen Cheng, Qun Niu, Hu Wei, Jiawen Bang, The DEM study of segregation phenomena of burden distribution during the charging process of blast furnace with two parallel hoppers, Ironmak. Steelmak. 47 (2020) 337–343.
[96] T.F. Zhang, J.Q. Gan, A.B. Yu, D. Pinson, Z.Y. Zhou, Segregation of granular binary mixtures with large particle size ratios during hopper discharging process, Powder Technol. 361 (2020) 435–445.
[97] M.A.J. Holmes, D.J. Penney, N.P. Lavery, S.G.R. Brown, A numerical investigation assessing the symmetry of burden charging in a blast furnace using different chute designs, Ironmak. Steelmak. 45 (2018) 551–559.
[98] Wenxuan Xu, Shusen Cheng, Changrong Li, Experimental study of the segregation of burden distribution during the charging process of bell-less top blast furnace with two parallel hoppers 2044, 2021, p. 12129.
[99] C.J. Coetzee, Calibration of the discrete element method and the effect of particle shape, Powder Technol. 297 (2016) 50–70.
[100] C.J. Coetzee, Review: calibration of the discrete element method, Powder Technol. 310 (2017) 104–142.
[101] Thomas Roessler, Christian Richter, André Katterfeld, Frank Will, Development of a standard calibration procedure for the DEM parameters of cohesionless bulk materials – part I: solving the problem of ambiguous parameter combinations, Powder Technol. 343 (2019) 803–812.
[102] André Katterfeld, C.J. Coetzee, Tim Donohue, Johannes Fottner, Andrew Grima, Álvaro Ramírez-Gómez, Dusan Ilic, Rimantas Kačianauskas, Jan Necas, Dingena Schott, Kenneth Williams, Jiri Zegzulka, Calibration of DEM Parameters for Cohesionless Bulk Materials under Rapid Flow Conditions and Low Consolidation, 2019.
[103] Aleksei Boikov, Roman Savelev, Vladimir Payor, Alexander Potapov, Universal approach for DEM parameters calibration of bulk materials, Symmetry 13 (2021).
[104] L. Benvenuti, C. Kloss, S. Pirker, Identification of DEM simulation parameters by artificial neural networks and bulk experiments, Powder Technol. 291 (2016) 456–465.
[105] Frederik Elskamp, Harald Kruggel-Emden, Manuel Hennig, Ulrich Teipel, A strategy to determine DEM parameters for spherical and non-spherical particles, Granul. Matter 19 (2017) 6.
[106] Huy Q. Do, Alejandro M. Aragón, Dingena L. Schott, A calibration framework for discrete element model parameters using genetic algorithms, Adv. Powder Technol. 29 (2018) 1393–1403.
[107] Christian Richter, Thomas Rößler, Günter Kunze, Andre Katterfeld, Frank Will, Development of a standard calibration procedure for the DEM parameters of cohesionless bulk materials – part II: efficient optimization-based calibration, Powder Technol. 360 (2020) 967–976.

[108] Christian Richter, Frank Will, Introducing Metamodel-based global calibration of material-specific simulation parameters for discrete element method, Minerals 11 (2021).
[109] M. Javad Mohajeri, Cees van Rhee, Dingena L. Schott, Replicating cohesive and stress-history-dependent behavior of bulk solids: feasibility and definiteness in DEM calibration procedure, Adv. Powder Technol. 32 (2021) 1532–1548.
[110] Marc P. Fransen, Matthijs Langelaar, Dingena L. Schott, Application of DEM-based metamodels in bulk handling equipment design: methodology and DEM case study, Powder Technol. 393 (2021) 205–218.
[111] Yu Yaowei, Henrik Saxén, Experimental and DEM study of segregation of ternary size particles in a blast furnace top bunker model, Chem. Eng. Sci. 65 (2010) 5237–5250.
[112] Aman Tripathi, Vimod Kumar, Arpit Agarwal, Anurag Tripathi, Saprativ Basu, Arijit Chakrabarty, Samik Nag, Quantitative DEM simulation of pellet and sinter particles using rolling friction estimated from image analysis, Powder Technol. 380 (2021) 288–302.
[113] K. Zhou, Z. Jiang, D. Pan, W. Gui, J. Huang, Influence of Charging Parameters on the Burden Flow Velocity and Distribution on the Blast Furnace Chute Based on Discrete Element Method, Steel Research Int. 93 (2022) 2100332, 10.1002%2Fsrin.202100332.
[114] Hiroshi Mio, Yoichi Narita, Shinroku Matsuzaki, Koki Nishioka, Seiji Nomura, Measurement of particle charging trajectory via rotating chute of 1/3-scale blast furnace and its comparing with numerical analysis using discrete element method, Powder Technol. 344 (2019) 797–803.
[115] Yu Yaowei, Henrik Saxén, Segregation behavior of particles in a top hopper of a blast furnace, Powder Technol. 262 (2014) 233–241.
[116] Sida Liu, Zongyan Zhou, Kejun Dong, Yu Aibing, David Pinson, John Tsalapatis, Numerical investigation of burden distribution in a blast furnace, Steel Res. Int. 86 (2015) 651–661.
[117] Arijit Chakrabarty, Saprativ Basu, Samik Nag, Ujjal Ghosh, Mantu Patra, Model study of Centre coke charging in blast furnace through DEM simulations, ISIJ Int. 61 (3) (2021) 782–791.
[118] Gerhard Holzinger, Magdalena Schatzl, Effect of chute start angle and hopper change on burden distribution during the charging process of a bell-less top blast furnace with two parallel hoppers, Powder Technol. 395 (2022) 669–680.
[119] Hiroshi Mio, Satoshi Komatsuki, Masatoshi Akashi, Atsuko Shimosaka, Yoshiyuki Shirakawa, Jusuke Hidaka, Masatomo Kadowaki, Hirokazu Yokoyama, Shinroku Matsuzaki, Kazuya Kunitomo, Analysis of traveling behavior of nut coke particles in bell-type charging process of blast furnace by using discrete element method, ISIJ Int. 50 (2010) 1000–1009.
[120] Yu Yaowei, Andreas Westerlund, Timo Paananen, Henrik Saxén, Inter-particle percolation segregation during burden descent in the blast furnace, ISIJ Int. 51 (2011) 1050–1056.
[121] W.J. Yang, Z.Y. Zhou, A.B. Yu, Discrete particle simulation of solid flow in a three-dimensional blast furnace sector model, Chem. Eng. J. 278 (2015) 339–352.
[122] Dingena Schott, Wouter Vreeburg, Carmen Molhoek, Gabriel Lodewijks, Granular Flow to a Blast iron Ore Furnace: Influence of Particle Size Distribution on Segregation of a Mixture, Springer International Publishing, 2016, pp. 621–628.
[123] Marc Holmes, A Numerical Simulation of Particulate Distribution of the Blast Furnace Raw Material Burden through the Paul Wurth Bell-Less Top Apparatus, PhD thesis, 2016.
[124] Nicolin Govender, Daniel N. Wilke, Wu Chuan-Yu, Ugur Tuzun, Hermann Kureck, A numerical investigation into the effect of angular particle shape on blast furnace burden topography and percolation using a GPU solved discrete element model, Chem. Eng. Sci. 204 (2019) 9–26.
[125] Deside Kudzai Chibwe, Geoffrey Michael Evans, Elham Doroodchi, Brian Joseph Monaghan, David John Pinson, Sheng Jason Chew, Charge material distribution behaviour in blast furnace charging system, Powder Technol. 366 (2020) 22–35.
[126] Gabriele Degrassi, Lucia Parussini, Marco Boscolo, Nicola Petronelli, Vincenzo Dimastromatteo, Discrete element simulation of the charge in the hopper of a blast furnace, calibrating the parameters through an optimization algorithm, SN Appl. Sci. 3 (2021) 242.
[127] Y. Tsuji, T. Tanaka, T. Ishida, Lagrangian numerical simulation of plug flow of cohesionless particles in a horizontal pipe, Powder Technol. 71 (1992) 239–250.
[128] Paulo Flores, Compliant contact force approach for forward dynamic modeling and analysis of biomechanical systems, Proc. IUTAM 2 (2011) 58–67.
[129] Jun Ai, J. Jian-Fei Chen, Michael Rotter, Jin Y. Ooi, Assessment of rolling resistance models in discrete element simulations, Powder Technol. 206 (2011) 269–282.
[130] C.M. Wensrich, A. Katterfeld, Rolling friction as a technique for modelling particle shape in DEM, Powder Technol. 217 (2012) 409–417.
[131] G. Lu, J.R. Third, C.R. Müller, Discrete element models for non-spherical particle systems: from theoretical developments to applications, Chem. Eng. Sci. 127 (2015) 425–465.
[132] Yoav Kallus, The random packing density of nearly spherical particles, Soft Matter 12 (2016) 3.
[133] Daniel Schiochet Nasato, Christoph Goniva, Stefan Pirker, Christoph Kloss, Coarse graining for large-scale DEM simulations of particle flow – an investigation on contact and cohesion models, Proc. Eng. 102 (2015) 1484–1490.
[134] Stef Lommen, Mohammadjavad Mohajeri, Gabriel Lodewijks, Dingena Schott, DEM particle upscaling for large-scale bulk handling equipment and material interaction, Powder Technol. 352 (2019) 273–282.
[135] Suranita Kanjilal, Simon Schneiderbauer, A revised coarse-graining approach for simulation of highly poly-disperse granular flows, Powder Technol. 385 (2021) 2.
[136] Dingena L. Schott, Stef W. Lommen, Ronald van Gils, Job de Lange, Martijn M. Kerklaan, Olaf M. Dessing, Wouter Vreugdenhil, Gabriel Lodewijks, Scaling of particles and equipment by experiments of an excavation motion, Powder Technol. 278 (2015) 26–34.
[137] M. Javad Mohajeri, Rudy L.J. Helmons, Cees van Rhee, Dingena L. Schott, A hybrid particle-geometric scaling approach for elasto-plastic adhesive DEM contact models, Powder Technol. 369 (2020) 72–87.
[138] Thomas Roessler, André Katterfeld, Scaling of the angle of repose test and its influence on the calibration of DEM parameters using upscaled particles, Powder Technol. 330 (2018) 58–66.
[139] Thorsten Pöschel, Clara Salueña, Thomas Schwager, Can we Scale Granular Systems? Powders & Grains 2001, 2001, pp. 439–442.
[140] Y.T. Feng, K. Han, D.R.J. Owen, J. Loughran, On upscaling of discrete element models: similarity principles, Eng. Comput. 26 (6) (January 2009) 599–609.
[141] Y.T. Feng, D.R.J. Owen, Discrete element modelling of large scale particle systems–i: exact scaling laws, Comp. Part. Mech. 1 (2014) 159–168.
[142] Masatoshi Akashi, Hiroshi Mio, Atsuko Shimosaka, Yoshiyuki Shirakawa, Jusuke Hidaka, Seiji Nomura, Estimation of bulk density distribution in particle charging process using discrete element method considering particle shape, ISIJ Int. 48 (2008) 1500–1506.
[143] Han Wei, Xiaojiu Tang, Yao Ge, Meng Li, Henrik Saxén, Yu. Yaowei, Numerical and experimental studies of the effect of iron ore particle shape on repose angle and porosity of a heap, Powder Technol. 353 (2019) 526–534.
[144] Han Wei, Yao Ge, Meng Li, Ying Li, Henrik Saxén, Zhijun He, Yu. Yaowei, DEM study of the porosity distribution of pellet sandpile formed by ternary size particles, Powder Technol. 360 (2020) 1337–1347.
[145] Arijit Chakrabarty, Rituparna Biswas, Saprativ Basu, Samik Nag, Characterisation of binary mixtures of pellets and sinter for DEM simulations, Adv. Powder Technol. 33 (1) (2022), 103358.
[146] Xiuhao Xia, Lianyong Zhou, Huaqing Ma, Changhua Xie, Yongzhi Zhao, Reliability study of super-ellipsoid DEM in representing the packing structure of blast furnace, Particuology 70 (2022) 72–81.
[147] Govind S. Gupta, S. Sarkar, A. Chychko, L.D. Teng, M. Nzotta, S. Seetharaman, Chapter 3.1 - process concept for scaling-up and plant studies, in: Seshadri Seetharaman (Ed.), Treatise on Process Metallurgy, Elsevier, Boston, 2014, pp. 1100–1144.
[148] Tamoghna Mitra, Henrik Saxén, Model for fast evaluation of charging programs in the blast furnace, Metall. Mater. Trans. B Process Metall. Mater. Process. Sci. 45 (2014) 2382–2394.
[149] Kiichi Narita, Shinichi Inaba, Isao Kobayashi, Okimoto Kenichi, Masakata Shimizu, Yabata Takeshi, Tamada Shinichi, Study of ore and coke distribution in blast furnase carried out on a full size model, Tetsu To Hagane J. Iron Steel Inst. Japan 65 (1979) 358–367.
[150] Hiroshi Takahashi, Masayuki Tanno, Jiro Katayama, Burden descending behaviour with renewal of deadman in a two dimensional cold model of blast furnace, ISIJ Int. 36 (11) (1996) 1354–1359.
[151] Juan Jimenez, Javier Mochón, Antonio Formoso, Jesús Sainz, de Ayala., Burden distribution analysis by digital image processing in a scale model of a blast furnace shaft, ISIJ Int. 40 (2) (2000) 114–120.
[152] Zongyan Zhou, Haiping Zhu, Yu Aibing, Bryan Wright, David Pinson, Paul Zulli, Discrete particle simulation of solid flow in a model blast furnace, ISIJ Int. 45 (2005) 1828–1837.
[153] Z.Y. Zhou, H.P. Zhu, A.B. Yu, B. Wright, P. Zulli, Discrete particle simulation of gas–solid flow in a blast furnace, Comput. Chem. Eng. 32 (2008) 1760–1772.
[154] B. Wright, P. Zulli, Z.Y. Zhou, A.B. Yu, Gas–solid flow in an ironmaking blast furnace — I: Physical modelling, Powder Technol. 208 (1) (2011) 86–97.
[155] Xu Jin, Nan Wang, Min Chen, Zongyan Zhou, Pengfei Wang, Evaluation of reduction behavior of blast furnace dust particles during in-flight process with experiment aided mathematical modeling, Appl. Math. Model. 75 (2019) 535–552.
[156] Yan Li, Shuxia Ren (Eds.), Basic Properties of Building Decorative Materials, Woodhead Publishing, 2011, pp. 10–24.
[157] Stef Lommen, Dingena Schott, Gabriel Lodewijks, DEM speedup: stiffness effects on behavior of bulk material, Particuology 12 (2014) 107–112.
[158] Y. Okuno, S. Matsuzaki, K. Kunitomo, M. Isoyama, Y. Kusano, Development of a mathematical-model to estimate burden distribution in bell-less type charging for blast-furnace, Tetsu to Hagane-Journal Iron Steel Institute Japan 73 (1) (Jan 1987) 91–98.
[159] Mingyin Kou, Wang Zeng, Zhong Zhang, Xuefeng She, Tianxiang Zhang, Baojun Zhao, Xiaodong Ma, Heng Zhou, Central coke charging and its effect on coke collapse at the throat of blast furnace by DEM simulation, Powder Technol. 408 (2022), 117784.
[160] Shigeru Ueda, Shungo Natsui, Zhengyun Fan, Hiroshi Nogami, Rikio Soda, Junya Kano, Ryo Inoue, Tatsuro Ariyama, Influences of physical properties of particle in discrete element method on descending phenomena and stress distribution in blast furnace, ISIJ Int. 50 (2010) 981–986.
[161] Wenjing Yang, Zongyan Zhou, David Pinson, Yu. Aibing, Periodic boundary conditions for discrete element method simulation of particle flow in cylindrical vessels, Ind. Eng. Chem. Res. 53 (2014) 8245–8256.
[162] Stef Lommen, Virtual Prototyping of Grabs: Co-Simulations of Discrete Element and Rigid Body Models, PhD thesis,, Delft University of Technology, 2016.
[163] Juan Rodriguez, Tommy Edeskär, Sven Knutsson, Particle shape quantities and measurement techniques: a review, Electr. J. Geotechn. Eng. 18 (2013) 169–198.
[164] Vasileios Angelidakis, Sadegh Nadimi, Stefano Utili, SHape Analyser for particle engineering (SHAPE): seamless characterisation and simplification of particle morphology from imaging data, Comput. Phys. Commun. 265 (2021), 107983.

[165] Vasileios Angelidakis, Sadegh Nadimi, Masahide Otsubo, Stefano Utili, CLUMP: a code library to generate universal multi-sphere particles, SoftwareX 15 (2021), 100735.
[166] Gabriel K.P. Barrios, Rodrigo M. de Carvalho, Arno Kwade, Luís Marcelo Tavares, Contact parameter estimation for DEM simulation of iron ore pellet handling, Powder Technol. 248 (2013) 84–93.
[167] Han Wei, Hao Nie, Ying Li, Henrik Saxén, Zhijun He, Yu. Yaowei, Measurement and simulation validation of DEM parameters of pellet, sinter and coke particles, Powder Technol. 364 (2020) 593–603.
[168] Micromeritics, Geopyc 1365 – Envelope Density Analyzer, 2017.
[169] Chengzhi Li, Tom Honeyands, Damien O'Dea, Roberto Moreno-Atanasio, The angle of repose and size segregation of iron ore granules: DEM analysis and experimental investigation, Powder Technol. 320 (2017) 257–272.
[170] Tinghua Li, Jiayuan Zhang, Wei Ge, Simple measurement of restitution coefficient of irregular particles, China Particuol. 2 (2004) 274–275.
[171] C.M. Wensrich, A. Katterfeld, D. Sugo, Characterisation of the effects of particle shape using a normalised contact eccentricity, Granul. Matter 16 (2014) 327–337.
[172] Y.C. Zhou, B.H. Xu, A.B. Yu, P. Zulli, An experimental and numerical study of the angle of repose of coarse spheres, Powder Technol. 125 (1) (2002) 45–54.
[173] Piotr Frankowski, Martin Morgeneyer, Calibration and validation of DEM rolling and sliding friction coefficients in angle of repose and shear measurements, AIP Conf. Proc. 1542 (1) (2013) 851–854.
[174] Hamzah M. Beakawi, S. Al-Hashemi Omar, Baghabra Al-Amoudi, A review on the angle of repose of granular materials, Powder Technol. 330 (2018) 397–417.
[175] Johan Bester, Philip Venter, Martin van Eldik, Discrete element model calibration for industrial raw material simulations, MATEC Web Conf. 347 (2021) 00036.
[176] Deside Chibwe, Optimised Burden Delivery for Blast Furnace Operations, PhD thesis,, University of Newcastle, Australia, 2019.
[177] Qiang Li, Mingxia Feng, Zongshu Zou, Validation and calibration approach for discrete element simulation of burden charging in pre-reduction shaft furnace of COREX process, ISIJ Int. 53 (2013) 1365–1371.
[178] Marc P. Fransen, Matthijs Langelaar, Dingena L. Schott, Including stochastics in metamodel-based DEM model calibration, Powder Technol. 406 (2022), 117400.
[179] N. Standish, A. Kilic, Comparison of stop-start and continuous sampling methods of studying segregation of materials discharging from a hopper, Chem. Eng. Sci. 40 (1985) 2152–2153.
[180] N. Standish, Studies of size segregation in filling and emptying a hopper, Powder Technol. 45 (1985) 43–56.
[181] M. Rahman, Dingena Schott, André Katterfeld, C.M. Wensrich, Influence of the software on the calibration parameters for DEM simulations, Bulk Solids Handl. 31 (2011) 396–400.
[182] D. E, Numerical investigation of mixed layer effect on permeability in a dynamic blast furnace, Engineering Reports 2 (2020), e12166, 10.1002%2Feng2.12166.
[183] Micromeritics, Density Analysis. Brochure. https://www.micromeritics.com/Repository/Files/Density_Brochure.pdf, 2022.
[184] Jong-In Park, Hun-Je Jung, Min-Kyu Jo, Oh. Han-Sang, Jeong-Whan Han, Mathematical modeling of the burden distribution in the blast furnace shaft, Met. Mater. Int. 17 (2011) 485–496.
[185] Zhanxia Di, Mingrong Huang, Xiaobin Zhou, Junhan Liu, Junjie Sun, Ping Wang, Hongtao Wang, The influence of central coke charging mode onthe burden surface shape and distribution of ablast furnace, 2022.
[186] D. Wang, M. Servin, T. Berglund, K.O. Mickelsson, S. Rönnbäck, Parametrization and validation of a nonsmooth discrete element method for simulating flows of iron ore green pellets, Powder Technol. 283 (2015) 475–487.
[187] Rikio Soda, Akira Sato, Junya Kano, Eiki Kasai, Fumio Saito, Masaki Hara, Takazo Kawaguchi, Analysis of granules behavior in continuous drum mixer by DEM, ISIJ Int. 49 (2009) 645–649.
[188] Shiyu Wei, Han Wei, Henrik Saxen, Yaowei yu., Numerical analysis of the relationship between friction coefficient and repose angle of blast furnace raw materials by discrete element method, Materials 15 (2022) 903.